UNLIMITED
UNCLASSIFIED

ILLIMITÉ
NON CLASSIFIÉ

Technical Report

Rapport technique

1988/10

TR-WE-50
NRC NO. 27491
TDC No. TP 8344E

WEAR AND CONTACT FATIGUE MODEL FOR RAILWAY RAIL

J. Kalousek

CA1
DTC 801
86
W21
c.2

Division of
Mechanical Engineering

Division de
génie mécanique

National Research Council Canada
Conseil national de recherches Canada

Canada

88-00340/

DIVISION OF MECHANICAL ENGINEERING PUBLICATIONS

DM **(Division of Mechanical Engineering Report)**
Scientific and technical information considered important, complete and a lasting contribution to existing knowledge.

TR **(Technical Report)**
Information less broad in scope but a substantial contribution to existing knowledge.

CTR **(Controlled/Classified Technical Report)**
A Technical Report with controlled distribution for national security, proprietary or other reasons.

LM **(Laboratory Memorandum)**
Preliminary or exploratory information with controlled distribution.

CAT **(Calibration Analysis and Test Report)**
Information on minor laboratory projects or services.

PUBLICATIONS DE LA DIVISION DE GÉNIE MÉCANIQUE

DM **(Rapport de la Division de génie mécanique)**
Informations scientifiques et techniques jugées importantes, complètes et susceptibles de contribuer de façon durable à l'avancement des connaissances courantes.

TR **(Rapport technique)**
Informations de moindre importance, mais pouvant contribuer substantiellement à l'avancement des connaissances actuelles.

CTR **(Rapport technique à diffusion contrôlée/classifiée)**
Rapport technique à diffusion contrôlée pour des raisons de sécurité nationale, de propriété intellectuelle et autres.

LM **(Mémoire de laboratoire)**
Informations préliminaires ou de nature exploratoire à diffusion contrôlée.

CAT **(Rapport d'étalonnage d'analyse et d'essai)**
Informations sur de petits projets ou des services de laboratoire.

UNLIMITED
UNCLASSIFIED

ILLIMITÉ
NON CLASSIFIÉ

WEAR AND CONTACT FATIGUE MODEL FOR RAILWAY RAIL

MODELE D'USURE ET DE FATIGUE DE CONTRACT DES RAILS DE CHEMIN DE FER

FINAL REPORT
April 85 to March 86

Library and Information Centre / Centre de Documentation (GSLA)
RECEIVED - REÇU LE
OCT 5 1987
Transport Canada / Transports Canada

J. Kalousek

Sponsor Organizations:

Transport Canada
Transportation Development Centre
Montreal, Canada

and

Association of American Railroads
Technical Research Center
Chicago, U.S.A.

Technical Report

1986/10

Rapport technique

TR-WE-50
NRC No. 27491
TDC No. TP 8344E

Dr. C. Dayson, Head/Chef
Western Laboratories/
Laboratoires de l'Ouest

Mr. J. Ploeg
Director/
Directeur

The contents of this report reflect the views of the author and not necessarily the official view or opinions of the Transportation Development Centre of Transport Canada.

Un sommaire en français de ce rapport est inclus avant la Table des matières.

Transport Canada / Transports Canada

Development / Développement

REPORT DOCUMENTATION FORM

1. Transport Canada Report No.	2. TDC Project No.	3. Recipient's Catalogue No.
TP 8344E	6433/6747	

4. Title and Subtitle	5. Report Date
Wear and Contact Fatigue Model for Railway Rail - Final Report	October 1986
	6. Performing Organization Report No.
7. Author(s)	8. Transport Canada File No.
J. Kalousek	D1465-366-5
9. Performing Organization Name and Address National Research Council of Canada (NRC) Tribology and Mechanics Laboratory 3650 Wesbrook Mall Vancouver, B.C. V6S 2L2	10. DSS File No.
	11. DSS or Transport Canada Contract No. 6433/6747
12. Sponsoring Agency Name and Address Transportation Development Centre (TDC) Guy Favreau Complex 200 Dorchester Blvd. W., Suite 601, West Tower Montreal, Quebec H2Z 1X4	13. Type of Report and Period Covered Final; 04/85-03/86
	14. Sponsoring Agency Code TDC 6433/6747
15. Supplementary Notes This is a cooperative project between the Transportation Development Centre and the Association of American Railroads	16. TDC Project Officer **D.W. Dibble**

17. Abstract

The research objective of the wear and contact fatigue model is to identify theoretical and practical measures aimed at the extension of rail life. The research efforts were carried out jointly by the National Research Council (NRC) of Canada and the University of Rhode Island (URI). At the NRC, several aspects of selected mechanical, metallurgical, and lubrication parameters on the wear and contact fatigue processes were studied; while the URI experimentally investigated contact fatigue crack initiation in the biaxial stress environment.

This report summarizes the results of the overall research program carried out during the course of four and a half years. It first describes the fundamentals of rail/wheel contact mechanics with respect to contact stresses microslip, tractions and plastic flow. It is followed by a discussion of the basic forms of wear and the quantitative wear rates obtained in laboratory tests from a number of commercial and developmental rail steels. Next, the results of laboratory tests concerned with the effect of lubrication on wear and contact fatigue are reported and discussed, together with several other practical aspects of rail wheel lubrication. The relationship between wear and contact fatigue crack initiation by plastic instability is explained. And finally a rail maintenance policy, aiming at a substantial rail life increase, consisting of thorough lubrication and light grinding is described and its economic benefits are estimated.

18. Key Words	19. Distribution Statement
Rail life, Wear, Fatigue, Lubrication and Metallurgy, Model	A limited number of copies are available from the Transportation Development Centre

20. Security Classification (of this report)	21. Security Classification (of this page)	22. No. of Pages	23. Price
Unclassified	Unclassified		----

TDC CDT 79-005
Rev 86

Canada

Transports Canada / Transport Canada

Développement / Development

FORMULE DOCUMENTAIRE DU RAPPORT

1. N° du rapport Transports Canada	2. N° de l'étude — CDT	3. N° de catalogue du destinataire
TP 8344E	6433/6747	

4. Titre et sous-titre	5. Date du rapport
Wear and Contact Fatigue Model for Railway Rail - Final Report	octobre 1986
	6. N° du rapport de l'organisme exécutant

7. Auteur(s)	8. N° de dossier Transports Canada
J. Kalousek	D1465-366-5

9. Nom et adresse de l'organisme exécutant	10. N° de dossier — ASC
Conseil National de Recherches Canada Laboratoire mécanique et tribologie 3650 Wesbrook Mall Vancouver (C.-B.) V6S 2L2	11. N° de contrat — ASC ou Transports Canada 6433/6747

12. Nom et adresse de l'organisme parrain	13. Genre de rapport et période visée
Centre de développement des transports (CDT) Complexe Guy-Favreau 200 ouest, boul. Dorchester, suite 601, tour ouest Montréal (Québec) H2Z 1X4	Final; 04/85-03/86
	14. Code de l'organisme parrain CDT 6433/6747

15. Remarques additionnelles	16. Agent de projet — CDT
Ceci est un programme de recherche conjoint, parrainé par le Centre de développement des transports et l'Association of American Railroads	**D.W. Dibble**

17. Résumé

Ce rapport décrit la recherche sur le modèle mathématique qui figure le processus d'usure et de fatigue des rails de chemins de fer et vise à prolonger la durée de vie de ces éléments. Ce programme de recherche a été lancé conjointement par le Conseil national de recherches du Canada (CNR) et l'Université du Rhode Island aux Etats-Unis. Au CNR, les travaux ont porté sur divers aspects touchant certains paramètres particuliers: mécaniques, métallurgiques et rhéologiques qui ont une influence sur le processus d'usure et de fatigue par contact. A l'Université du Rhode Island, on a cherché à approfondir expérimentalement le phénomène de fissuration par fatigue sous contraintes biaxiales. Le rapport récapitule les résultats du programme global qui s'est échelonné sur les quatre dernières années et demie. D'abord, il rappelle les notions fondamentales touchant la mécanique du contact roue-rail sur les plans des contraintes, du glissement microgéométrique, des charges de traction et de l'écoulement plastique. Il traite ensuite des formes fondamentales d'usure et des taux d'usure obtenus en laboratoire sur des aciers à rail de type tant commercial qu'expérimental. En outre, il donne et commente les résultats des essais visant à mettre en évidence l'effet de la lubrification sur l'usure et la fatigue par contact ainsi que divers autres aspects pratiques de la lubrification des rails, de même qu'il explique la relation entre usure et fissuration par fatigue due aux déformations plastiques. Enfin, il décrit une méthode de maintenance des rails visant à en augmenter sensiblement la durée de vie par une lubrification poussée, accompagnée d'un reprofilage léger, dont il présente les avantages économiques escomptés.

18. Mots-clés	19. Diffusion
Durée des rails, usure, fatigue, lubrification, métallurgie, modèle	Le Centre de développement des transports dispose d'un nombre limité d'exemplaires.

20. Classification de sécurité (de ce rapport)	21. Classification de sécurité (de cette page)	22. Nombre de pages	23. Prix
non classifié	non classifiée		----

CDT/TDC 79-005
Rev 86

Canada

ACKNOWLEDGEMENT

A substantial input from Prof. H. Ghonem, University of Rhode Island, U.S.A., and Dr. D.M. Fegredo, Department of Energy, Mines and Resources, Canada towards the development of the model described in this report is most gratefully acknowledged.

The financial support provided by the Transportation Development Centre (Canada) and the Association of American Railroads towards the research described in this report, is also most gratefully acknowledged.

ABSTRACT

This is the final report on a research program jointly carried out at the National Research Council of Canada (NRCC) and the University of Rhode Island (URI), U.S.A. The program was aimed at the development of a wear and contact fatigue model for railway rail which, by establishing or identifying the relationships between relevant variables, could identify some practical measures to extend rail life. The author of this report believes that the objective of the research program was achieved with respect to preventing wear and such surface defects as shelling, spalling, rail corrugations, and in controlling the plastic flow of rail material. A rail maintenance method, consisting of thorough lubrication and light but frequent grinding, should completely eliminate rail surface damage due to wear and contact fatigue. Provided that the incidence of fatigue ("Sperry") defects is also brought under control, a significant increase in rail life will result. Analysis of fatigue defects is not included in our model.

The first section of this report describes the fundamentals of rail/wheel contact mechanics with respect to contact stresses, microslip and associated traction forces, and plastic flow of rail steel. It describes the phenomenon of pummelling - an intermittent movement of the contact zone from the center of the rail to its side and back. The relative frequency of contact at a specific location on the rail is of critical importance in correctly interpreting field or laboratory wear and contact fatigue data. Simplified formulae to calculate the maximum compressive and shear contact stresses at the rail's top and gauge face are presented. The strong effect of contact geometry on contact stresses is explained and the effect of lubrication on the surface and subsurface stress distribution is shown. Although lubrication contributes to the reduction of rail plastic flow, rail hardness appears to have a stronger effect.

The next section discusses the four basic forms of wear: severe adhesive, mild adhesive, oxidative and abrasive. It reports the quantitative wear rates obtained in the laboratory tests from a number of commercial and developmental rail steels. The correlation between our laboratory tests and the controlled field wear tests was found to be satisfactory. Laboratory tests have shown that increasing the rail hardness beyond the 360-380BHN range becomes ineffective in controlling adhesive wear, although some further improvement can be achieved by reducing the sulphur content. Lubrication controls gauge face wear most effectively, however, it reduces the wear rate on top rail surfaces to an unacceptably low level which contributes to the development of contact fatigue cracks.

The lubrication section opens with a brief review of lubrication theory followed by a description of the composition and desirable selection criteria for rail greases. Comparative performance tests with respect to chemical and mechanical extreme pressure (EP) additives were carried out on several experimental batches of rail grease. These tests indicated that the most effective lubrication was obtained with one or, at most, two EP additives. Since the rate of grease dispensation should be equal to the rate at which the grease is consumed in the rail/wheel interface, a series of laboratory retentiveness tests were performed. These tests showed that the rate of exhaustion of the lubricant increases with increasing axle load and curvature.

The contact fatigue section opens by reminding the reader that although the load has a strong negative effect on contact fatigue, the negative effect of counterformal wheel/rail geometry is disasterous. The contact fatigue crack propagation theory is reviewed and the effect of lubrication, which accelerates the propagation of the cracks, is noted. Then a mechanism of surface crack initiation - by plastic instability is described. Using a specially designed test specimen which was subjected to a biaxial compressive and shear cyclic stress environment, the relationships governing the plastic instability of one commercial rail steel were established. It was found that, in the case of plastic instability, lubrication decreases the onset of crack initiation which, when related to wear rates, was used to estimate the grinding interval.

The last section brings forward arguments in support of light but frequent grinding. This is called preventive grinding and it is most effective when used on adequately lubricated railway lines. Rather than using heavy grinding to correct rail surface defects such as corrugations, weld batter or distortion of rail profile due to cumulative plastic flow, preventive grinding simply prevents the development of such defects. The grinding criteria, desirable grinding depth, period and patterns are described and discussed.

The author believes that the combination of thorough lubrication and preventive grinding will provide the railway industry with a means to substantially increase rail life in curves and tangent tracks alike. It will also enable the railways to be in full control over the rail corrugation problem and a rail grinding program.

SOMMAIRE

Ceci est le rapport final du programme de recherche réalisé conjointement par le Conseil national de recherches du Canada (CNRC) et l'Université du Rhode Island (URI) aux É.-U. Le programme visait à mettre au point un modèle de fatigue de contact et d'usure des rails de chemin de fer qui, en établissant ou en identifiant les relations entre les variables pertinentes, permettrait d'identifier quelques mesures pratiques pour prolonger la durée utile des rails. Les auteurs du rapport croient que l'objectif du programme de recherche a été atteint sur le plan de la prévention de l'usure et des défauts de surface, comme l'écaillage et l'usure ondulatoire des rails, et sur le plan du contrôle de l'écoulement plastique des matériaux constituant les rails. Une méthode d'entretien des rails consistant en une lubrification à fond et un meulage léger mais fréquent devrait éliminer complètement les dommages de surface des rails résultant de l'usure et de la fatigue de contact. On pourra accroître de façon appréciable la durée utile des rails dans la mesure où on pourra exercer un contrôle sur la production des défauts de fatigue ("Sperry"). L'analyse des défauts de fatigue n'est pas incluse dans notre modèle.

La première section du rapport décrit les aspects fondamentaux de la mécanique de contact roue-rail ayant trait aux contraintes de contact, au micropatinage et forces de traction associées, et à l'écoulement plastique des aciers pour rails. Elle décrit le phénomène de matraquage, un mouvement de va-et-vient de la zone de contact entre le centre du rail et son côté. La fréquence relative du contact en un point précis du rail joue un rôle critique dans l'interprétation des données de fatigue de contact et d'usure obtenues sur le terrain ou en laboratoire. On présente des formules simplifiées de calcul des contraintes de contact de cisaillement et de compression maximales sur le dessus du rail et sur sa face intérieure. On explique l'effet marqué des caractéristiques géométriques du contact sur les contraintes de contact et on montre l'effet de la lubrification sur la distribution des contraintes au-dessous de la surface et en surface. Bien que la lubrification contribue à réduire l'écoulement plastique des rails, la dureté des rails semble avoir un effet plus prononcé.

La section suivante traite des quatre types fondamentaux d'usure: usure d'adhérence prononcée, usure d'adhérence modérée, usure par oxydation et usure abrasive. Elle donne les taux d'usure quantitatifs obtenus dans les essais de laboratoire portant sur un certain nombre d'aciers pour rails commerciaux et d'aciers au stade de la mise au point. On a trouvé une corrélation satisfaisante entre les résultats de nos essais en laboratoire et les taux d'usure contrôlés sur le terrain. Les essais de laboratoire ont montré que l'accroissement de la dureté des rails au-delà d'un nombre de Brinell de 360 à 380 ne permettait pas de réduire davantage l'usure d'adhérence, mais que la réduction de la teneur en soufre permet une certaine amélioration. La lubrification limite l'usure de la face intérieure des rails de façon très efficace, mais elle réduit le taux d'usure du dessus des rails à un niveau tel qu'il s'y forme des fissures de fatigue de contact.

La section de la lubrification débute par un examen rapide de la théorie de la lubrification, suivi d'une description de la composition et des critères souhaitables de sélection des lubrifiants pour rails. On a effectué, sur plusieurs lots expérimentaux de lubrifiants pour rails, des essais de performance comparatifs d'additifs d'extrême pression (E.P.) chimiques et mécaniques. Ces essais ont montré que le lubrifiant le plus efficace contenait un ou au plus deux additifs E.P. Étant donné que le taux de distribution du lubrifiant devrait être égal à son taux de consommation à l'interface roue-rail, on a effectué une série d'essais de capacité de rétention en laboratoire. Ces essais ont montré que le taux d'épuisement du lubrifiant croît avec la charge aux essieux et la courbure.

À la section de la fatigue de contact, on commence par rappeler au lecteur que la charge a un effet négatif marqué sur la fatigue de contact et que l'effet négatif des interfaces roue-rail non conformes est désastreux. On examine la théorie de la propagation des fissures de fatigue de contact et on mentionne l'effet de la lubrification, qui accélère la propagation des fissures. On décrit ensuite un mécanisme de production de fissures de surface, par instabilité plastique. À l'aide d'un échantillon d'essai de conception spéciale soumis à des contraintes cycliques de cisaillement et de compression biaxiales, on a établi les relations que caractérisent l'instabilité plastique d'un acier commercial pour rails. On a trouvé que, dans le cas de l'instabilité plastique, la lubrification réduit la production de fissures, ce qui, mis en relation avec les taux d'usure, a permis d'estimer l'intervalle de meulage.

Dans la dernière section, on présente des arguments en faveur d'un meulage léger mais fréquent, qu'on appelle meulage préventif. Ce type de meulage est le plus efficace lorsqu'il est effectué sur des rails lubrifiés adéquatement. Au lieu d'effectuer un meulage prononcé pour corriger les défauts de surface, par exemple les surfaces ondulées, les dépressions dans les zones de soudure ou la déformation du profil des rails résultant de l'écoulement plastique cumulatif, on effectue un meulage préventif qui empêche tout simplement la formation de ces défauts. On décrit et on analyse les critères de meulage, la profondeur, la période et les modes de meulage souhaitables.

Les auteurs croient que la combinaison de la lubrification à fond et du meulage préventif constituera pour l'industrie ferroviaire une méthode permettant d'accroître de façon appréciable la durée utile des rails dans les courbes et les voies en alignement. Elle permettra aussi de résoudre entièrement le problème de l'usure ondulatoire des rails et de réaliser un programme de meulage des rails.

CONTENTS

		Page
	REPORT DOCUMENTATION PAGE (TDC)	(iii)
	FORMULE DE DOCUMENT POUR RAPPORT (TDC)	(iv)
	ACKNOWLEDGEMENT	(v)
	ABSTRACT	(vi)
	SOMMAIRE	(viii)
1.0	INTRODUCTION	1
2.0	CONTACT MECHANICS	2
2.1	Frequency of Contact	3
2.2	Contact Stress	4
2.3	Microslip and Tractions	6
2.4	Plastic Flow	8
3.0	WEAR	11
3.1	Dry Wear	11
3.1.1	Severe adhesive (gouging) wear	11
3.1.2	Mild adhesive (oxidative) wear	11
3.2	Lubricated Wear	11
3.2.1	Surface fatigue wear (delamination)	11
3.2.2	Abrasive wear	12
3.3	Rail/Wheel Wear Apparatus	12
3.4	Test Procedures	13
3.5	Test Results	15
3.5.1	Wear rates of commercial steels	15
3.5.2	Correlation of laboratory tests to field conditions	17
3.5.3	Wear rates of developmental rail steels	18
3.5.4	Effect of sulphur content on adhesive wear	19
4.0	LUBRICATION	20
4.1	General Aspects of Lubrication	20
4.2	Effect of Lubrication on Traction Forces	21
4.3	Lubricants	22
4.4	Retentiveness	24

CONTENTS (Cont'd)

		Page
5.0	CONTACT FATIGUE	26
	5.1 Crack Propagation	26
	5.2 Crack Initiation	27
	5.3 Effect of Lubrication on Contact Fatigue Crack Initiation and Propagation	29
6.0	RAIL GRINDING	29
	6.1 Corrugations	29
	6.2 Corrective Grinding	31
	6.3 Preventive Grinding	31
	6.3.1 Grinding depth	32
	6.3.2 Grinding period	32
	6.3.3 Grinding profile	33
	6.4 Rail Life	35
7.0	CONCLUSIONS	35
8.0	REFERENCES	38
	DOCUMENTATION PAGE (NRC)	

LIST OF TABLES

Table		Page
1	Variability of p_o/k ratios with location and hardness of the rail.	43
2	Hardness, dry wear rates and chemical composition tested commercial steels.	44
3	Microstructure, hardness and dry wear rates of experimental rail steels.	45
4	Effect of grease composition on wear rates.	46
5	Results from four ball and Timken tests.	47

LIST OF ILLUSTRATIONS

Figure		
1	Severe adhesive (gouging) wear: a) "moonshine" on railway ties b) worn gauge face of high rail.	48
2	Contact fatigue: a) shelly spots on high rail, b) flaking on low rail.	49

CONTENTS (Cont'd)

		Page
3	Relative frequency of contact (pummelling) diagram for high and low rails in 8° curve.	50
4	Change in the geometry of contact between rail's top and gauge face contact zones as function of angle-of-attack.	51
5	Distribution of contact stress with respect to depth at x=y=0.	52
6	Definitions of creep components.	53
7	Friction streaks observed on worn high rail located in 8° curve.	54
8	Distribution of slip vectors within the flange contact.	55
9	Plastic flow observed on the crossection of high rail removed from 8° curve.	56
10	Effect of traction on elastic and shakedown limits.	57
11	Shear stress τ_{yz} in the plane perpendicular to the direction of travel for a) dry contact, b) grease-sand lubricated contact.	58
12	Wear particles: a) cross section of severe adhesive wear particle, b) oxidative wear particles.	59
13	a) Rail's top surface abraded by crushed sand particles, b) cross section of delamination wear particles generated by surface fatigue wear.	60
14	Schematics of rail/wheel wear test apparatus.	61
15	Dimensions of rail and wheel discs used in wear apparatus.	62
16	Wear rates observed on commercial rail steels with: a) no lubrication, b) lubricated by grease - 20% sand mixture, c) lubricated by grease.	63
17	New and worn profiles of low and high rail discs: a) Steel A - standard carbon b) Steel G - new head hardened.	64
18	a) Plastic flow of metal into the gauge face area, where it is worn away; b) narrowing of gauge caused by plastic flow.	65

CONTENTS (Cont'd)

		Page
19	Correlation of gauge face wear rates on the same rail steels tested at Facility for Accelerated Service Testing (FAST) and rail/wheel wear apparatus.	66
20	Effect of lubrication breakdowns on the average gauge face wear rates.	67
21	Wear rates converted to surface recess of material.	68
22	Wear rates observed on experimental rail steels:	69
23	a) Gauge corner cross section of high rail with microstructure made from nodular iron, b) wear surface microstructure of adhesively worn rail steel.	70
24	Effect of sulphur inclusion density on adhesive wear.	71
25	Schematics of contact in a) partial-Elastohydrodynamic lubrication and b) boundary lubrication.	72
26	Effect of lubrication on L/V ratio of low rail disc.	73
27	Retentivity tests a) $\psi = 20'$ b) $\psi = 40'$.	74
28	Lubrication breakdown as function of load and angle of attack.	75
29	Compressive σ_z and shear τ_{yz} stress distribution at the depth a) $z = 0$, b) $z = 0.5a$ and c) $z = 1.5a$.	76
30	Ductile shear fracture of rail material.	77
31	Biaxial specimen with loads applied in the shear and compression directions.	78
32	Number of cycles to crack initiation by plastic instability with respect to maximum shear stress for different values of η.	79
33	Relationship between wear and surface fatigue crack initiation for 8° curve.	80
34	Rail corrugation profiles a) at FAST under dry conditions b) in Canadian Rockies under lubricated conditions.	81
35	Schematics of a) corrective and b) preventive grinding on a) longitudinal and b) transverse sections of the railhead.	82

CONTENTS (Cont'd)

		Page
36	Modified frequency histogram for preventively ground rails on 8° curve.	83
37	Effect of preventive grinding on wear rates in lubricated 8° curve.	84
38	"Flat" and "contour" grinding profiles.	85
39	Basic (tangent track) rail grinding pattern for 44 grinding train recommended for territories travelled by wheels with modified Heumann profile.	86
40	Left hand curve rail grinding pattern for 44 stone grinding train recommended for territories travelled by wheels with modified Heumann profile.	87

WEAR AND CONTACT FATIGUE MODEL FOR RAILWAY RAIL

1.0 INTRODUCTION

Rail life is governed either by damage which occurs at the immediate surface layer of the rail head or by fatigue failures which occur deeper in the railhead or at any point within the cross-section of rail.

At the surface level there are two competing damage mechanisms which limit the rail life. One is wear and the other is contact fatigue. In its severe form, wear can remove a substantial volume of steel, specifically at the gauge face of high rails in curves [Fig. 1a,b]. Contact fatigue is characterized by substantial and often rapid cracking of the subsurface layer. It is manifested by head checks, spalls or shelly spots found at the gauge corner of the high rail [Fig. 2a] or flaking [Fig. 2b] observed on the low rail in curves or occasionally in a tangent track. The rail with headchecks, spalls, flakes or shelly spots most often becomes corrugated.

Any inadequately maintained rail may develop fatigue defects such as "tache oval", detail fracture, pull-apart and others. When the frequency of these defects per track mile reaches a specific limit the entire section of track thus affected is usually, for safety reasons, relayed with new rail. Since the mechanism of formation of what is termed "Sperry" defects is different from that of contact fatigue, the analysis of the former is not included in our study.

Wear and contact fatigue are affected by a large number of variables. The specific values of these variables are given by operating conditions. The variables may be divided, in general, into three groups: mechanical, metallurgical and rheological (lubrication). In the last two decades, the mechanical and metallurgical variables affecting wear have received considerable attention. The effect of load and creepage (1 - 3), hardness and interlamellar spacing (4, 5), sulphur content (6) and humidity (7) on dry wear rates have been well researched and quantified.

When wear in curves changes from mild to severe [Fig. 1a,b] lubrication is delivered to the rail/wheel flange interface by either track-mounted or vehicle-born lubricators. The wear is then reduced not only at gauge face but also on top running surfaces. Numerous railway engineers noted that lubrication of track reduces rolling resistance and thereby saves fuel. Presently the lubrication of railway track is becoming commonplace even in straight track, not to prevent wear but to improve the economy of railway operation by reducing fuel consumption on locomotives.

Lubrication of bearings and gears leads to a complete separation of their moving components due to the formation of elastohydrodynamic (EHD) film. The occurrence of such film in rail/wheel contact is very unlikely. Under extreme conditions a partial-EHL regime may develop but for the most part, the rail,

when lubricated, is subject to boundary lubrication. The lubricant contamination of rail running surfaces results in insufficient adhesion for the locomotive wheels and sand is supplied to bring the adhesion to a manageable level. Ultimately the rails are lubricated with a mixture of lubricant and finely pulverized sand. (No machinery other than the rail/wheel interface is subject to boundary lubrication by grease-sand mixtures.) Prolonged lubrication of rail reduces wear and leads to the development of contact fatigue.

Two different forms of contact fatigue-related damage have been observed in railway rail: squats and shelly spots. High speed, light axle load traffic, typical of some British and Japanese railway lines, leads to the development of "squat" or "black spot." The description and analysis of squats can be found in References 8 and 9. However, squats have not, to the author's knowledge, been observed in North America. Both squats and shelly spots occur due to lower rate of wear, which can be attributed to light axle loads in the case of squats, and boundary lubrication in the case of shelly spots. This report will limit its analysis to contact fatigue defects of the shelly spot and flake variety [Fig. 2ab].

The first portion of this report reviews the fundamentals of rail/wheel interaction and contact mechanics.

2.0 CONTACT MECHANICS

The amount of wear or contact fatigue damage is not uniformly distributed across the rail head's running band. Although the running band on the top surface is typically 63.5mm (2.5") wide, the typical dimension of a contact circle or ellipse between the rail and the wheel of a loaded 100t capacity car, if a circle, does not exceed 16mm (5/8"). Hence four such circles or ellipses, assuming that some are elongated in the direction of travel and some perpendicular to it, can be fitted side by side across the running band of both right and left rails.

Furthermore, the dynamic instability of freight car trucks, known as hunting, or the severe mismatch of the rolling radii on wheels of the same wheelset may result in a flange contact in tangent track. These are rather isolated phenomena and do not cause significant wear or damage to the rail. On the other hand, flange contact in curves, due to angular misalignment of wheelset referred to as yaw angle or angle-of-attack, is frequent enough and causes undesirable gauge side wear (sidecutting) in curves. The contact area between wheel flange and gauge side of the rail is, in most instances, a thin ellipse elongated in the direction of travel (10). The width of the gauge side wear band could be 6.35 to 19.05mm (1/4 - 3/4") wide and about two to five such ellipses could be fitted into this band.

To better understand the reason that wear and contact fatigue damage is not uniformly distributed across the rail surface, let us assume a simple model in which the top running surface band is divided into four equally spaced segments A, B, C and D while the gauge contact is considered as one segment E [Fig. 3]. Assume a cube of a unit volume material is placed beneath the center of each segment and subjected to a load equal to the average load acting on the corresponding segment.

The wear or fatigue damage of each material element (A to E) is significantly affected by:

(i) Total number of loading cycles, which depends on the frequency of contact

(ii) Contact stresses

(iii) Amount of microslip and friction forces (tractions)

(iv) Rate of plastic flow

Each of these parameters and its influence on the model described above will now be discussed.

2.1 Frequency of Contact

Although there exists a number of theoretical models of dynamic or quasistatic nature, known as hunting or curve steering models, one would have to examine numerically the interaction between at least several hundred wheelsets with random wheel tread geometry and loading distribution to obtain a realistic single frequency of contact distribution for a particular section of track. To our knowledge, no result of any such study is available and thus we are limited to a qualitative approximation of the contact frequency.

Presumably, the frequency of contact distribution may change as a function of rail wear or the level of maintenance applied to rolling stock and other operational variables. In order to derive a reasonable frequency diagram for a sharp curve, where both wear and contact fatigue become most severe, let us consider field measurements of angle of attack and lateral forces. Most North American freight cars are equipped with a three piece truck; the leading wheelsets of these trucks show high positive angle of attack and high L/V forces while, for the trailing wheelsets, the values of both angles of attack and L/V forces are spread around zero or moderately negative values. Thus, in sharp curves most leading wheelsets are displaced towards the gauge side of high rail. Many of these will come to hard flange contact with the rail. Hard flanging is synonymous with a two-point contact between a single wheel and a high rail, one at a gauge side and the other on the top of the rail, or a three point contact between a wheelset and a pair of rails. Most of the trailing wheelsets, on the other hand, contact the rails on their top running surfaces, with some of the wheelsets having a negative angle-of-attack, and are displaced towards the low rail. Therefore, the area of contact on the rails passed by a sequence of leading and trailing wheelsets will intermittently move from the gauge corner towards the center, or field side of high rail and from field side towards the center, or gauge corner of low rail - a phemonemon we will refer to as "pummelling".

Most leading wheelsets would contact the naturally worn (unground) rails in a curve at location A while the majority of trailing ones would contact the rail at locations B, C, D [Fig. 3]. We assume that a frequency of contact distribution, shown in Fig. 3, is reasonably typical of field conditions.

2.2 Contact Stress

For any given load, geometry of contact and elastic properties of material, the size and shape of contact area and the distribution of contact stresses beneath it can be established using the Hertz theory. As mentioned previously, the contact areas on top running surfaces (locations A to D in Figure 3) are mildly elliptical with major axis aligned either in the direction of travel or perpendicularly to it. On the other hand, the gauge face contact area (location E) is a long thin ellipse. Figure 4 shows an example of the two types of ellipses - the near circular one located at "B", and the elongated one at "E". The imprints of the contact ellipses shown in Figure 4 were obtained using an aluminum foil inserted into a 1/10 scale model of wheel/rail interface and pressed together. For details see Reference 10.

Thus we will not commit too great an error if we replace ellipses at the locations A-D with a circular contact area and those at E with line contact. We can then use the following formulas (11):

	Line contact (flange)	Circular contact (top running surface)	
Semi contact width or contact radius:	$b = 2\left[\frac{P'R}{\pi E^*}\right]^{1/2}$	$a = \left[\frac{3}{4}\frac{PR}{E^*}\right]^{1/3}$	(1)
Maximum contact pressure:	$p_o = \frac{2P'}{\pi b} = \left[\frac{P'E^*}{\pi R}\right]^{1/2}$	$p_o = \frac{1}{\pi}\left[\frac{6PE^{*2}}{R^2}\right]^{1/3}$	(2)
Maximum shear stress:	$\tau_{max} = 0.3\ p_o$ at $(x = 0,\ z = 0.73b)$	$\tau_{max} = 0.31\ p_o$ at $(r = 0,\ z = 0.48a)$	(3)

where:

b	semi-contact width (line contact)	
a	radius of contact circle (point contact)	
p_o	maximum contact pressure	
τ_{max}	maximum shear stress	
$(E^*)^{-1}$	contact modulus	$\frac{1}{E^*} = \frac{1 - \nu_1^2}{E_1} + \frac{1 - \nu_2^2}{E_2}$
E_1, E_2	Young's moduli of wheel and rail	
ν_1, ν_2	Poisson's ratios	
$(R)^{-1}$	effective curvature	$\frac{1}{R} = \frac{1}{R_1} + \frac{1}{R_2}$

R_1, R_2 wheel and rail head radii (assuming a conical tread wheel). For flange line contact take R_2 to be the gauge corner of rail or flange tip radius ($R_1 = \infty$). Assume the length of flange contact $\ell = 6a$, as calculated at locations A,B,C or D.

p' load/unit length $\qquad p' = \frac{P_F}{\ell} \approx \frac{\mu W}{\ell}$

W wheelset load

P_F flange load

μ coefficient of adhesion

From the knowledge of the Hertz stress value, p_o one can describe the entire contact stress field. The surface pressure distribution is a circle, i.e. $p = p_o [(1-x^2/a^2)]^{0.5}$, in the case of line contact.

The variation of three principal stresses with depth for a circular contact at $r = 0$ is shown in Figure 5 (12). For pure rolling, the shear stress at the surface is zero and reaches its maximum value at the depth equal to a quarter the size of the contact area. However, in rolling-sliding contacts with tractions, the τ_{max} gradually moves closer to the surface and, at approximately $\mu = 0.3$, τ_{max} is located at the surface. The exact solution in a closed form for all stress components at any point beneath or in the proximity of circular contact area with or without tractions, is given by Hamilton (13).

It is apparent from the given formulas for circular contact that the Hertz stress is more sensitive to changes in geometry than load. Thus the contact between the flange and gauge corner of high rail or between the false flange and field side of low rail will yield, for the same load, higher contact stress values than at the center of the rail. For the centrally located wheelset loaded by 30 tonnes (66,000 lbs) Johns and his co-workers (14) calculated $p_o = 1500$ MPa (218,000 psi) for new rail/wheel profiles and $p_o = 830$ MPa (120,000 psi) for a worn wheel/rail profile. However, when the wheelset with worn profiles was offset toward either side by 1 to 2.5 cm (.4" to 1") the same load yielded p_o in the range 1500 to 3000 MPa (218,000 to 436,000 psi).

As the wear on the rails and wheels progresses, each location on the rail surface experiences a wide range of contact stress values. It is beyond the scope of this report to give the frequency distribution (or even the average value) of contact stresses because these change with track location, traffic patterns, maintenance policies and many other variables. However for the purposes of further analysis, we choose the values of 1150 MPa (≈ 170,000 psi), 1800 MPa (≈ 260,000 psi) and 2500 MPa (≈ 360,000 psi) to be average values at locations B and C, D and A, respectively. These stress values may be considered typical of 8° curves subject to heavy haul traffic.

2.3 Microslip and Tractions

Most wheelsets are subject to a combination of rolling and sliding. Pure rolling would occur if a wheelset with cylindrical treads, neither driven nor braked, was to roll in a straight line over perfectly aligned track. Realistically, however, rolling of a wheel over the rail is not ideal and an appreciable amount of sliding can develop due to the conicity of wheel profiles, rail cant, unequal wear on wheels belonging to the same wheelset, track irregularities and curvature. The non-dimensional measure of the amount of sliding, or more accurately that of microslip, is termed creepage. Creepage has three components, longitudinal, lateral and spin, and although one of the components may be predominant, the others are always present.

The nature of each creepage component, using the example of a disc rolling on a cylinder, is depicted in Figure 6. When the peripheral speeds of the disc and cylinder are in the same direction but of different magnitudes, which may be the case if one of the rolling bodies is driven or braked, the creepage is termed longitudinal. The slip between the asperities of respective surfaces and the resulting friction force T_x are also in the longitudinal direction [Fig. 6a]. The yaw misalignment between the disc and cylinder, but otherwise rotating at the same peripheral speed, gives rise to lateral creepage. The disc and cylinder "rub" each other in a direction perpendicular to the rolling direction. The resulting traction force T_y is also perpendicular to rolling [Fig. 6b]. Finally, when the disc is tilted with respect to the cylinder, the asperities rub each other in a circular motion, although the center of this circular motion is located away from the contact area. The circular rubbing generates spin moment M. The traction forces T_x and T_y and moment M increase at first linearly with creepage. For the dry surfaces the rate of this increase is given by Kalker's coefficients f_{11}, f_{12}, f_{23} and f_{33} (15). If spin and lateral creepage are simultaneously present, the coefficient f_{23} accounts for the spin moment produced by lateral creepage and vise versa as indicated by the following equations.

$$\begin{aligned} T_x &= f_{11}\gamma_1 \\ T_y &= f_{22}\gamma_2 + f_{23}\omega_3 \\ M &= f_{23}\gamma_2 + f_{33}\omega_3 \end{aligned} \qquad (4)$$

Once the tractions T_x, T_y and M reach the adhesion limit, a condition of saturation, their value becomes independent of creepage and equal to the product of coefficient of friction and normal load.

In the case of a yawed and offset freight car wheelset which is not braked, the longitudinal creepage is given by the rolling radii difference between right and left wheels. The lateral and spin creepages are given by the amount of yaw and effective conicity respectively. A number of formulae, taking into account different influencing factors, were developed to calculate creepages. These

can be found in several References (16 - 19). As an example two types of formulae are shown below:

(after reference 16)

$$\gamma_1 = \frac{\Omega R \cos\delta \cos\psi - V}{V}$$

$$\gamma_2 = \sec\delta \sin\psi$$

$$\omega_3 = \frac{tg\delta}{R}$$

(after reference 19, right wheel only)

$$\gamma_1 = \frac{1}{V}\left[V\left(1 - \frac{r}{r_o}\right) + a\dot{\psi}\right] \quad (5)$$

$$\gamma_2 = \frac{1}{V}\left[\dot{y} + r\phi - V\psi\right]\cos(\delta - \phi) \quad (6)$$

$$- \frac{1}{V}\left(\dot{z} - a\dot{\phi}\right)\sin(\delta - \phi)$$

$$\omega_3 = \frac{1}{V}\left[\dot{\psi}\cos(\delta - \phi) + \Omega \sin\delta\right] \quad (7)$$

Where

a	- half of wheelset contact distance
V	- wheelset forward velocity
R	- curve radius
r_0	- centered wheel radius
r	- wheel contact radius
y, z	- lateral and vertical coordinates
γ_1, γ_2	- longitudinal and lateral creepages
ω_3	- spin creepage
Ω	- wheelset rotational velocity
ϕ .	- roll angle
ψ, $\dot{\psi}$	- wheelset yaw angle and angular-velocity
δ	- conicity of contact (contact angle)

Once the creepages at right and left contact points are established, Kalker's computer algorithms DUVOROL and CONTACT (20) are used by many researchers to calculate traction forces within the sloping portion of traction-creepage curves. These computer programs are also used to calculate the distribution of microslip vectors within the rail wheel interface, an example of which is shown in Reference 3. The microslip, however, can also be directly observed on the rail or wheel surfaces.

When hard wheel asperities rub against the rail surface, they leave marks in the form of streaks. Figure 7 shows streaks observed at different locations on the surface of a worn high rail of 8° curve. At location D, the orientation of the streaks appear to be random. As pointed out previously, relatively few wheelsets contact the rail at this location and those which do, do not exhibit any consistent pattern of misalignment. On the other hand, all the wheelsets contacting locations C to A exhibit a strong lateral creepage component. The wheels rub the high rail towards the gauge corner and the rubbing is

most severe at location A. As the rail/wheel contact point moves from location C to A, the length of rubbing marks increases in direct proportion to the wheelset's angle of attack. The curving of the streaks at location A is due to spin component. Overall, it is the lateral component of creepage which dominates in sharp curve. The length of slip vectors observed at locations A,B,C and D ranges from 20 to 200μm.

As the locations A to D could be subject to a combination of rolling and sliding, hard flange-gauge face contact (location E) experiences sliding only. Under this contact condition three different types of streak marks can be observed, as shown in Figure 8. In each case, the length of streaks is substantially longer than those observed at locations A - D. The typical length of a slip mark observed at E is 2.5mm. The direction of slip vectors and that of friction force are governed by the relative position of the top surface and flange contact areas and the relative tilt of flange and gauge face. The magnitude of flange force is a product of flange load and a coefficient of friction.

Based on the above analysis we conclude that the rail's top running bands (both high and low rail), in sharp curve, are subject to a combination of rolling and sliding while the gauge side of high rail is subject to sliding only. This is a governing factor in estimating the plastic flow behaviour for each case.

2.4 Plastic Flow

In the presence of high contact stress the rail material undergoes plastic deformation whose rate is not uniform across the rail head profile. Figure 9 shows the lateral component of plastic flow on a worn high rail with hardness of 325 VNH - the same rail for which the surface streaks are shown in Figure 8. The plastic flow is most severe at the gauge corner, location A, where the contact stress and slip are largest. At locations B and C less plastic flow takes place. Most of the high rail surface layer flows towards the gauge side. However, at the field side the flow is in the opposite direction and the point at which the reversal takes place is called the inflection point. At this point, although the material is work-hardened, little or no plastic flow occurs.

A similar plastic flow pattern could be observed on the low rail. Most of the surface layer flows towards the field side and the flow is most severe at location A. In fact, for both high and low rail the dominant direction of lateral component of plastic flow is towards the center of the curve. The inflection point in both cases is located in the vicinity of the boundary between segments C & D but moves further away from the center of the curve with increasing curvature.

To explain the fundamental principles governing the plastic flow, we will use the two-dimensional shakedown theory developed by Johnson and his co-workers (21). (A three dimensional theory concerned with lateral plastic flow in the rail head is currently under development.)

The two-dimensional analysis considers a rigid cylinder, with or without longitudinal creepage, in contact with an elastic-perfectly plastic Von Misses material. The resistance of material to plastic flow is evaluated in terms of p_o/k, where k may be interpreted as either the yield stress in simple shear of Y/3, where Y is yield stress in uniaxial tension. In terms of hardness, $k = 1/6VHN$, where VHN is Vickers hardness number in units of kg/mm^2. Depending on the magnitude of contact stress p_o the material is subjected to three characteristic deformation regimes which for the case of zero creepage are:

$p_o/k < 3.1$	- elastic deformation	
$3.1 < p_o/k < 4.0$	- shakedown	(8)
$p_o/k > 4.0$	- continuing incremental plastic deformation	

In the first regime, the deformation is elastic and no plastic flow takes place. Once the elastic limit is exceeded, the initial plastic deformation introduces the residual stress which makes further plastic flow unlikely. This process takes place during the first few loading cycles and is known as shakedown. The maximum stress for which it occurs is called shakedown limit. In each loading cycle, during which the stress exceeds the shakedown limit, the subsurface layer of material will flow by a rather small but finite increment.

The elastic and shakedown limits decrease with an increasing ratio of tractive force to normal load (T/N) as shown in Figure 10. This decrease can be attributed to the maximum value of shear stress τ_{max}, which increases with the increasing T/N. Tractions also bring the τ_{max} closer to the surface, at first gradually and then more rapidly and at T/N = 0.3 it reaches the surface. Assuming the average value of T/N for a wheelset with saturated lateral creepage in unlubricated territory is = 0.30 and in lubricated territory 0.18, the dry rail will experience maximum shear stress at the surface but the lubricated rail will experience it below the surface. The shear stress patterns for the above two cases and various depths are shown in Figure 11.

Next, let us examine the average p_o/k ratios at locations A to D for plain carbon and head-hardened rails. These are shown in Table 1.

For the material to flow, the shakedown limit must be exceeded. Since the shakedown limit for a three-dimensional stress field subject to lateral tractions is not available to us, let us use as a guide only, the one shown in Figure 10. For dry and lubricated track the shakedown limits are at $p_o/k = 2.6$ and 3.2, respectively. But at location B & C the ratio of average contact stress with respect to k is, for the plain carbon rail, also 2.6. Thus, the dry plain carbon rail will incrementally flow during half of the total loading cycles. At location A, every single wheelset will produce incremental plastic flow because the shakedown limit at $p_o/k = 2.6$, is much lower than the $(p_o/k)_{av} = 5.6$ and is caused by actual wheel loading.

Lubrication raises the shakedown limit to $p_o/k = 3.2$ and reduces the plastic flow regardless of the type of rail used. However, as shown in Table 2, a stronger effect in plastic flow reduction can be achieved by increasing the hardness of the rail. Thus the hardest of premium rails (super rails), with an average railhead hardness of 380 BHN, will experience increments of plastic flow at the locations B, C, & D only during loading cycles with above or well above average contact stresses. Yet, more than half of the wheelsets contacting hard rails at A will contribute to the plastic flow.

The gauge face (location E) of dry, plain carbon rail typically exhibits less plastic flow than the locations B & C. Only a few of the wheelsets contacting high rail at location E exceed the shakedown limit and, as pointed out previously, the maximum shear stress in dry contacts is located at the surface. For lubricated gauge face contact, although the shear stress is located beneath the surface, the $(p_o/k)_{av}$ is sufficiently low to result in any appreciable plastic flow. Although the premium rails, based on the arguments presented in this section, should not flow at all at location E, the metallographical observation of immediate surface layer will always show some plastic deformation. This deformation is caused by asperity-asperity contact, some aspects of which are covered in later sections of this report.

In summary, plastic flow is reduced by increasing the hardness of the rail and by decreasing the adhesion limit between wheel and rail.

3.0 WEAR

No other branch of railway engineering uses terminology as confusing as the one dealing with wear. Adhesive, delamination, smearing, abrasive, tribo-oxidative, type I, II and III, flow fatigue, corrosive, surface fatigue, flaking, severe and mild adhesive and perhaps several other adjectives are used to describe the rail/wheel wear phenomenon. Although some of the above terms are synonymous, several different wear mechanisms can indeed take place. These mechanisms are given by a specific mechanical and lubrication condition. Four generally recognized wear mechanisms take place at the surfaces of heavy haul rail and are termed in this report as: mild adhesive, severe adhesive, surface fatigue and abrasive wear. The first two types occur in an unlubricated (dry) environment and the other two in a lubricated environment.

3.1 Dry Wear

3.1.1 Severe adhesive (gouging) wear

This wear occurs in the dry flange/gauge side interface [Figure 3 location E]. It generates a lot of wear debris which is highly visible on railway tracks [Fig. 1a]. Its appearance inspired other descriptions, such as, gouging, snowflaking, moonshine or dandruff - to name a few. The actual wear mechanism is due to localized welding of wheel and rail asperities which form junctions. Subsequent separation of the surfaces breaks off these junctions producing large wear particles up to 0.5 mm thick and 3 mm across [Fig. 12a]. This mechanism yields high wear rates and produces rough gauge side and flange surfaces.

3.1.2 Mild adhesive (oxidative) wear

This primarily occurs on top surfaces of dry rail [Fig. 3 locations A - D]. The wear rates can change in a wide range, depending on Hertz pressure and amount of slip. The wear debris associated with this mode varies accordingly in size, about 3 to 50 μm in thickness and 10 to 500 μm in length. The particles contain a heavily deformed and oxidized mixture of rail and wheel material containing numerous microcracks. Similar but less numerous cracks can be observed in the immediate surface layer of rail and wheel materials [Fig. 12b] suggesting that the generating mechanism of such particles is of a cyclic nature. In addition, these particles may sequentially adhere to the wheel and rail surfaces several times before they are released from the system.

3.2 Lubricated wear

3.2.1 Surface fatigue wear (delamination)

This form ocurs in all lubricated or lubricant contaminated contacts [Fig. 3, locations A - E]. Surface fatigue wear must not be confused with contact fatigue. Although both processes imply some kind of fatigue mechanisms, surface fatigue wear occurs at a very shallow depth, not exceeding 0.05 mm (0.002"). Contact fatigue cracks, on the other hand, could reach a depth of about 5 mm (0.2"). In surface fatigue wear the asperity-asperity contacts are always separated by a film of lubricant. As a consequence no material is removed from the tips of these rather shallow asperities.

With the increasing number of contact events, microcracks form parallel to the surface due to the presence of manganese sulphide inclusions or to plastic instability of the material (to be discussed in detail in Section 5.2). Thousands of asperity to asperity contacts may occur and form such cracks, and the particle thus formed does not delaminate immediately. It is removed after an appreciable but undetermined number of loading cycles. For this reason, the delamination wear rates are very low.

3.2.2 Abrasive wear

This mechanism occurs in lubricated track when sand is discharged by locomotives to improve adhesion. Two variations of this mechanism occur. The sand's quartz grains are crushed by wheels into microscopic particles which are imbedded in the rail and/or wheel and abrade the other surface. Also, the sand particles, when mixed with a lubricant or its residues, form a paste which abrades both rail and wheel in a process identical to that of polishing by using a polishing paste. In most instances, both abrasive mechanisms are present. Wear rates, however, are extremely low because of short sliding distances generated by creepage and the small grain size (< 2 μm) of sand particles. Because of these very low wear rates, this form of abrasive wear is conducive to the development of surface fatigue wear. Thus in lubricated and sanded environments surface fatigue and abrasive wear mechanisms occur simultaneously and any wear rate measured represents a sum of abrasive and surface fatigue wear rates. The characteristic appearance of abraded surface and associated delamination particles are shown in Figures 13a,b.

We have studied the above wear mechanisms in the laboratory using an apparatus which is described in Section 3.3.

3.3 Rail/Wheel Wear Apparatus

The apparatus was designed to simulate, on a reduced scale, the interaction between a railway wheelset and a pair of rails. As shown in Figure 14, the top wheel discs are rigidly connected and represent a "wheelset." The bottom discs, simultaneously driven by a 14.7 kW (20 HP) variable speed reversible motor represent rails. The cross-sectional profiles of wheel or rail discs are machined on a numerically controlled lathe and can be made to fit any kind of rail or wheel profile used by the railroads. The profiles are, however, scaled down by a factor of ten. The dimensions of the specimens permit them to be produced from rail heads and wheel tires, as shown in Figure 15. With the exception of residual stress patterns, the original metallurgical properties of the as-produced wheels or rails are preserved.

The apparatus can simulate tangent track running or curving. Curve negotiation is simulated by yawing the wheelset axis with respect to rail axis. This is achieved by rotation of the flexure pivots assembly about the vertical axis located at the center of the wheelset. The lateral and vertical softness of these flexure pivots enable the

wheelset to move laterally into a flange contact or to move downward to compensate for wear and plastic flow.

The wheelset is loaded by a gravitational lever system provided with another set of flexure pivots and a thrust bearing to minimize the effect of applied load on the measurement of lateral and spin components of rail wheel disc tractive forces. This ensures that the occurrence of flange contact is the function of yaw misalignment, geometry of rail and wheel disc profiles and lubrication, but independent of the wheelset loading system. The orthogonal components of a load vector transmitted between right and left sets of rail/wheel discs are measured by loadcells as shown in Figure 14.

Several additional subsystems are attached to the apparatus to complete the simulation of operational field conditions. These include yaw (angle-of-attack) drive, brakes, water and grease dispenser and a fixture to grind the rail discs. The repeatability of test procedures is insured by a microprocessor which, following a pre-programmed sequence, operates all the functions of the test apparatus. The microprocessor is also used to periodically record the revolution counts distribution of rail/wheel forces and the history of longitudinal and lateral creepages during the test. A combined mechanical and electronic instrument, capable of tracing any shape with an accuracy of $\pm 2\,\mu m$, is used periodically to record the evolving wear and plastic flow induced profile changes of tested wheel and rail discs.

3.4 Test Procedures

The above described features of the test apparatus allow a wide variety of test procedures to be developed. Since the effect of load, hardness and longitudinal creepage on wear have been established previously (1 - 5), we decided to subject our specimens to conditions as complex and severe as might be found in the field. In one of the several tests we developed, the rail discs are subjected to an equivalent of 51 million gross tonnes (60 MGT in U.S. customary units) of traffic experienced by rails laid in a 235m radius (8°) curve, located in a single main line track which is subjected to intermittently changing lubrication and experiences heavy axle load in both directions.

The test, designated as "full sequence", consists of sixty periods during which both inner (low) and outer (high) rail discs experience 40,000 loading cycles (revolutions). The wheelset load throughout the entire sequence was 7,000 N. It produced p_o = 1,800MPa between the inner and outer rail wheel disc in the case of a centrally located wheelset, and p_o = 2500MPa between the outer pair of rail/wheel discs for a laterally displaced wheelset.

Within each period the yaw angle was alternated each 2,500 revolutions between 10', 18', 36', and 40' of arc. These values represent the mean yaw angles typical of the four wheelsets of a freight car negotiating a 235m radius (8°) curve (22). This subjected the discs to some degree of pummelling. However, the spread of pummelling,

or more accurately, the standard deviation of the position of contact area and contact stress distribution curves is appreciably larger in the field than in the laboratory. This is because the rail in the field is in contact with a different wheelset each loading cycle but the "rail disc" is in contact with the same "wheelset" throughout the whole test. The dual direction of traffic was simulated on the wear apparatus by reversing the direction of disc rotation each 20,000 revolutions. At the same time, the setting of yaw angles changed from a positive to a negative value to maintain the same orientation of curvature.

In territories with lubricated railway track there are periods of dry wear which may occur intentionally, for example, by shutting off the lubricators to allow the inspection of the rails by the Sperry rail defect detection car, or unintentionally in most cases due to inadequate maintenance of lubricators. This intermittent occurrence of dry wear in curves was simulated on the rail wheel apparatus in the following manner:

Step 1: The first period of 40,000 revolutions was run dry at an ambient temperature of 19°C and relative humidity of 45%. The disc surfaces were cooled by blowing air. This air stream also transported the loose wear particles from the wearing surface to the nearby magnets.

Step 2: The next nineteen periods (760,000 revs.) were lubricated by a calcium soap-based grease mixed with 20% quartz sand. The grease contained a mineral oil with a viscosity of 19.8cSt (at 40°C), and the following EP additives: 11% graphite and 2.5% molybdenum disulphide. The sand, regardless of its initial grain size, was crushed into particles ranging in size from .5 to 2μm. The grease-sand paste which formed in the interface yielded a boundary lubrication regime and a coefficient of adhesion of .18.

Step 3: Same as Step 1.

Step 4: The remaining 39 periods (1.56×10^6 revs.) were lubricated by the same grease used in Step 2, but without any sand. The contamination of grease by wear particles could not be prevented, thus producing a boundary lubrication regime with the limiting coefficient of friction in the range of .09 to .12. The grease only lubrication, though less realistic in terms of field conditions than lubrication by a grease-sand mixture, was used to enhance the rate of contact fatigue damage to rail discs.

During each test the wear was measured after each step by weighing the discs with an accuracy of 0.05%. The disc profiles were taken and wear debris was collected at the same time. Upon the completion of the test, the specimens were subjected to metallographical examination.

3.5 Test Results

The wear research reported in this section can be loosely divided into four groups:

a. evaluation of wear resistance of selected commercial rail steels.

b. application of laboratory tests to field conditions.

c. evaluation of wear resistance of selected experimental rail steels.

d. evaluation of the effect of sulphur content on adhesive wear.

3.5.1 Wear rates of commercial steels

The chemical composition, hardness and dry wear rates of tested rail discs manufacutured from full scale rails are shown in Table 2. All wheel discs were made from AAR Class C wheel steel, having the same chemical composition as plain carbon rail but heat-treated for hardness of BHN 360. Dry, grease-sand and grease-only wear rates are shown in the form of a bar diagram in Figure 16. As indicated by different scales in each of the Figures 16a, b and c, these lubrication regimes produce vastly different wear rates. Compared to dry wear experienced by high rail discs, the grease-sand and grease-only lubrication reduces wear on an average, 20 and 200 times, respectively.

In dry regime, the high rail discs experienced appreciably higher wear rates than low rail discs. The gauge face material was removed by the mechanism of adhesive wear. Out of the four wear mechanisms discussed previously only the severe adhesive one can be distinctly controlled by metallurgical properties — namely, hardness of the steel.

Top surfaces of rail discs, on the other hand, are subject to oxidative wear and the effect of hardness on wear rates is rather weak. The layer of oxidized wear particles which remain on a rail disc surface for an appreciable number of loading cycles contains several different oxides of iron, each of different shear strength. As the humidity affects the formation of a particular type of oxide, the wear rates and adhesion limit are more strongly affected by humidity than the mechanical properties of the steel. Jamison (7) has shown that for plain carbon steel, decreasing the relative humidity from 50 to 25% increases the oxidative wear rates by a factor of 10. Our measurements, during which the humidity was constantly maintained, indicate that the hardness difference between plain carbon and the most recent premium rails affects the oxidative wear by only a factor of 2 (see W_L in Table 2). Thus, the hardness of steel has a strong effect on gouging and a weak one on oxidative wear rates.

The high rail discs wear rates W_H were determined by weighing, and include the sum of gouging and oxidative wear mechanisms. To separate the two might seem, at first, difficult because the top surface of high rail discs, judging from the shape of worn rail profiles shown in Figure 17, appear to wear more on the top than do low rail discs. This difference might be caused either by an increased rate of oxidative wear brought about by increased spin creepage, due to higher conicity of high rail discs, or by the plastic flow which gradually delivers the metal into the gauge face where it is worn away [Fig. 18a]. Although both mechanisms are present, we believe the plastic flow is stronger. Thus, we will not error greatly if we assume that the oxidative wear rates on the top surfaces of both rails are the same. The gauge face adhesive wear rates can then be taken as $W_F = W_H - W_L$.

The commercial steels tested are arranged in Figure 16, with the exception of the last experimental heat, in order of their increasing resistance to adhesive wear. The arrangement might not necessarily be "correct" since the repeatability of wear testing is not absolute. Although we do not repeat every test, the greatest difference in dry wear rates, in the six tests we have repeated, was 25%. Nevertheless, commensurate with customary railway practice, the commercial steels tested could be divided, with respect to their resistance to gauge face wear, into three groups: plain carbon, premium and super-premium. Apart from plain carbon rail, we rate Algoma Cr, and its derivative, Heat Cr-MoI, Russian FHT, Sysco Cr-Cb, and Bethlehem FHT as premium rails; and Nippon NHH, Broken Hill HH, British Steel enhanced Cr, Nippon Cr-HH and experimental heat of Algoma AWC340 as super-premium rails.

As Figure 16 indicates, grease-sand lubrication yields appreciably lower wear rates than the adhesive or oxidative wear mechanisms. As mentioned previously, grease-sand lubrication removes metal by abrasive and surface fatigue wear mechanisms. Thus, in some cases the low rail, in others the high rail discs, exhibit more wear, depending on the random manner by which the sand is distributed throughout the rail wheel disc interfaces. Since high rail disc wear rates represent both gauge face and top surface rates, the amount of material removed from the gauge face is low and does not govern the rail life anymore.

Similar observations can be made about wear rates produced by grease-only lubrication [Fig. 16c]. Since, in absence of sand, no abrasive wear mechanism is present, the bit of material which wears off is removed by the surface fatigue wear. However, the numerical values of wear rates observed in Figure 16c are also affected by a release of large flakes generated by contact fatigue mechanism [see Section 5.0]. Although we do not know how the removal of metal is divided between surface fatigue wear and contact fatigue flakes, we have observed flaking or shelly spots on the discs having wear rates larger than 0.2 μg/cycle. Acknowledging that grease only wear rates do not occur on the top rail surfaces because of sanding, we suggest that these may occur in some instances at the gauge face surface, where the fresh supply of grease

dilutes, if not eliminates, the sand contamination. When the rate of recess of material due to wear is less than the rate of plastic flow, the rail actually "swells" towards the gauge [Fig. 18b] making it narrower. This condition is sometimes referred to as "negative gauge face wear".

3.5.2 Correlation of laboratory tests to field conditions.

The laboratory tests described above demonstrate that lubrication can effectively eliminate the adhesive (gouging) gauge face wear in curves. The gauge face dry and lubricated wear rates obtained in our tests correlate well with the controlled field data as obtained at the Facility for Accelerated Service Testing (FAST). The correlation of adhesive wear is shown in Figure 19 which is reproduced from Reference 23. FAST lubrication tests have also confirmed that the adhesive gauge face wear rates could be reduced by a factor of 100 or better through effective lubrication.

However, tests on revenue lines suggest that lubrication reduces gauge face wear by a factor significantly less than 100, often as little as 5 or 3. Such a discrepancy can be explained by lubrication breakdowns, which can occur both in the laboratory and in the field. If, for example, lubrication breakdown had occurred on a certain length of a lubricated territory and had lasted for one week, at the ratio of dry to lubricated wear of 100:1, the volume of rail steel removed from gauge face during that one week could require a two year period of wear under lubricated conditions. Thus lubrication breakdown can reduce the apparent effectiveness of lubrication to a theoretical ratio of 1:5. This ratio will, however, be lowered further as additional material is removed, due to the conversion from dry to lubricated wear regimes during which the rough surface generated by adhesive wear becomes gradually smooth.

Our laboratory tests, as well as FAST experience, showed that effective lubrication can thoroughly obliterate the metallurgy or hardness effect on abrasive and contact fatigue wear. If, however, the lubrication breakdown occurs, then, because of the presence of dry adhesive wear, the ratio between averaged "dry and lubricated" wear, with respect to the type of the rail tested, is maintained [see Fig. 20].

To demonstrate the dramatic effect of lubrication, even of the grease-sand variety, let us plot the wear rates in the form of material recess with respect to depth. This can be easily done by dividing the rates shown in Figure 16 by specific gravity and top or gauge surface band areas which are, in the case of our discs, 13.2 and 4.3 cm^2, respectively. Let us also use the rates obtained with Algoma Cr, since this rail steel was used in the surface fatigue crack studies described later on. Setting the oxidative wear rate $(\Delta_T)_{dry}$ to a slope of 1, then the slopes of adhesive gauge face wear $(\Delta_G)_{dry}$ and the grease-sand lubricated wear at gauge face $(\Delta_G)_{lub}$ and top $(\Delta_T)_{lub}$ are 18:1, 1:4.3 and 1:6.5, respectively. The lines so generated are shown in Figure 21.

3.5.3 Wear rates of developmental rail steels

The field and laboratory testing of commercial rails have shown that lubrication can reduce gauge face wear to an insignificant level. However, in some instances where the lubrication cannot be effectively maintained or where a high adhesion limit is desirable, the adverse effects of adhesive wear must be controlled by means other than lubrication. Thus, it may be desirable to know if increasing the steel hardneses beyond the current level of BHN 380 would result in further significant gains in wear resistance. Furthermore, although previous studies indicate that the pearlite resistance to adhesive wear is superior to bainite or tempered martensite, the latter two microstructures might have a better resistance to rail fatigue failures. We have, therefore, investigated the wear resistance of these microstructures at three hardness levels BHN 360, 390 and 425 (HRC 38, 42 and 45). Two additional microstructures, nodular iron and Chrome Vanadium pearlitic steel are also included. The nodular iron, originally developed as a railway wheel material, could be considered for a production of wear resistant frogs.

The identification code of tested materials, their microstructure hardness and dry wear rates are shown in Table 3. The chemical composition of rail discs A to I was 0.72%C, 0.81%Mn, 0.28%S, 0.022%S, 0.79%Cr and 0.21%Mo. The composition of nodular iron was 3.3C, 0.66 Mn, 2.5Si, 0.28Mo and .73Cu and that of Cr-V steel was 0.28C, 0.095Mn, 0.30Si, 0.024S, 1.2Cr, 0.3V and 0.017N. The details of heat-treating procedures of discs A-I can be found in reference (24).

The same full sequence test procedures were used as described in Section 3.2. The dry and lubricated wear rates are shown in Figure 22. Keeping in mind that the hardness range of discs A-I is appreciably higher than that of tested commercial steels, the following observations were made:

a) The microstructures can be rated in the following order of decreasing gauge face wear resistance: pearlite, bainite and tempered martensite. In particular, the adhesive wear of tempered martensite is ten times that of pearlite at BHN 360 (HRC39);

b) The adhesive gauge face wear rates decrease with increasing hardness for tempered martensite and bainite microstructures but not at all for pearlite. Surprisingly, the pearlite showed identical adhesive wear rates at all three hardness levels.

Since all the discs had the same chemical composition and inclusion content, this suggests that at the upper hardness range, the hardness is not a controlling factor in the increased resistance of pearlite to adhesive wear. Thus, the difference in wear rates observed in commercial steels with the hardness range of BHN 360-400 might be caused by other than metallurgical factors.

The oxidative wear rates, typified by those measured on the top running surfaces of low rails W_L, are much lower for all three microstructures than the adhesive one. Again a weak hardness effect on oxidative wear rates can be observed for tempered martensite and bainitic microstructures but virtually none for pearlite [Table 3].

The surface fatigue wear rates obtained with grease only lubrication are extremely low with respect to the adhesive one. Again, microstructure and hardness do not play significant roles in deciding wear performance but high rail discs consistently showed higher rates than low rail discs. The yet to be discussed gauge corner shelling of high rail discs undoubtedly contributed to the differences observed.

The wear resistance of nodular iron and Chrome Vanadium pearlitic steel for all four wear mechanisms followed the pattern of high hardness pearlite. This is somewhat surprising in the case of nodular iron since its microstructure consists of bainitic matrix with dispersed graphite nodules [Fig. 23a] and hardness of BHN 320 (HRC 34). Its high resistance to adhesive wear can be explained by the release of the nodular graphite and its lubrication of the gauge face/flange interface.

3.5.4 Effect of sulphur content on adhesive wear

In the previous section we have shown that a fine pearlite should continue to be used in premium rails in preference to tempered martensite or bainite and that no useful purpose is served in achieving pearlite hardness beyond BHN 360-380 (HRC 38-40). Thus, to further increase the resistance of rail steels to adhesive wear, it becomes necessary to adopt routes other than the indefinite increase in hardness. One possible route is to control the sulphur content of steel.

The near surface microstructure of rail steel subjected to adhesive wear shows a number of cracks parallel to the surface [Fig. 23b]. The energy dispersive x-ray analysis indicated that most of these cracks contain sulphides, particularly MnS. As the hardness of MnS is only VHN 170, it deforms with the steel matrix at a rate equal to that of the plastic flow of steel. Therefore, the original sulphide inclusions begin to deform soon after entry into the sheared layer and continue to elongate as the surface is approached. Although such an elongated MnS inclusion constitutes a crack, scanning electron and optical microscopic observations indicate that these cracks do not propagate or grow beyond the range of plastic deformation of metal even when fairly close to the surface. However, the increased density of MnS inclusions in the undeformed metal results in increased "precracking" of the subsurface sheared layer. As a consequence, the resistance to adhesive wear is reduced.

On the other hand, the silicon and aluminum oxides (SiO_2 and Al_2O_3) are hard at ≈ VHN 800 and 2500, respectively, and do not deform with the metal matrix. Therefore, these inclusions do not deform at the rate of metal flow and thus do not "precrack" the sheared layer to the same extent as sulphide inclusions do. Thus, the hard inclusions have a minor effect on adhesive wear rates. It should be pointed out, however, that oxide inclusions can initiate fatigue cracks, the growth of which, if undetected, could lead to fatigue failure ("Sperry" defects) in rails (25).

The above postulated mechanisms were confirmed by the tests detailed in Reference 26. Figure 24 shows the dry adhesive wear rates of high rail discs as the function of the inclusion density, measured in units of inclusion length/unit area, for as-rolled and oil quenched and tempered (OQ&T) experimental rail steels. The wear results show marked linear increases in wear rate with increases in the density of sulphides. A wear rate - hardness dependence also exists such that softer microstructures have steeper wear rates/sulphide lengths than the OQ&T ones. Therefore much larger differences in the adhesive wear rates occur for widely different hardnesses at high sulphur levels. Hard oxides, as expected, fail to increase adhesive wear rates.

4.0 LUBRICATION

Provided that lubrication breakdowns could be avoided, the damage done by adhesive gauge face (gouging) wear can be effectively controlled. While lubrication breakdowns can be induced purposely - by shutting off the lubricators to allow the utrasonic inspection of rails, its occurrence is generally due to poor maintenance where either the broken lubricating parts are not replaced in time, or in some instances the lubricators are simply allowed to run dry. The use of a "wrong" type of lubricant could also lead to a lubrication breakdown. In this section we will try to concentrate on the problems associated with:

a) the rate at which a lubricant should be dispensed and,

b) the type of lubricant that should be used.

To analyze these problems, we will first briefly review the basic principles of lubrication.

4.1 General Aspects of Lubrication

Three lubrication regimes, elastohydrodynamic (EHL) partial-EHL, and boundary can occur between the lubricated surfaces. The full EHL occurs at the specific film thickness $\lambda = 3.5$ to 5, where the surfaces are completely separated by the film of lubricant. Since the viscosity of most lubricants increases with pressure, the pressurized lubricant carries the entire load within the Hertzian area of contact. In the partial EHL regime, at $\lambda = 1.5$ to 3.5, some asperities of both surfaces penetrate the film and carry a portion of the load, the remainder being carried by pressurized lubricant [Fig. 25a]. At $\lambda = 1.5$, none of the load is carried by lubricant. The entire load is supported by asperities which themselves are separated by a thin layer of lubricant or additives contained, as indicated in Figure 25b. The specific film thickness, λ, is the ratio of minimum film thickness h_{min} and the composite surface roughness. Several formulae were developed to calculate h_{min}. These are functions of speed of motion between the surfaces, pressure-viscosity coefficient of lubricant, load and material properties and can be readily found in References 27 and 28.

Carrying out the calculations it becomes quickly apparent that full EHL does not occur in lubricated rail/wheel interfaces because these surfaces are generally too rough and the slip speeds too low. Partial-EHL may, however, be realistically maintained between flange and gauge face surfaces, if these are sufficiently smooth. Thus, the

most prevailing regime of rail/wheel lubrication is boundary. In lubricated territories it is always present between the rail's top and wheel tread surfaces [loc. A-D, Figure 3] and occasionally at location E when insufficiently lubricated. However, the presence of lubricant on the top rail surface is not always obvious. It can be easily proven by washing the appropriate section of rail surface with a solvent soaked swab. The chemical analysis of a black spot, seen on the swab after washing, usually reveals the polymerized residues of the original petrochemical lubricant and, more plentifully, its additives. Although it is the top surface of high rail which first becomes contaminated, the lubricant contamination invariably spreads onto the top surfaces of low rails of the neighboring reverse curves.

4.2 Effect of Lubrication on Traction Forces

To investigate this effect, we measured the lateral over vertical (L/V) force ratio on the low rail disc in the rail/wheel wear apparatus for four lubrication regimes: dry, grease and sand, grease and wear debris and grease only. This type of measurement was selected because the low rail always experiences a single point contact and at higher values the lateral force is primarily a function of angle-of-attack. Once the adhesion coefficients on both top rail surfaces are the same, the flange force can be approximated as twice the measured lateral force on the low rail.

New rail and wheel discs were used for the test. As in all the wear tests, the rail discs had 1/10th scale 132 lb AREA profile tilted 1:40 towards the gauge and the wheel discs had 1/10th scale "CN profile A" which is essentially a worn wheel profile. The wheelset load was 7000N. The angle of attack was initially increased by steps of 4' and a larger one later during the test as indicated by the measurement points in Figure 26. The apparatus was also instrumented by lateral displacement transducer to determine the onset of flanging.

The dry regime resulted in oxidative wear on the top surface with the maximum L/V reached at 0.36. At the gauge face surface, although not measured, the coefficient of adhesion was presumed to be in the range of 0.5 to 0.6. The L/V became saturated at 0.18 when lubricated by a grease-sand mixture, and at 0.08 to 0.09 when lubricated by grease or grease contaminated by wear particles. The L/V measurement clearly indicates that, for any given angle-of-attack, the lubrication reduces the value of lateral force on top surfaces of rails. Consequently, it also reduces the magnitude of the flange force.

The surprising aspect of this test was an early occurrence of hard flanging in the dry regime. The wheelset flanged at angle-of-attack $\psi = 4'$. In the case of the grease lubrication regime the value was $\psi = 32'$. The delayed onset of hard flanging caused by lubrication suggests that, in lubricated territories, the wheelsets come into hard flange contact with the gauge side of the rail less frequently.

4.3 Lubricants

Oils (including spent crankshaft oil) and greases are both used to lubricate rail and wheels. According to presently emerging practices, usage of oils is preferred in vehicle borne, and grease in track-side mounted lubricant dispensing equipment. The dispensation of oils or greases by vehicle borne lubricators was shown to be effective in reducing the rolling resistance of trains and wear of locomotive wheels (29), while grease dispensed by track-side mounted lubricators or hy-rail vehicles primarily controls the adhesive gauge face wear in curves. Since our report is concerned with wear in curves, we will have a closer look at the properties of grease.

A lubricating grease is a solid or semisolid lubricant consisting of a thickening agent and a liquid lubricant. Other ingredients imparting special properties may be included. The grease is usually identified by the reference to thickener, fluid component and additives as follows:

thickener:
- calcium soap
- sodium soap
- lithium soap
- other soaps (aluminum, barium, and strontium)
- clays (bentonite, hectorite, etc.)

fluid
- mineral oil
- synthetic oil (diesters, fluorocarbons and silicones)

additives:
- oxidation inhibitors
- corrosion inhibitors
- load carrying agents
- others (structure modifiers, metal deactivators, stringiness additives and dyes)

From the railway engineer's point of view, the most desirable grease selection criteria are as follows:

a. ability of the grease to stay on the surface (stickiness)

b. ability to be delivered at low temperatures (pumpability)

c. ability to separate surfaces under the conditions of high contact stress (antiwear-lubricity).

The ability of grease to stay on the rail surface is influenced by its water wash-out resistance and dropping point. For example, calcium soap grease which has good water resistance might be preferred to sodium soap grease which has poor water resistance. However, the dropping point of both greases is low ≈ 93°C (200°F) for calcium and ≈ 150°C (300°F) for sodium base grease. The grease with a high dropping point should be used in mountainous territories where the

wheel tires become fairly warm due to prolonged braking periods on the downhill sections of track. Santa-Fe railroad measured the temperature of the wheel tires at the bottom of a particular hill and found the average temperature to be ≈ 150°C (300°F) with some tires at ≈ 288°C (550°F). Thus the usage of lithium base or clay base greases with a dropping point of 177°C (350°F) and 260°C (500°F) respectively, might be preferable.

Lubrication breakdown and high wear rate may occur at low temperature if the grease stops being pumpable. Canadian railroad requires that grease is still pumpable at -40°C (-40°F). For the southern United States this criterion is less severe. The pumpability of grease is controlled by the kinematic viscosity of mineral oil. For a grease to be pumpable at -40°C (-40°F) the viscosity should be in the range of 20 - 30 cSt at 40°C (104°F) depending on the other grease ingredients.

The antiwear-lubricity properties of grease are enhanced by load carrying or extreme pressure (EP) additives. These can be divided into two groups:

mechanical
- graphite
- molybdenum disulfide (MoS_2)
- powdered metals (lead, copper and zinc)

chemical
- sulphurized fatty oils
- dethiocarbamates
- various sulphur/phosphorous compounds

The mechanical group of additives is often referred to as fillers, since they fill in the asperity valleys and spread the load otherwise carried by asperity peaks. The MoS_2 and graphite also form a film on the tip of asperities thereby preventing metal-to-metal contact.

The chemical additives, on the other hand, react with the metal and form a protective layer over the asperity when it comes into contact. The chemical reaction only occurs at high contact pressures during which the temperature of asperities reaches about 600°C (1112°F). The sulphur or phosphorous iron compounds thus formed reduce friction and prevent metal-to-metal contact. Thus the chemical EP additives form a protective film when and where needed.

To determine a load carrying performance of the EP additives commonly used in curve greases we tested five variants of clay base grease in the four ball friction and wear, Timken and rail/wheel wear apparatuses. The grease variants were as follows:

a. base grease (BG) consisting of clay and mineral oil
b. BG with 7.75% graphite
c. BG with 2.5% chemical EP additive
d. BG with 2.25% MoS_2
e. BG with graphite, EP, and MoS_2

In the rail/wheel wear tests the wear rates and L/V ratio at the low rail were evaluated for two angle-of-attack settings of 12' and 40'. The load between each pair of chromium alloyed rail discs and class C steel disc was 3500N (≈ 800 lb). For comparison purposes we also ran a dry wear test under identical test parameters.

The results are shown in Table 4. Notwithstanding the scatter of data typical of lubricated wear tests, the only difference in wear rates worth mentioning is the one observed on high rail discs at angle-of-attack $\psi = 40'$. It appears that BG & MoS_2 gives the best wear rate while BG only and BG + all additives are least effective in reducing the lubricated wear rates. However, the interpretation of the lubricated wear data are more meaningful when compared to the dry test. Compared to dry wear rates BG & MoS_2 and BG and all additives yield a reduction in wear rates of 220:1 and 133:1, respectively. Both reductions are significant and adequately protect the rail from gauge face wear.

The results from four-ball friction and wear (ASTM D-2266) and Timken (ASTM D-2509) tests are shown in Table 5. Unlike the wear apparatus test the four ball wear test indicates that BG & EP has the best ability to prevent wear while the Timken test singled out BG & MoS_2 as the lubricant with the highest load carrying ability (highest OK value). We should point out that a new multipurpose ring on block test machine was used to perform the Timken tests. Although this machine gave a consistently lower Timken OK value than the original Timken test machine, we believe that the relative standing of the OK values should not be affected by the type of machine used.

All of the above tests indicate that overloading of the grease with load carrying agents appears to be less effective in controlling wear than the usage of one or, at most, two EP additives. Regardless of how many EP additives a lubricant has, with respect to dry wear rates, any differentiation between lubricants is not significant. As shown in Figure 20, keeping the rail wheel interface lubricated all the time appears to be more important than the type or number of load carrying agents a particular lubricant may contain.

4.4 Retentiveness

A question often asked by railway engineers is how much grease should be used to maintain an adequate lubrication in curves? Although a fully satisfactory answer can only be obtained by a field test, the lubricator grease dispensation rates should equal the rate at which the grease is consumed in the rail/wheel interface. To determine the relative standing of these rates we have run a series of lubrication breakdown or retentiveness tests on the rail wheel wear apparatus.

To eliminate the unwanted influencing factors from our tests, such as the effect of difference in rail or wheel profiles, the effect of surface roughness and that of surface texture, we have adopted the following test procedures:

Step 1: Pre-run: A new set of chromium rail and class C wheel discs with 132ℓb. AREA and CN profile A respectively, were run dry for 30,000 revolutions at an angle-of-attack of 20' and load of 3500N (≈ 800ℓb)/pair of discs. The rail-wheel profile became conformal and the surface layers work-hardened.

Step 2: Conditioning run: The purpose of this run was to prepare the rail disc surface for the actual lubrication breakdown test carried out in step 4. Thus this step was run under the same load, angle-of-attack, and with the same grease type used in step 4 for 450,000 revolutions. Step 2 should ensure that the surface roughness, surface fatigue deterioration of rail material and its contamination by layers of solid lubricants or products of chemical EP additives are identical to surface conditioning in step 4.

Step 3: Disc preparation: The excess grease from the previous step was removed from the disc surface by a gentle bath in the solvent. Such a bath removed the petrochemical fractions of the grease from the disc running surfaces but left the solid surface films untouched. Using a syringe, 2g of fresh grease were then deposited and evenly spread by a spatula on the disc surfaces.

Step 4: Retentiveness test: The discs were run at the desired load and angle-of-attack until the breakdown occurred. The L/V ratio on the low rail disc was measured, stored, and displayed by the light-emitting diode each 500 revolutions until the completion of the test.

The last step established how long a known quantity of grease will last in the rail wheel interface without replenishment. The effect of lubricant deterioration on the L/V ratio is shown in Figure 27. At first, the freshly lubricated surfaces yielded low L/V values and the surface fatigue wear characteristic of this mode of lubrication did not generate any wear particles noticeable to the naked eye. After some period the grease started to deteriorate and the L/V ratio started to steadily increase. We presume that the wear mode was still that of contact fatigue as no change in the surface texture or generation of wear particles was observed. When L/V approached its maximum, the disc surface texture suddenly became rougher and less shiny. The wear mode changed to oxidative and adhesive on top running and gauge face surfaces respectively, and the generation of numerous adhesive wear particles became noticeable to the naked eye. The sudden change in wear mode marks the final stage of the lubrication-breakdown process. For rolling-sliding contacts the duration of this process, called retentiveness, is a function of creepage and load as shown in Figure 28. The points in this figure are the lubrication breakdown points taken from Figure 27.

In the above tests we measured the lubricant retentiveness on top running surfaces. In fact, before the lubricant at the gauge face

can start breaking down, the lubricant on the top surfaces must first break down to increase the flange force and frequency of flanges coming into hard contact with the gauge side of the rail disc. The situation in the field is actually somewhat more complicated since the excess lubricant at the gauge face periodically recontaminates the rail's top surface until all the lubricant supply is exhausted. Nevertheless our retentiveness tests closely agree with those carried out at FAST (29) even though they used a different technique to detect the lubrication breakdown. At FAST, the deterioration of the lubricant was monitored in terms of temperature rise of the railhead.

The retentiveness test clearly indicates that the breakdown or exhaustion of lubricant increases with increasing axle load and curvature.

5.0 CONTACT FATIGUE

Like any other form of metal fatigue, contact fatigue failure occurs in two stages - crack initiation and crack propagation. The time until failure is customarily given by a contact stress and number of cycles relationship (S-N curve). The endurance testing of discs in rolling contact or complete bearing assemblies have shown that contact fatigue is inversely proportional to the cube of the load which is, in turn, proportional to the ninth power of the Hertzian stress (30, 31). This means that doubling of load, at constant geometry, results in a ninefold decrease in fatigue life. Doubling contact stress, which in rail/wheel contact is rather commonplace, as discussed in Section 2.0, decreases the contact fatigue life about five hundredfold. It, therefore, should be of no surprise that the largest gains in contact fatigue life of rails or wheels could be achieved through the control of rail and wheel profiles. However, lubrication also has a strong effect on contact fatigue crack propagation and initiation.

5.1 Crack Propagation

Once the crack is initiated, it generally propagates in a direction parallel to the surface or inward along the lines of plastic flow. Owing to the presence of large compression stresses, the contact fatigue cracks are propagated by the shear stress i.e., Mode II. It was suggested by McClintock (32) and shown by Hearle and Johnson (33) and Regan et al. (34) that the stress intensity factor K_{II} at the crack tip and, consequently, the rate of crack propagation is greatly influenced by friction at the rail wheel interface as well as friction between the walls of the crack μ_c. In particular, the cracks with μ_c at near zero levels, i.e., when contaminated by lubricant, will propagate faster than the dry cracks with $\mu_c \approx 0.4$ to 0.6. The analysis carried out by Nishida et al. (35) suggests that the crack stops propagating when K_{II} reaches a threshold value. They experimentally confirmed that a specific type of crack propagated at $\mu_c \approx 0.2$ but did not propagate at $\mu_c \approx 0.5$.

Although all of the above mentioned studies investigated the cracks propagating in or opposite to the direction of travel, we assume that the "flaking" and "shelly spot" cracks, which propagate in the direction perpendicular to that of travel, behave in a similar manner. That is, those cracks which either reach or initiate at the surface and become contaminated by the lubricant will propagate at an accelerated rate due to low μ_c and high K_{II}, while the cracks which do not become contaminated by lubricant, i.e., subsurface cracks or when lubrication is not used, will propagate at much lower rates, if at all. Needless to say, the problem of laterally propagating contact fatigue cracks deserves and requires further study.

5.2 Crack Initiation

Contact fatigue crack initiation is less explored than the propagation since the mechanism of the former is difficult to assess. The initiation sites can generally be divided into two categories - surface and subsurface. Past studies have suggested that microscopic flaps of metal forming over the surface irregularities (36) or small circular indentations (8) could initiate cracks at the surface, while the subsurface initiation is primarily attributed to the presence of inclusions (37, 38). Under the auspices of this study, we have investigated the possible involvement of plastic instability in generation of cracks within the surface layer of material. The major cause of the instability is the incremental accumulation of plastic flow due to biaxial (compressive and parallel to surface shear stresses) loading cycle [Fig. 11]. This phenomenon is known as ratchetting or incremental collapse and is illustrated in Figure 29. When the ductility limit of the surface layer is reached, ductile fracture will take place, as shown in Figure 30, resulting in the sudden appearance of a surface crack.

We have investigated surface crack initiation experimentally using a specially designed test specimen subject to cyclical biaxial loading in a hydraulically-actuated fatigue tester Figure 31. All test specimens were machined from the head of chromium alloyed rail [steel B in Figure 16]. The biaxial loading of the specimen followed the cycle of Hertzian compressive and shear stresses acting at the rail surface [Fig. 29] as closely as the controls of the fatigue tester permitted. Because the ratio between shear and compressive stress at the rail/wheel interface is given at saturated creepage by the coefficient of friction μ, the biaxial fatigue tester simulated the effect of lubrication at the rail/wheel interface by simply varying the shear/compressive stress ratio.

We found the following relationships between the contact stresses and the number of cycles to crack initiation (i.e. separation of test specimens):

$$\tau_{max} = CN_f^{-\alpha} \quad ; \quad \alpha = \alpha_o + B\sigma_{max} \qquad (1)$$

$$\sigma_{max} = C_1 N_f^{-\beta} \quad ; \quad \beta = \beta_o e^{b\eta}$$

where:

N_f - number of cycles to crack initiation

σ_{max}, τ_{max} - maximum compressive and shear stress respectively

C, C_1, B, β_o, b - experimental constants

$\eta = \tau_{max} / \sigma_{max}$ - represents the coefficient of friction

For the chromium alloyed steel the experimental constants were determined as follows:

$C = 2767$ to 3010 MPa ; $C_1 = 7382$ MPa

$\alpha_0 = 0.265$; $B = 4.45 \times 10^{-5}$

$\beta_o = 0.18$; $b = 1.73$

For further details see Reference 39.

Most surface cracks, once they appear, lead to the formation of wear particles. However, when such particles remain in place for sufficient time, due to good lubrication, the surface cracks will branch into deeper layers of rail steel and will continue their growth as contact fatigue cracks.

The effect of lubrication on surface crack initiation is shown in Figure 32. Three curves with shear to compressive ratio of 0.10, 0.18 and 0.30 are shown. The selected ratios are typical of:

(a) $\mu \simeq 0.1$ - delamination wear taking place at gauge face under lubricated conditions

(b) $\mu \simeq 0.18$ - delamination and mild abrasive wear on top surface contaminated by grease and sand

(c) $\mu \simeq 0.3$ - mild adhesive (oxidative) wear on dry rail's top surface

The relationship between the wear rates and surface and contact fatigue crack initiation is shown in Figure 33. The wear rates of chromium alloyed steel were converted into the average "surface recess" rates, as shown in Figure 21. Although the surface cracks can generate at any depth ranging from 5 μm to 50 μm, the line TL indicates that, for a rail head contaminated with grease and sand, the average rate of recess is only 2.4 μm/MGT. This implies that to generate and remove a 30μm thick wear particle from the rail surface takes about 12.5 MGT.

Next, the surface crack initiation points were related to the MGT's using the pummelling diagram [Fig. 3] and contact theory of rough surfaces. At $\mu \simeq .18$, the average rate of surface recess-line TL is less than the time it takes to generate the surface crack and associated particle - point K. Therefore, enough time between the crack generation and particle removal is available for some surface cracks to branch into the subsurface layer and become contact fatigue cracks. At the wear rate represented by line TD ($\mu \simeq .3$) the material is removed from the surface faster than the time needed to generate surface crack — shown by point J. Therefore, in dry wear, the forming surface cracks are removed early and cannot branch into contact fatigue crack.

5.3 Effect of Lubrication on Contact Fatigue Crack Initiation and Propagation

In general, the number of cycles required to initiate surface cracks by plastic instability decreases with increasing contact stress and increasing coefficient of friction at the rail/wheel interface. Thus the effect of lubrication on the initiation of surface cracks is opposite to its effect on crack propagation. While the contamination of crack cavities by the lubricant speeds up contact fatigue crack propagation, the contamination of the rail/wheel interface by the lubricant delays the initiation of both surface and contact fatigue cracks. Preventive grinding, which is to be discussed in Section 6.0, takes advantage of these seemingly opposite effects of rail lubrication.

6.0 RAIL GRINDING

The grinding criteria presently used by most railway engineers are essentially corrective ones. These specify certain limits for the rail surface deterioration with respect to corrugations, joint or weld batter or rail profile distortion beyond which rail grinding is desirable. The rail corrugations or battered welds are by far the most frequently cited reasons for rail grinding and a brief discussion of their development is appropriate.

6.1 Corrugations

The initiation and growth of contact fatigue cracks is always followed by development of corrugations. We may call these "contact fatigue corrugations" (40) as opposed to "roaring rail" (41),"stick-slip" (42) or "dynamic" (43, 44) corrugations. Although such adjectives

are seldom used by the investigators it is unfortunate that any type of random or cyclical unevenness of rail surface is termed corrugation. Usage of a suitable adjective simply acknowledges that there are different mechanisms of corrugation formation. Even within the domain of seemingly identical operating conditons, that of heavy haul railway lines, two different types of corrugations occur depending on whether lubrication is used or not.

The growth of heavy haul "dry" rail corrugations was studied at FAST (45). These corrugations developed on the low rail in curve, they were rather regular in shape [Fig. 34a] and had the mean wavelength of ≈ 200mm (8"). The mechanism of their formation consisted of plastic flow and "mild" (called oxidative in this report) wear phenomena. Although the wear mechanism was the same at corrugation peak and valley, the magnitude of the slip distance and creepage force fluctuated. These fluctuations were caused by wheelset vibrations which, in turn, were excited by fluctuations in the retarding component of flange friction force. As soon as the lubrication was applied to the gauge face of high rail the vibrations disappeared and the corrugations on the low rail stopped growing. This occurred despite the uneven distribution of lubricant between high and low rails at FAST where, typically, the high rail was lubricated but the top surface of the low rail remained uncontaminated by lubricant and continued to experience dry oxidative wear.

On the other hand, in lubricated heavy haul lines with frequent reversed curves, the top surfaces of both high and low rails become quickly contaminated with lubricant or its residues and experience a combination of abrasive and surface fatigue wear. These rail surfaces develop contact fatigue corrugations brought about by the initiation and growth of contact fatigue cracks.

Surface crack initiation is accelerated (as discussed previously) by lubrication breakdowns, high contact stresses or variations in the properties of rail material. For example, the steel in the weld's heat-affected zone is seldom of the same hardness and cleanliness as that of the original rail material. The hard or soft welds develop high or low spots. In both cases the high contact stresses associated with unevenness of the rail, and a plastic flow in softer regions contribute to early initiation of surface cracks. Certain track irregularities also contribute to the initiation of cracks. For example, the cracks initiate quickly at locations of wide gauge because of increased incidence in contact between false flanges of worn wheels and field side of low rail. Thus, two or three individual low spots, in addition to low spots at welds, may appear along any single length of low rail in a curve. When these low spots reach a certain limit, say .5mm (0.020"), they dynamically excite the wheelset and trigger the growth of additional low spots in the direction of heavy traffic. At the same time, new low spots continue to form due to development of new cracks at the less severe track irregularities. At the final stage, the contact fatigue corrugations are nothing more than a random assembly of low spots at various stages of their development. An example of vertical profile of contact fatigue corrugated rail which is "random" both in wavelength and depth, is shown in Figure 34b.

The only method presently available to control the growth of rail corrugations is to grind or plane the rail surfaces. Previous studies have shown that grinding can effectively alleviate the growth of contact fatigue corrugations (46). However, based on the analysis of contact fatigue crack initiation and propagation phenomena we are certain that present grinding practices could be modified to entirely eradicate the occurrence of rail corrugations.

6.2 Corrective Grinding

Any rail grinding program which allows the corrugations to develop to any depth before these are ground constitutes a corrective method of grinding. The grinding criteria usually specify that grinding should commence when corrugation growth or weld batter reach a specific limit, let us say, 0.5 mm (0.020"). However, at the time the corrugation reaches such depth the grinding equipment is not always available and, as a rule, the corrugations grow beyond the desired depth prior to grinding. Any corrugations which are 0.5 mm (0.020") deep or deeper already contain clusters of fully developed contact fatigue cracks which propagate at a fast rate through the surface layer of rail steel to the depth of several millimeters.

Figure 35 schematically shows an example of a thorough corrective grind in a curve where the average corrugation depth is 0.625mm (0.025"), with some reaching the depth of 1.5 mm (0.060"). To make the rail surface flat, several passes with a large grinding train are made until 2mm (0.080") of material is removed with respect to the corrugation peaks. Although the rail is corrugation-free after the grinding, many cracks are left behind, especially at the locations of original corrugation valleys. Since the grinding cannot remove the lubricant from the crack cavities, these cracks will continue their growth upon the passage of the first train. However, the initial growth of corrugations may be slow due to the absence of dynamic effect.

6.3 Preventive Grinding

The aim of preventive grinding is to maintain the rail surface free from corrugations all the time. Providing the gauge face wear is effectively controlled by thorough lubrication, the preventive rail grinding criteria are as follows:

a) to remove the surface layer before it becomes plastically unstable, i.e. before the surface cracks appear

b) to minimize the frequency of contact for each element of material at rail surface

c) to minimize contact stresses

d) to improve the steering of freight car trucks

The first criterion dictates the depth and period of grinding while the other three affect the grinding profile.

6.3.1 Grinding depth

The depth of cut is given by the depth at which the surface cracks are generated. As discussed in the previous section, this depth is on average 25 μm(0.001") with some cracks generated at 50 μm (0.002"). Therefore, the grinding need not be any deeper, with the exception of location A [Fig. 3], than 50μm (0.002"). At location A we estimated, using Figures 3 and 32, that surface cracks will generate early, at ≈ 0.5MGT. This gives an unrealistically short grinding period and we suggest that enough material is removed from the gauge corner of high rails and the field side of low rails to avoid rail/wheel contact at these locations altogether.

6.3.2 Grinding period

Preventing the occurrence of rail/wheel contact at location A alters the frequency histogram. A new pummelling diagram, typical of a preventive grinding profile, is shown in Figure 35. Using Figures 32 and 36 we estimate that the surface cracks in the sharp curves (>2.5°) will not appear before 10MGT and 6MGT at locations B & C and location D, respectively. New rail may initiate surface cracks very early, say at <5MGT, due to the presence of mill scale, a decarburized layer, and other surface imperfections and irregularities.

Based on the above arguments, it is proposed that new rail, whether located in curves or tangent track, is preventively ground immediately or as soon as practical after laying. Thereafter, the preventive grinding period for a sharp curve should be 5MGT. The total amount of material removed due to wear and grinding from the top surface of lubricated and preventively ground rail located in sharp curves is approximately equal, as shown in Figure 37, to the amount of material removed by oxidative wear in an unlubricated curve.

Since in shallow curves (<2.5°) the number of wheelsets which negotiate the curve at a saturated lateral creepage is reduced, say by 50%, we propose that the preventive grinding period is doubled on these curves to 10MGT. Taking into account the creepage considerations only, we find that, in tangent track, surface cracks initiate at ≈ 30 to 50MGT. At the welds, however, they will initiate much earlier and a grinding period of 15MGT is recommended.

The grinding periods of 5, 10 and 15MGT for sharp and mild curves and tangent track are based on laboratory studies carried out on one type of rail steel (chromium alloyed) and under the conditions of thorough (uninterrupted) lubrication. It is quite conceivable that these periods could be somewhat extended for a thoroughly lubricated track containing better quality rail particularly if the gauge corner of such rail is ground conformal to the flange root area of passing wheels immediately after this rail is laid into the track. On the other hand, a combinatin of frequent lubrication breakdowns and grinding to incorrect profiles may result in the development of contact fatigue cracks within the 5, 10 15MGT grinding intervals. Obviously, further research and field tests of preventive grinding are needed before any modification or extention of grinding periods could be proposed.

To summarize, preventive grinding requires that a single pass of the grinding train remove no more than 0.050 μm(0.002") of material each 5, 10 and 15MGT in sharp (>2.5°), mild (<2.5°) curves and tangent track, respectively. This can easily be achieved by dividing each siding-to-siding section of a single line track, typically 18 km (10 miles) long, into several sections: a section of sharp curves, two sections of mild curves and three sections of tangent track. The grinding train passes over the territory each 5MGT and grinds all the sharp curves, half of the mild curves and a third of tangent track sections, so that all the mild curves and tangent track are ground once each 10 and 15MGT, respectively. Even with an appreciable number of curves, the grinding train could cover a siding-to-siding length of track in 1 to 1 1/2 hour and 800 km (500 miles) of main line track in 8 to 10 working days.

6.3.3 Grinding profile

The grinding profiles traditionally used in corrective grinding can be conveniently divided into two groups: "flat" and "contour" grinding profiles [Fig. 38]. Usually, the "flat" grinding profile is used in tangent track while a "contour" grinding is used in curves. All the contour profiles are variations of a profile originally developed in Australia to alleviate the gauge face wear in mild curves on Mount Newman and Hamersley Iron Railways (47). Simply put, contour grinding increases the rolling radii difference between wheels in contact with high and low rail by forcing all wheelsets to contact the rails at or in close proximity of locations A [Fig. 3]. This is achieved by removing enough material from the field side of high and the gauge corner of low rails (i.e. locations D and partly C) so that wheel contact at these locations is prevented. Because the locations A, for reasons given earlier, have an extremely short contact fatigue life, the wheel contact must also be prevented at this location, even though it is counterproductive from the point of view of maximizing the rolling radii difference. The latest version (1985) of the Australian profiles focuses on the reduction of contact stresses at location A), rather than preventing the contact altogether. Thus a running band of about 1" - 1 1/2" is left at the center of both high and low rails. The contour profiles of this type have two disadvantages. Firstly, they are ineffective in preventing hard flanging in sharp curves and secondly, they increase the frequency of contact at locations B and C. If, in addition, the rail crown is ground to a small radius, say 10cm (4"), resulting in substantially increased contact stresses, the contact fatigue life at locations B & C is severely reduced (see Section 5.0), at least until plastic flow of rail head metal restores the crown radius and contact stresses to the original level.

Although such profiles, contoured on both sides of the rail head, were found useful by several railroads as suitable corrective grinding patterns, in general, they do not satisfy the preventive grinding criteria. To minimize the frequency of contact it is not necessary to profile the gauge corner of low rails and the field side of high rails, especially in sharp curves where the steering by rolling

radii difference becomes ineffective. In this way some of the loading cycles at B & C are transferred to location D. The rail crown should be ground to the radius of 10" to 14" to minimize the contact stresses at locations B & C.

The stresses at the gauge corner of high rail could be minimized by grinding it to an equal or slightly larger radius than the flange root radius of heavy haul wheels passing over the ground territory (i.e. ≈ 21mm (13/16") if AAR wheel profile is used and ≈ 12.7mm 1/2" if Modified Newmann (Radford) wheel profile is used). Such accuracy in rail grinding, however, is difficult to achieve in practice.

The grinding crew may find it easier to increase the depth of cut to 0.2 - 0.3mm (0.008 - 0.01") at location A, thereby preventing the wheel/rail contact at the gauge corner for most of the passing wheelsets. Nevertheless, the desired gauge corner radius should be maintained to the best ability and skill of the grinding equipment and crew.

The steering of vehicles in sharp curves could be improved if the spin difference between high and low rail contacts is minimized. The conicity (cant) at running surface of high rail, due to plastic flow and wear, increases while that of low rail decreases. The resulting spin difference increases the wheelsets' angle of attack and hence the flange force. For the modified Heumann and AAR wheel profiles the conicity (cant) on both high and low rail top surfaces should be 1:20 regardless of the installed cant of the rails given by the tieplates.

An example of developmental preventive grinding profiles, for a 44 stone grinding train, suitable for territories travelled by wheels with modified Heumann profile, are shown in Figures 39 and 40. The basic stone pattern, to be used in tangent track, is shown in Figure 39. For tangent track the profiling stones (four per rail) are not used and the rail crown stones are set to grind the rail's top surface to a radius of 30 to 35 cm (12" - 14"), inclined in a ratio of 1:20 towards the gauge on both rails. The gauge corner stones, set at 13°, 20°, and 32°, are intended to maintain the naturally worn rail profile, rather than alter it - i.e. these stones do not remove enough material to prevent contact at gauge corner of right and left rails. On the other hand, in curves, the profiling stones (two each at gauge corner of high rails and field side of low rails) are used and some of the crown stones are rearranged in such a manner as to prevent contact between wheel and rail at location A for most of the rail grinding interval. Figure 40 shows the left hand curve patterns. In right hand curves, the right-hand profiling stones are used (the left-hand ones are out of engagement) which, together with appropriate rearrangement of some of the crown stones, will yield a pattern symmetrically opposite to the one shown in Figure 40.

Grinding patterns similar to the above can be designed if more stones are available. All preventive grinding patterns should, with

respect to Figure 38, "contour" the gauge corner of high and field side of low rails but leave the field side of high and gauge corner of low rails "flat". To achieve the desired depth of cut of ≈ 0.050mm (0.002") the setting of power consumption at grinding motors, type of stone and the speed of the grinding train have to be determined by field tests.

6.4 Rail Life

Rail life in curves, namely that of the outer (high) rail in curves is most severely limited by dry wear. As shown in Figure 33, line GD, gouging wear removes the rail material from the gauge face of the rail at a high rate requiring rail in an 8° curve to be replaced every 40 to 100 MGT (depending on rail type).

As shown in Figure 16, lubrication can effectively arrest gauge face wear but it contaminates the rail's top surface and brings about the initiation and growth of contact fatigue cracks which develop into head checks, shelly spots and flakes, and cause the rail to corrugate. Whether the rail is lubricated and correctively ground or lubricated and preventively ground, the rail becomes condemnable if more than 19mm (0.75") (measured vertically) is removed from the rail head surface. If we use the previously mentioned example of corrective grinding (Figure 35a) which removes 2mm(0.080") of material from the rail head surface each 25MGT, then the rail becomes thin at 235MGT. Although this represents a substantial increase in rail life with respect to dry wear, a further increase can be achieved if the rail is ground preventively.

Figure 37 predicts that the combined material removal from the top of chromium alloyed rail due to wear and preventive grinding is 16 μm/MGT. In fact, a somewhat increased wear rate will occur due to the roughening of the rail surface by the grinding stones and we feel that the combined wear-grinding rate of 25 μm/MGT (0.001"/MGT) is more realistic. At this rate the high and low rails in sharp curves become thin at 750MGT and at about twice and three times this period in mild curve and tangent track respectively. This, compared to corrective grinding, represents a threefold increase in rail life.

7.0 CONCLUSIONS

The wear and contact fatigue model presented in this report attempts to formulate the relationship between two different forms of surface damage. The first one (wear) removes the material from the surface in the form of small particles at rates which can vary from very large to negligible. At zero or insufficient wear the surface layer of material is subject to fatigue deterioration consisting of initiation and growth of surface and subsurface cracks and subsequent development of contact fatigue corrugations. Wear could be particularly troublesome on gauge face surfaces of high rails in curves. Thorough lubrication eliminates gauge face wear, but unfortunately it reduces the wear rate on the top surfaces of both rails to a point beyond which contact fatigue corrugations develop. The optimum rate of material removal from the rail top surfaces must therefore be low enough to yield a reasonable rail life, yet large enough to prevent the development of contact fatigue corrugations.

Experimental studies have shown that, in the case of Chromium alloyed rail of hardness ≈ 320 BHN the optimum rates of material removal are 0.025mm (0.001")/MGT, 0.016mm (0.00066")/MGT and 0.0083mm (0.00033")/MGT for sharp and mild curves and tangent track respectively. Such rate of material removal can be achieved by a combination of lubrication and preventive grinding. Preventive grinding removes thin layers of metal at relatively frequent intervals. At the above quoted material removal rates the 136 b. AREA Chromium rail should last 750MGT, 1500MGT and 2250MGT in sharp and mild curves and in tangent track respectively, providing the rail is not removed from the track for fatigue ("Sperry") defects. Lubricated and preventively ground rail should remain corrugation free for its entire life.

Longer rail lives could conceivably be achieved with micro-alloyed head hardened rails, particularly if careful attention is given to grinding profiles. These profiles should conform to wheel profiles prevailing on heavy haul cars used over the ground (and lubricated) territory.

The following concluding remarks can be made with respect to contact mechanics:

- maintenance of wheel and rail profiles has a strong effect on the location of contact and magnitude of contact stresses.

- the plastic flow of rails is reduced by increasing the rail hardness (strong effect) and by decreasing the adhesion limit (weaker effect).

With respect to dry, gauge face wear:

- gouging wear is most effectively controlled by lubrication even if the lubricant is contaminated by sand.

- increasing the hardness of rail also results in appreciable reduction in dry wear rates, however, no further gains can be made beyond the hardness level of 360-380BHN.

- limiting the sulphur content to 0.015% or less enhances the rail's resistance to dry wear.

With respect to lubrication:

- lubricant applied to the flange/gauge face interface always contaminates the rail's top surfaces and:

    - reduces wear

    - reduces rail/wheel forces

    - reduces plastic flow

    - causes rail to corrugate

- sharp curves and heavy axle loads consume lubricant at faster rates than mild curves and light axle loads (empty cars), respectively.

- the composition of lubricant does not appreciably affect its anti-wear performance with respect to dry wear.

- overloading of lubricant with anti-wear additives appears to be less effective in controlling wear than usage of one or at most two additives.

With respect to contact fatigue:

- doubling of contact stresses results in a five hundredfold decrease in contact fatigue life.

- the accumulation of plastic flow at the top surface layer of rail material leads to the sudden appearance of surface cracks (a mechanism referred to as "plastic instability").

- lubrication delays the surface crack initiation by plastic instability but significantly accelerates the propagation of contact fatigue cracks.

- lubrication breakdowns (intentional or unintentional) appreciably reduce contact fatigue life and should be avoided.

With respect to rail grinding:

- an ideal rate of material removal exists at which the growth of contact fatigue corrugations is prevented and rail life is maximized.

- a further increase in rail life can be achieved if the rail is ground to a profile conformal to prevailing wheel profile. Further research in this area is desirable.

8.0 REFERENCES

1. Beagley, T.M. "Severe Wear of Rolling/Sliding Contacts". Wear, Vol. 36 (1976), 317-335.

2. Bolton, P.J.
   Clayton, P. "Rolling-Sliding Wear Damage in Rail and Tyre Steels". Wear, Vol. 93 (1984), 145-165.

3. Kalousek, J.
   Rosval, G.
   Ghonem, H. "Lateral Creepage and its Effect on Wear in Rail Wheel Interface". Contact Mechanics and Wear of Rail/Wheel Systems, J. Kalousek, R.V. Dukkipati and G.M.L. Gladwell eds., University of Waterloo Press, 1982, 373-393.

4. Heller, W.
   Schweitzer R.
   Weber L. "Modern Developments in Rail Steel Metallurgy and Production". Canadian Metallurgical Quarterly, Vol. 21, No. 1, pp. 3-15, 1982.

5. Steele, R.K. "Rail: its Behaviour and Relationship to Total System Wear". Second International Heavy Haul Railway Conference Proceedings, Colorado Springs, 1982, Paper 82-HH-24, pp. 227-276.

6. Fegredo, D.M.
   Kalousek, J.
   Shehata, M.T.
   Palmer, A. "The Effect of Sulphide and Oxide Inclusions on the Wear Rates of Standard and Alloy Rail Steels". Third Int. Heavy Haul Railway Conference Proceedings, Vancouver, 1986, pp. IB-14-1 to -13.

7. Jamison, W.E. "Wear of Steel in Combined Rolling and Sliding". ASLE Paper No. 80-LC-5B-1.

8. Clayton, P.
   Allery, M.B.P. "Metallurgical Aspects of Surface Damage Problems in Rails". Canadian Metallurgical Quarterly, Vol. 21, No. 1, pp. 31-46, 1986.

9. Masumoto, H.
   Sugino, K.
   Nisida, S.
   Kurihara, R.
   Matsuyama, S. "Some Features and Metallurgical Considerations of Surface Defects in Rail due to Contact Fatigue". Rail Steels - Developments, Processing and Use. ASTM STP 644, D.H. Stone and G.G. Knupp, Eds., ASTM, 1978, pp. 233-255.

10. Kalousek, J. "Contact Geometry Between Wheel Flange and Rail". National Research Council of Canada, Division of Mechanical Engineering Technical Report TR-WE-41, NRC No. 23208, March 1984.

11. Johnson, K.L. "Contact Mechanics". Cambridge University Press, 1985.

12. Seely, F.B.
Smith, J.O. "Advanced Mechanics of Materials". Wiley, pp. 342-378, 1952.

13. Hamilton, G.M. "Explicit Equations for the Stresses Beneath a Sliding Spherical Contact". Proc. Instn. Mech. Engrs., Vol. 197C, pp. 53-59, 1983.

14. Johns, T.G.
Sampath, S.G.
Bell, J.C.
Davies, K.B. "Engineering Analysis of Stresses in Railroad Rails". Batelle Columbus Labs., Report FRA/ORD-81/51, Oct. 1981.

15. Kalker, J.J. "On the Rolling Contact of Two Elastic Bodies in the Presence of Dry Friction". Thesis, Delft, 1967.

16. Gilchrist, A.O.
Brickle, B.V. "A Re-Examination of the Proneness to Derailment of a Railway Wheelset". Journal of Mechanical Engineering Science, Vol. 18, No. 3, 1976.

17. Marcotte, P.P.
Mathewson, K.J.R.
Young, R. "A Practical Model of Rail Vehicle Curve Negotiation". Proceedings of 7th Symposium of the Int. Association for Vehicle System Dynamics, Cambridge, 1981.

18. Elkins, J.A.
Eickhoff, B.M. "Advances in Nonlinear Wheel/Rail Force Prediction Methods and their Validation". ASME - Journal of Dynamic Systems, Measurement and Control, Vol. 104, pp. 133-142, 1982.

19. Horak, D.
Wormley, D.N. "Nonlinear Stability and Tracking of Rail Passenger Trucks". ASME - Journal of Dynamic Systems, Measurement and Control, Vol. 104, pp. 256-263, 1982.

20. Kalker, J.J. "Introduction to the Fortran IV Programs DUVOROL and CONTACT for the Solution of 3-D Elastostatic Half-Space Contact Problems With or Without Friction". Delft University of Technology, Dept. of Mathematics Report 82-29, 1982.

21. Johnson, K.L.
Jeffries, J.A.
"Plastic Flow and Residual Stresses in Rolling and Sliding Contacts".
Proceedings of Symposium on Fatigue in Rolling Contact, Paper 5, Institute of Mechanical Engineers, London, 1963, pp. 50-61.

22. Pak, W.
Izbinsky, G.
Soares, H.
"Wheelset Angle-of-Attack Measurement of Regular Train Consists".
Track/Train Dynamics, Vol. 3, Transport Canada Report TP4183E, pp. 113-123, 1982.

23. --------
"Track Train Dynamics Newsletter - Wheel/Rail Wear Project Status".
Railway Age, Dec. 1984, pp. 51-52.

24. Kalousek, J.
Fegredo, D.M.
Laufer, E.E.
"The Wear Resistance and Worn Metallography of Pearlite, Bainite and Tempered Martensite Rail Steel Microstructures of High Hardness".
Wear of Materials, ASME, 1985, pp. 212-231, and in Wear, 105 (1985) pp. 199-222.

25. Chipperfield, C.G.
Blicblau, A.S.
"Modelling Rolling Contact Fatigue in Rails".
Rail International, Jan., 1984, pp.

26. Fegredo, D.M.
Shehata, M.T.
Palmer, A.
Kalousek, J.
"The Effect of Inclusion Type and Control on the Wear of an Alloy Rail Steel".
In Strength of Metals and Alloys, Pergamon Press, 1985, pp. 1563-1568.

27. Winer, W.O.
Cheng, H.S.
"Film Thickness, Contact Stress and Surface Temperatures".
Wear Control Handbook, M.B. Peterson and W.O. Winer eds., ASME, 1980, pp. 81-141.

28. Dowson, D.
Higginson, G.R.
"Elastohydrodynamic Lubrication".
2nd Ed., Oxford: Pergamon, 1977.

29. Reiff, R.P.
"Rail-Wheel Lubrication. A Strategy for Improving Wear and Energy Efficiency".
Third International Heavy Haul Conference, pp. IA-3-1 to IA-3-9, 1986.

30. Palmgren, A.
"Ball and Roller Bearing Engineering".
SKF Industries Corp., Philadelphia, Pa. 3rd edn. 1959.

31. Fujita, K.
Yoshida, A.
"Effect of Hardness Difference on the Surface Durability and Surface Failure of Steel Rollers". Bull. JSME, Vol. 20, No. 140, Feb. 1977, pp. 232-239.

32. McClintock, F.A. "Plastic Flow Around Crack Under Friction and Combined Stress". ICF4, Fracture, Vol. 4, pp. 23-39, 1977.

33. Hearle, A.D.
Johnson, K.L. "Mode II Stress Intensity Factors for a Crack Parallel to the Surface of an Elastic Half-Space Subjected to a Moving Point Load". Cambridge University Report, CUED/C-Mech/TR26, 1983.

34. O'Regan, S.D.
Hahn, G.T.
Rubin, C.A. "The Driving Force for Mode II Crack Growth Under Rolling Contact". Wear, Vol. 101, pp. 333-346, 1985.

35. Nishida, S.I.
Sugino, lK.
Urashima, C.
Masumoto, H. "Study on Contact Rolling Fatigue of Rails". Bull. JSME, Vol. 28, No. 243, pp. 1819-1824, 1985.

36. Martin, T.A.
Eberhardt, A.S. "Identification of Potential Failure Nuclei in Rolling Contact Fatigue". Trans. ASME 89, 1967, pp. 932-942.

37. Suh, N.P. "Surface Interactions". Tribological Technology, Vol. 1, pp. 37-208, Martinus Nijhoff Publishers, 1982.

38. Sugino, K.
Miyamoto, K.
Nagumo, M.
Aoki, K. "Structural Alterations of Bearing Steels Under Rolling Contact Fatigue". Trans. Iron Steel Inst. Japan, V. 10 (1970) pp. 98-111.

39. Ghonem, H.
Kalousek, J. "Study of Surface Crack Initiation due to Biaxial Compression/Shear Loading". Proceedings of Second International Symposium on Contact Mechanics and Wear of Rail/Wheel Systems". University of Waterloo Press, (to be published in 1987).

40. Kalousek, J.
Klein, R. "Investigation into Causes of Rail Corrugations". AREA Bulletin 656, Vol. 77, pp. 429-448, 1976.

41. Frederick, C.O.
Bugden, W.G. "Corrugation Research on British Rail". Rail Corrugations, Institut fur Luft-und Raumfahrt, Technische Universitat Berlin, ILR-BERICHT 56, 1983, pp. 7-34.

42. Krause, H.
Senuma, T. "Investigation into the Influence of Dynamic Forces on the Tribological Behaviour of Bodies in Rolling/Sliding Contact with Particular Regard to Surface Corrugations". Trans ASME, J of Lub. Tech., Vol. 103, pp. 26-34, 1981.

43. Clark, R.A.
Foster, P.
"Mechanical Aspects of Rail Corrugation Formation".
in Rail Corrugations, Institute fur Luft-und Raumfabrt, Technische Universitat Berlin, ILR-BERICHT 56, 1983, pp. 145-180.

44. Mair, R.I.
"Natural Frequency of Rail Track and its Relationship to Rail Corrugation".
The Institution of Engineers, Australia, Vol. CE 19, No. 1, 1977, pp. 6-11.

45. Devine, T.J.
Daniels, L.E.
Blume, N.
"Rail Corrugation Investigations at FAST: December, 1979 through August 1981".
in Proceedings of FAST Engineering Conference, Report No. FRA/TTC-82/01 pp. 165-174.

46. Lamson, S.T.
"Rail Profile Grinding".
CIGGT Report No. 82-7, Transport Canada Report No. TP 3998E, 1982.

47. Lamson S.T.
Longson, B.H.
"Development of Rail Profile Grinding at Hamersly Iron".
Proceedings Second International Heavy Haul Railway Conference, ASME, paper 82-HH-33, 1982, pp. 372-379.

Location	Ratio of actual stress to the yield in shear p_o/k	
	Plain carbon (260BHN) k = 450 MPa	Head hardened (micro-alloyed) (380BHN) k = 654 MPa
A $(p_o)_{av}$ = 2500	5.6	3.82
D $(p_o)_{av}$ = 1,800	4.0	2.75
B & C $(p_o)_{av}$ = 1150	2.6	1.76
E $(p_o)_{av}$ = 800(dry)	1.7	1.22
$(p_o)_{av}$ = 500(lub)	1.1	.76

Table 1: Variability of p_o/k ratios with location and hardness of the rail

CODE	RAIL TYPE	BHN (approx)	DRY WEAR RATE µg/cycle		CHEMICAL COMPOSITION						
			low rail	high rail	C	Mn	Si	S	P	Cr	Others
A	Standard AREA	260	4	46.5	.76	.85	.26	.015	.014	.01	
B	Algoma Cr.	310	4	27.3	.72	.79	.35	.030	.018	1.39	
C	Algoma Cr-MoI (Experimental Heat)	320	3.3	22.5	.70	.99	.25	.021	.007	.80	Mo=.15
D	Russian FHT	330	4.8	20.0	.77	.81	.175	.05	.022	.095	Cu=.180
E	Sysco Cr-Cb	330	7.5	17.5	.68	.95	.47	.025	.017	.83	Nb=.037
F	Bethlehem FHT	360	3.3	16.5	.78	.80	.18	.045	.021	.10	Cu=.185
G	Nippon NHH	370	2.75	11.5	.78	.94	.23	.022	.022		
H	BHP HH	370	3.4	9.6	.81	.94	.23	.023	.019		
I	British Steel Cr	380	1.7	4.9	.75	.95	.34	.024	.029	.96	
J	Nippon Cr-HH	380	1.7	3.9	.78	.82	.78	.005	.018	.51	
K	Algoma AWC340 (Experimental Heat)	350	2.1	7.5	.77	.90	.45	.017	.029		

Table 2: Hardness, dry wear rates and chemical composition of tested commercial steels

CODE	Microstructure	Hardness (Approx.)		Dry wear rate	
		BHN	HRC	Low R µg/rev	High R µg/rev
A	Tempered Martensite	360	38	4.25	81
B		390	42	2.6	43
C		425	45	2.0	25.5
D	Bainite	360	38	5	37.5
E		390	42	2.0	16
F		425	45	1.75	14
G	Pearlite	360	38	1.25	9.8
H		390	42	1.0	9.8
I		425	45	1.0	9.8
J	Nodular Iron	320	34	2.25	14.5
K	Pearlite (Cr-V)	360	38	1.9	12.3

Table 3: Microstructure, hardness and dry wear rates of experimental rail steels

GREASE TYPE	ANGLE OF ATTACK Ψ	LOW RAIL		HIGH RAIL	NO LUBRICATION	
		L/V	WEAR RATE µg/cycle	WEAR RATE µg/cycle	LOW RAIL Ψ=40'	HIGH RAIL Ψ=40'
BASE GREASE (B.G.)	20' 40'	0.08 0.13	0.07 0.08	0.32 0.49	4.2	57.2
B.G. + GRAPHITE(G)	12' 40'	0.05 0.13	0.03 0.03	0.03 0.39		
B.G. + EP	12' 40'	0.04 0.11	0.03 0.02	0.09 0.26		
B.G. + MoS_2	12' 40'	0.07 0.12	0.03 0.03	0.03 0.07		
B.G. +G+EP+MoS_2	12' 40'	0.08 0.13	0.20 0.26	0.10 0.43		

Table 4: Effect of grease composition on wear rates

GREASE TYPE	FOUR BALL FRICTION AND WEAR			TIMKEN	
	SCAR DIA. (mm)	SPEC. TEMP. (°C)	COEFF. OF FRICTION	SCAR WIDTH (mm)	OK VALUE (LB)
BASE GREASE (B.G.)	0.719	39	0.07	0.7	12
B.G. + GRAPHITE(G)	0.652	42	0.06	1.4	18
B.G. + EP	0.569	41	0.06	1.9	27
B.G. + MoS_2	0.622	40	0.09	1.0	30
B.G. +G+EP+MoS_2	0.630	44	0.09	1.1	18

FOUR BALL: SPEED = 1200 RPM
LOAD = 40 KG
TIME = 60 MIN

TIMKEN: SPEED = 800 RPM

Table 5: Results from four ball and Timken tests

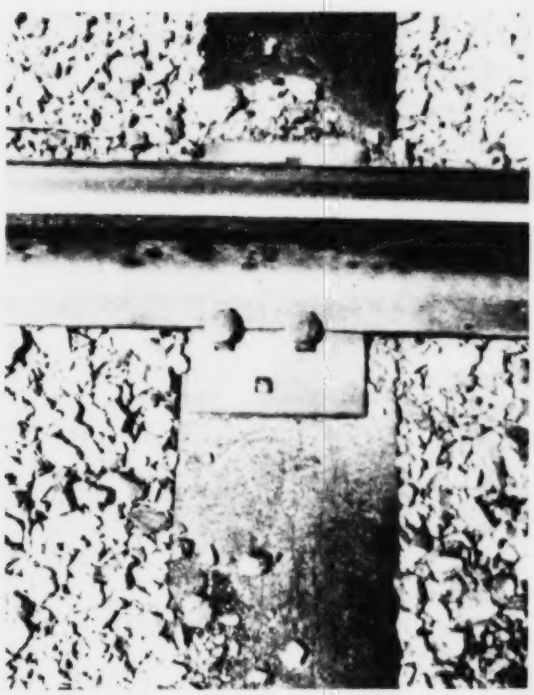

(a)

(b)

Fig. 1: Severe adhesive (gouging) wear:
a) "moonshine" on railway ties
b) worn gauge face of high rail

(a)

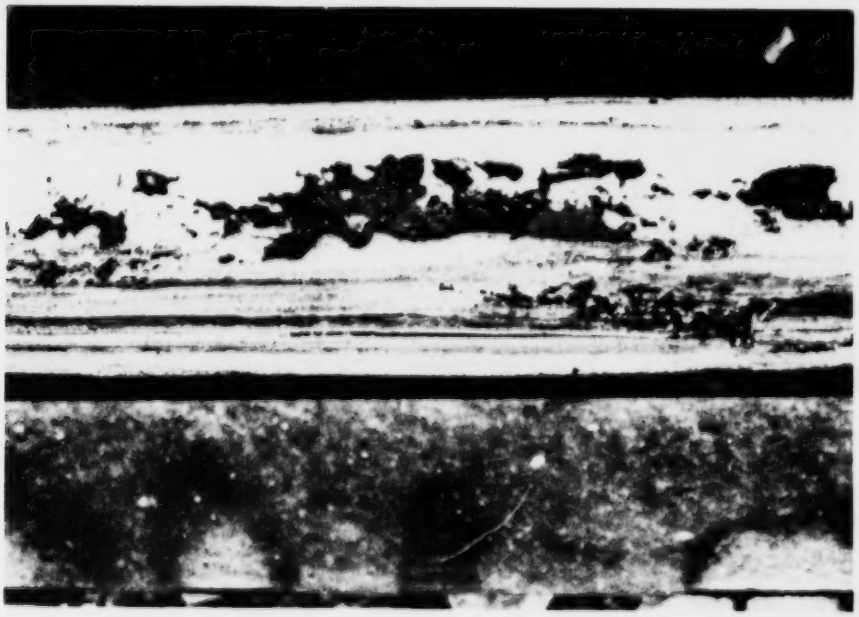

(b)

Fig. 2: Contact fatigue: a) shelly spots on high rail
b) flaking on low rail

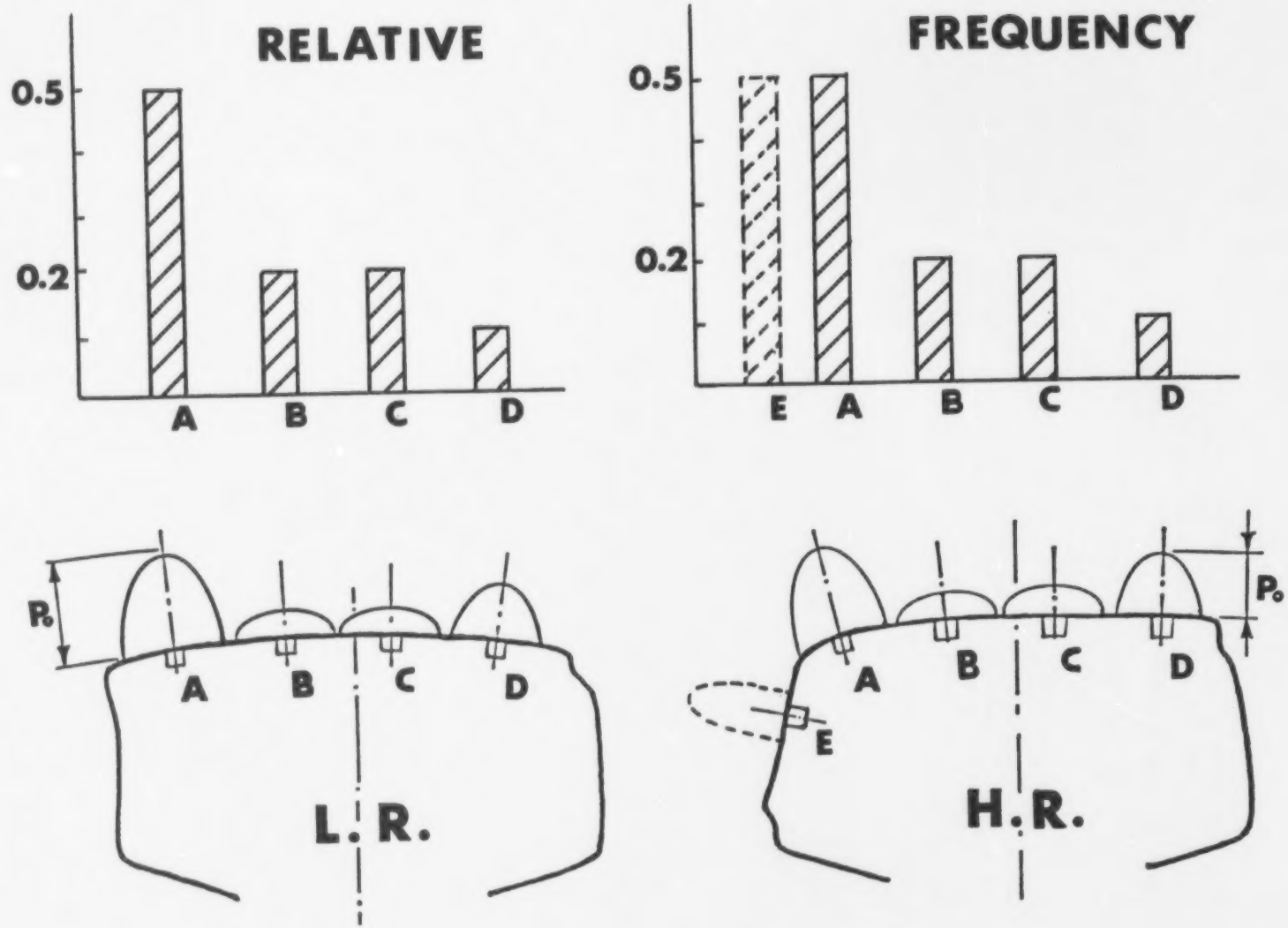

Fig. 3: Relative frequency of contact (pummelling) diagram for high and low rails in 8° curve

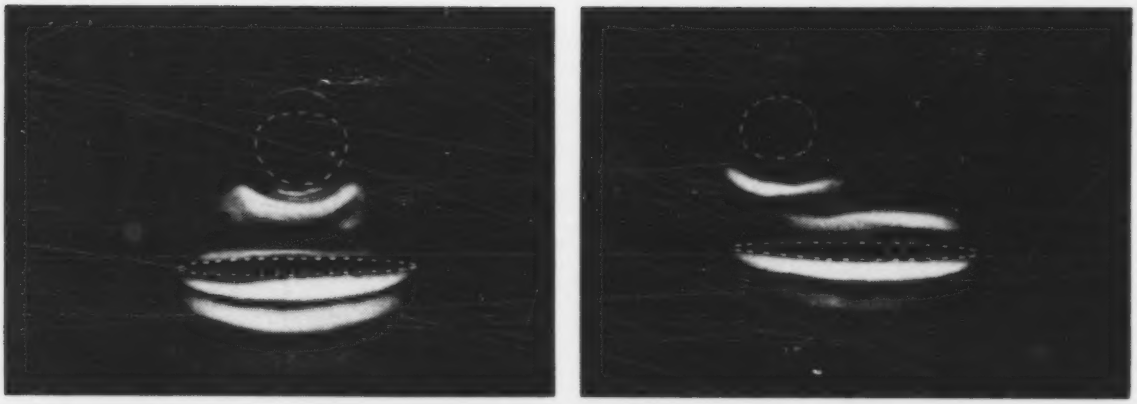

a) $\psi = 0$ b) $\psi = 30'$

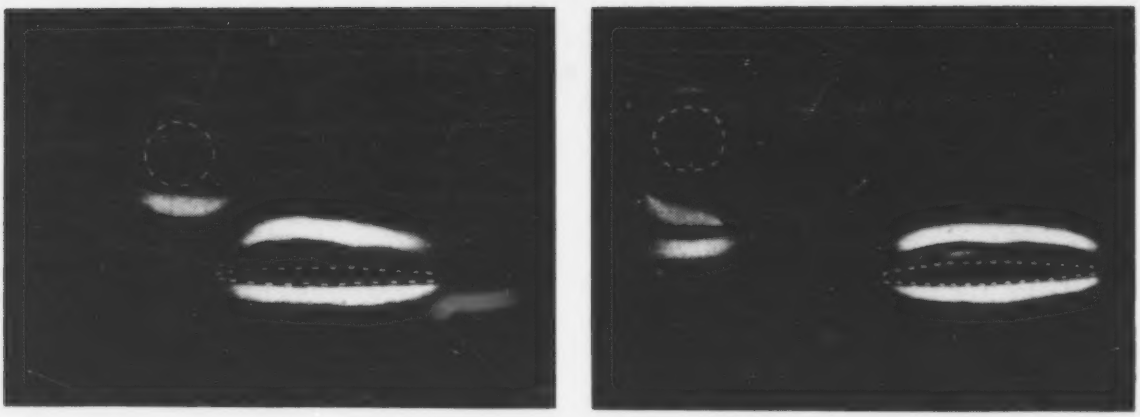

c) $\psi = 60'$ d) $\psi = 120'$

Fig. 4: Change in the geometry of contact between rail's top and gauge face contact zones as function of angle-of-attack

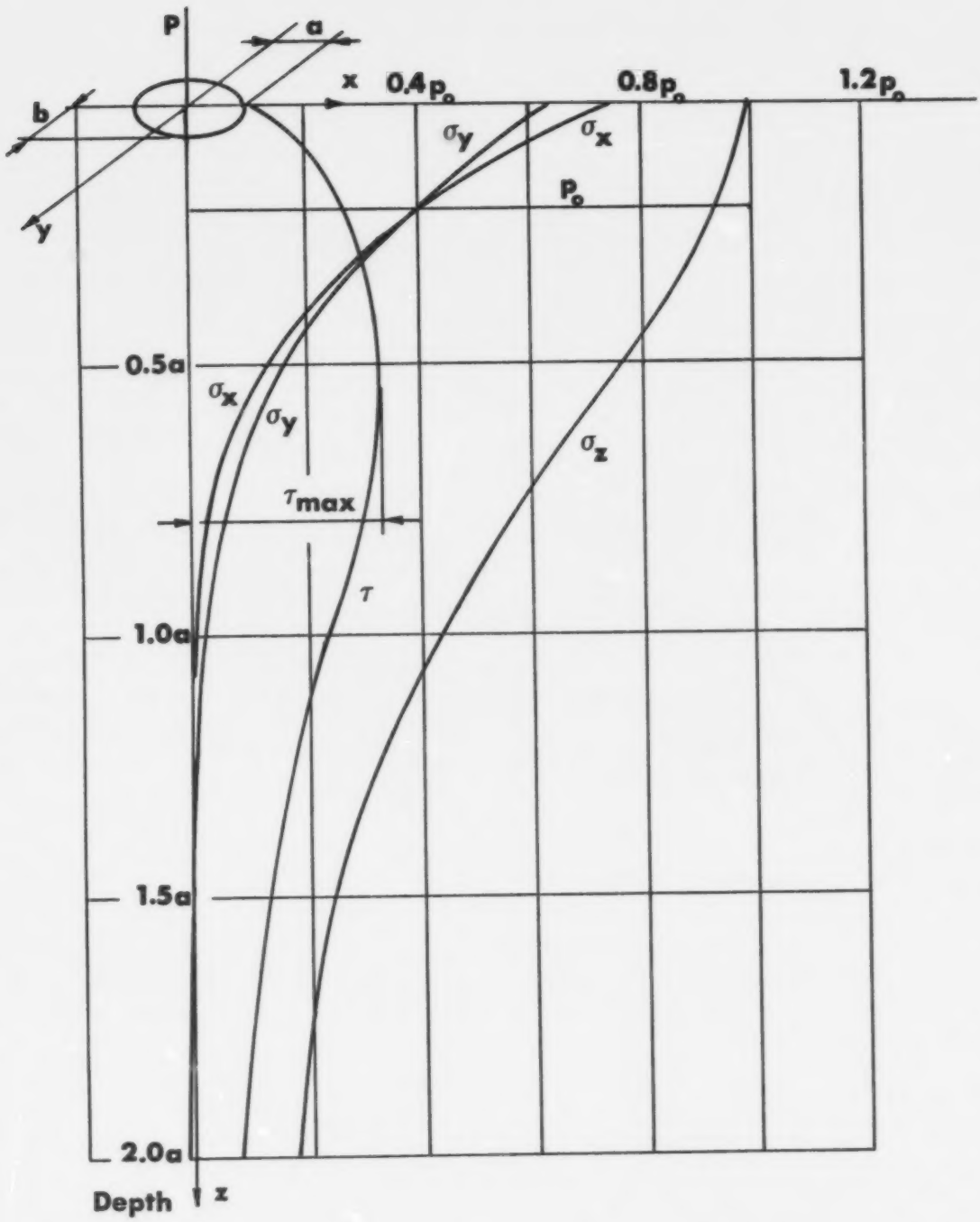

Fig. 5: Distribution of contact stress with respect to depth at x=y=0. σ_x, σ_y, σ_z are principal compressive stresses; τ is octahedral shear stress

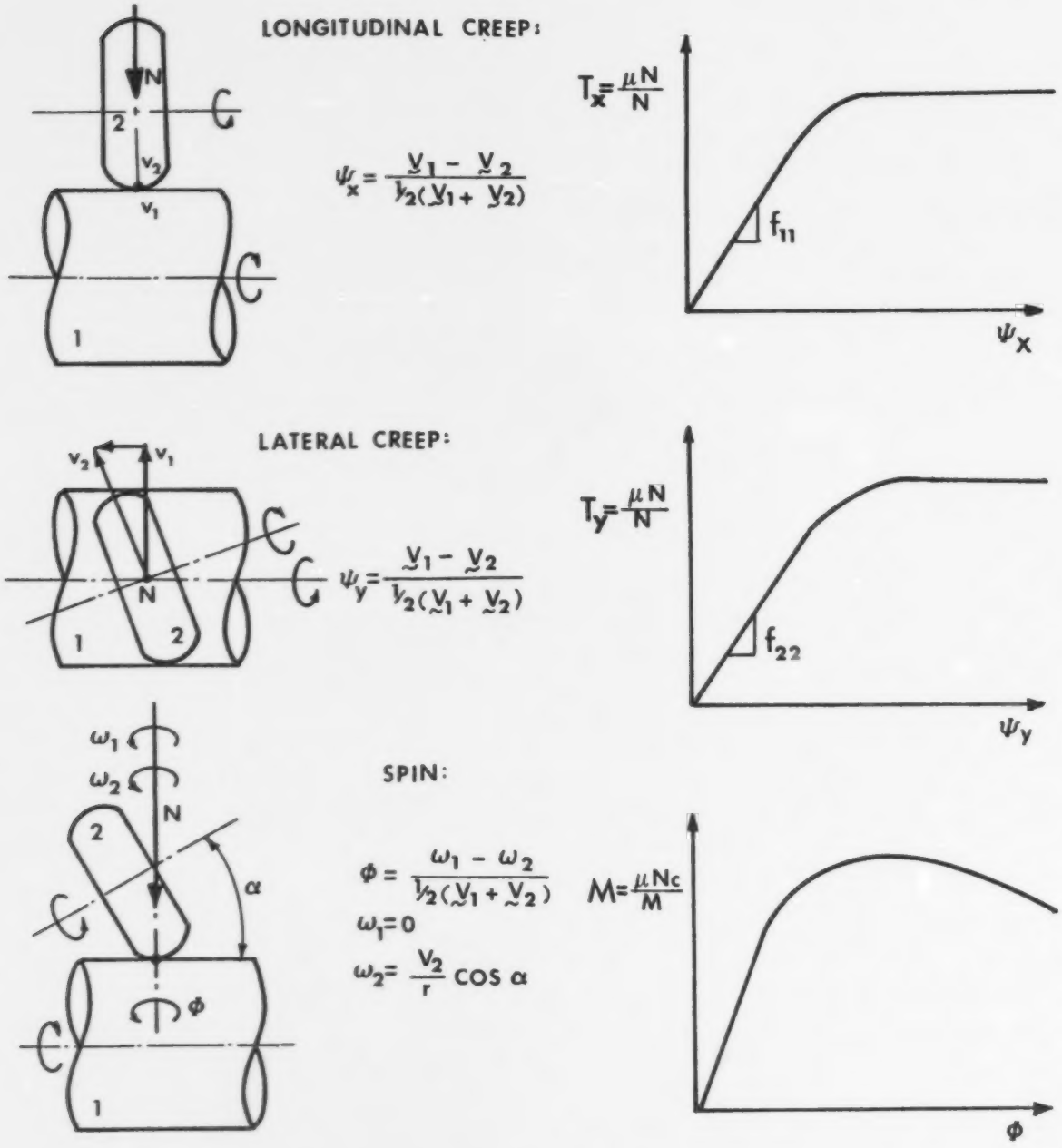

Fig. 6: Definitions of creep components

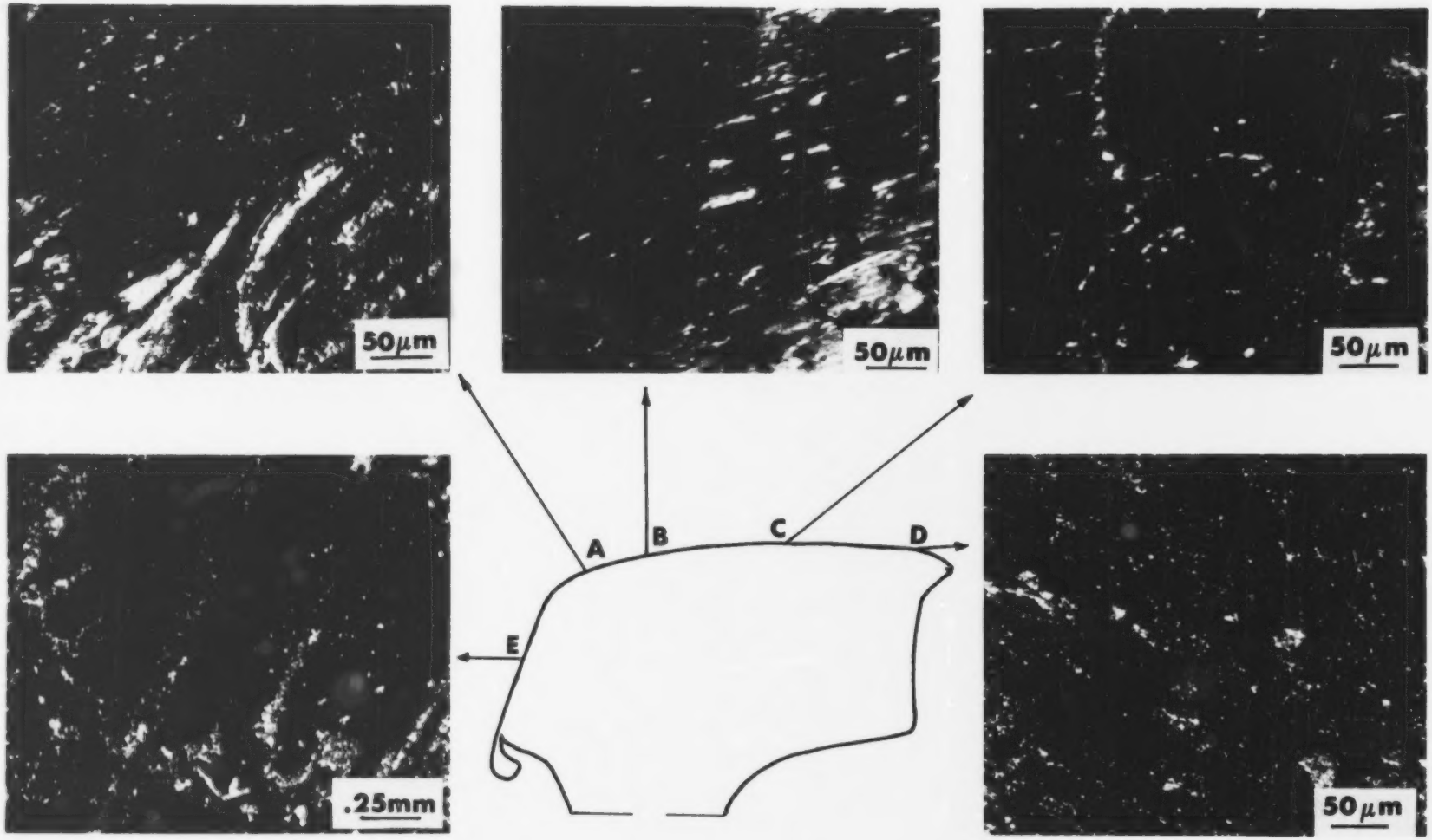

Fig. 7: Friction streaks observed on worn high rail located in 8° curve

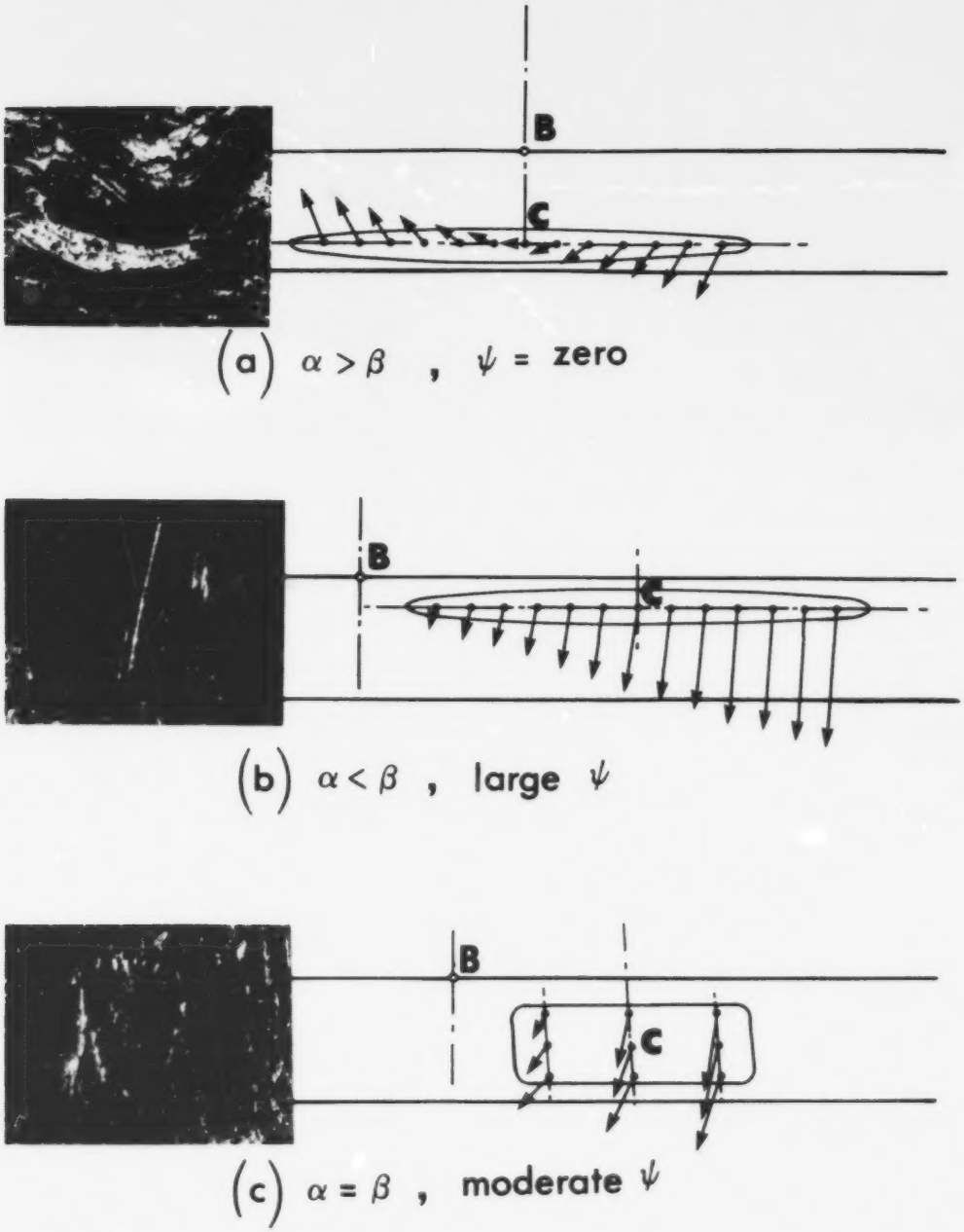

Fig. 8: Distribution of slip vectors within the flange contact. α, β - flange cone and gauge face inclination angles respectively, ψ - angle-of-attack

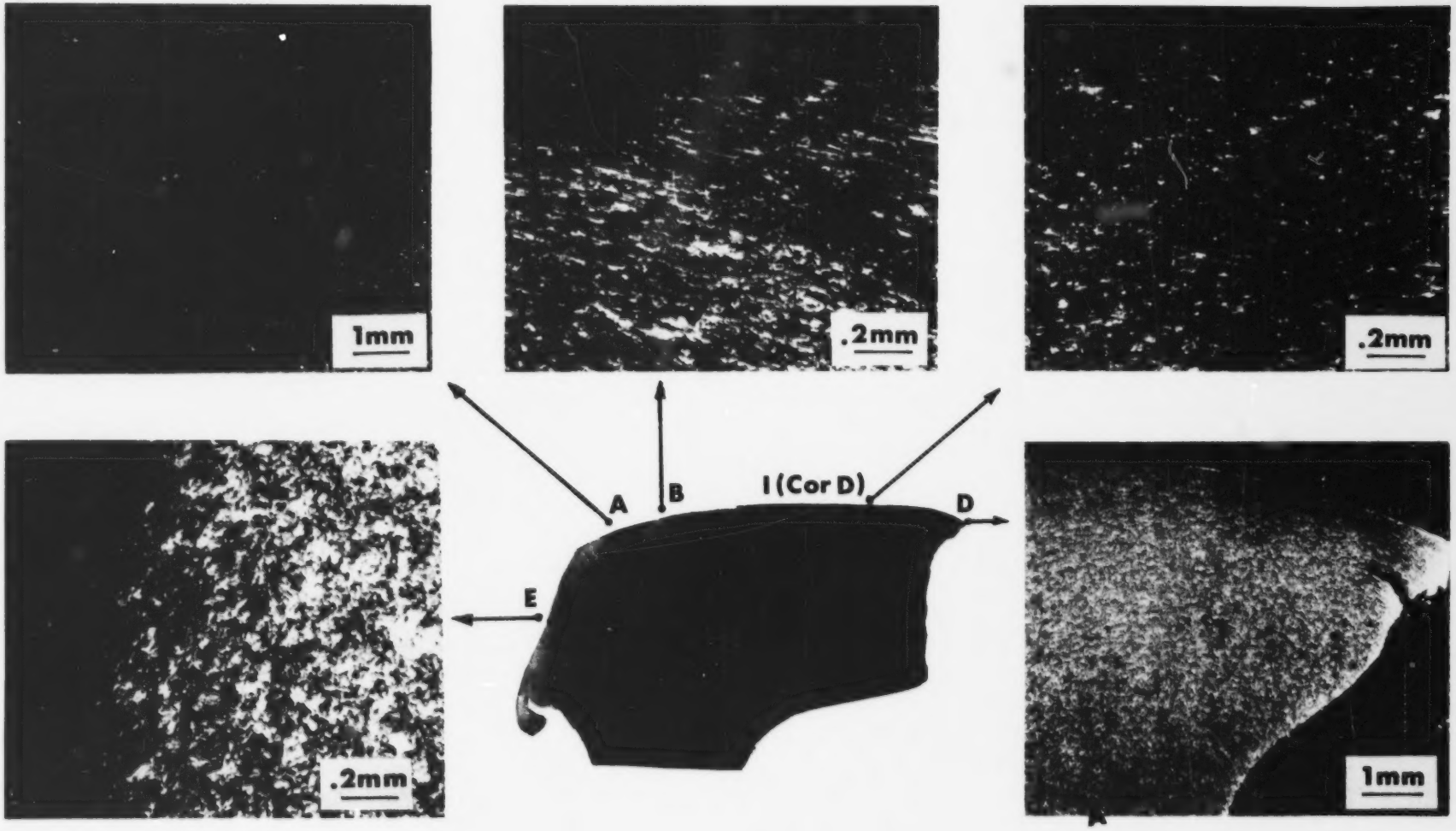

Fig. 9: Plastic flow observed on the crossection of high rail removed from 8° curve

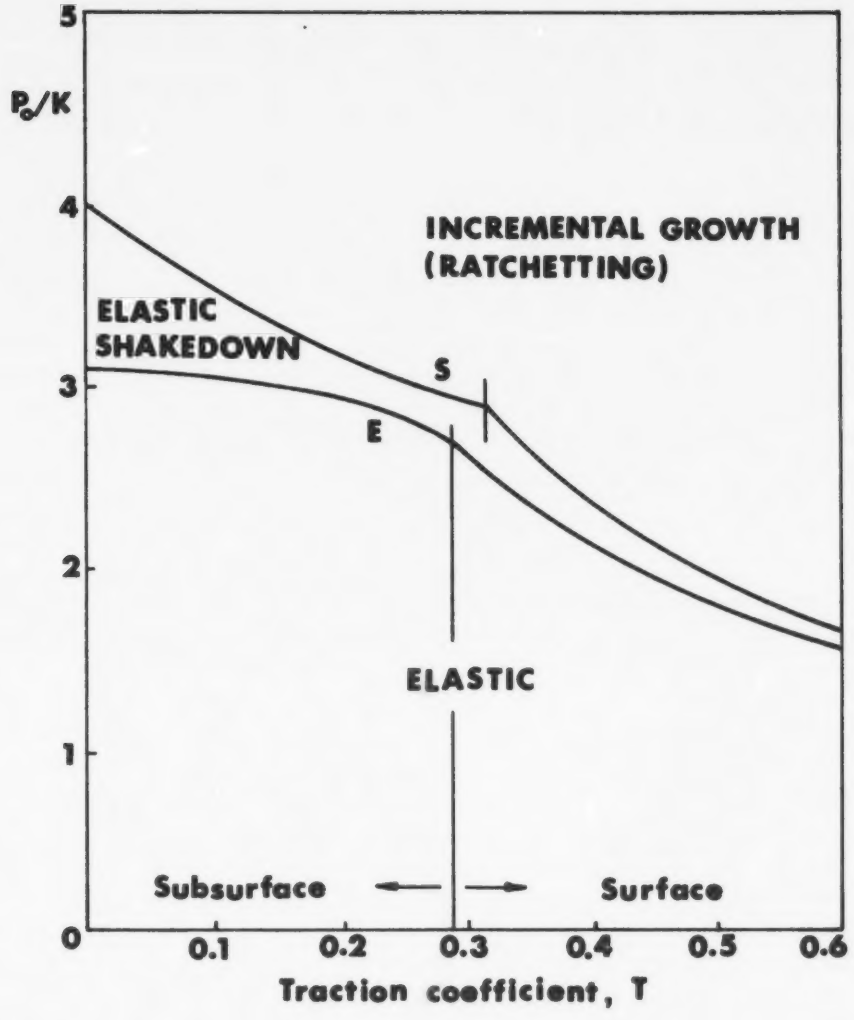

Fig. 10: Effect of traction on elastic and shakedown limits
E - elastic limit, S - shakedown limit

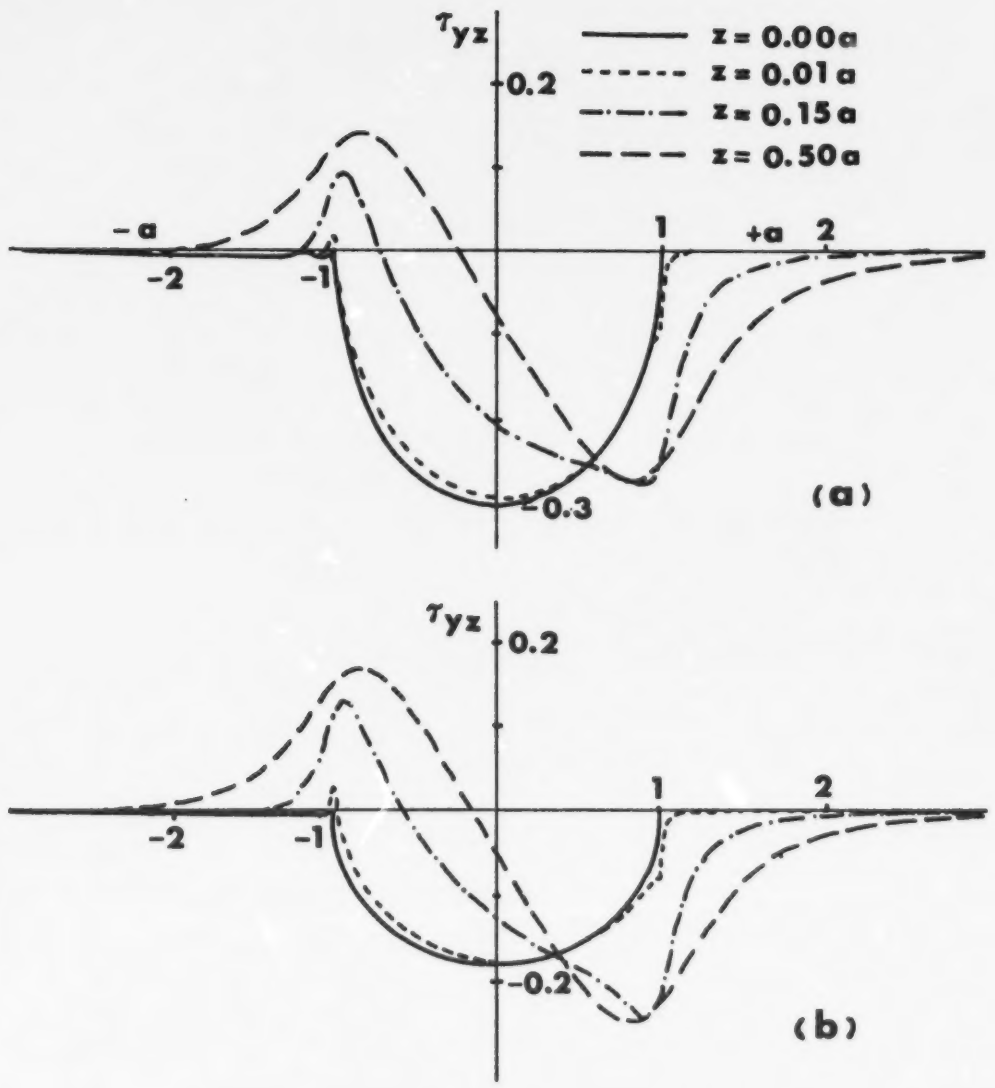

Fig. 11: Shear stress τ_{yz} in the plane perpendicular to the direction of travel for a) dry contact, $\mu = 0.3$ and b) grease-sand lubricated contact, $\mu = 0.18$ at depths as indicated

(a)

(b)

Fig. 12: Wear particles: a) crossection of severe adhesive wear particle
b) oxidative wear particles

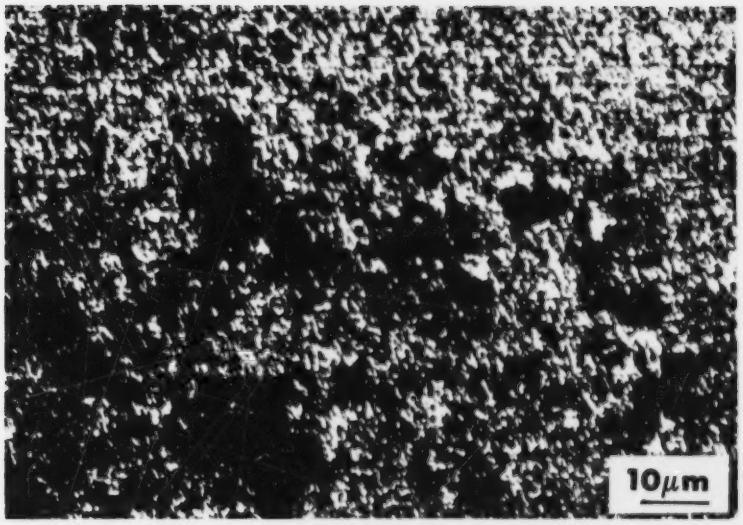

(a)

(b)

Fig. 13: a) rail's top surface abraded by crushed sand particles
b) crossection of delamination wear particles generated by surface fatigue wear

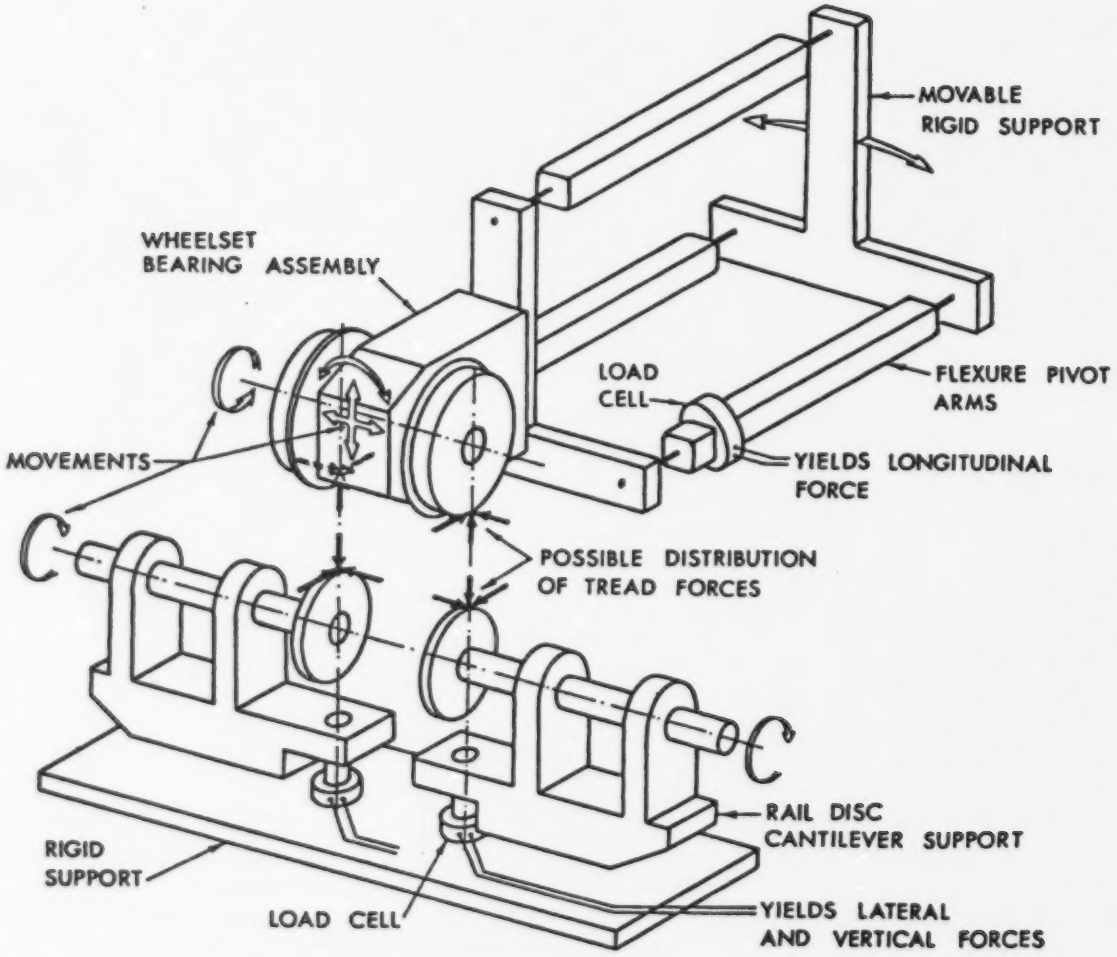

Fig. 14: Schematics of rail/wheel wear test apparatus

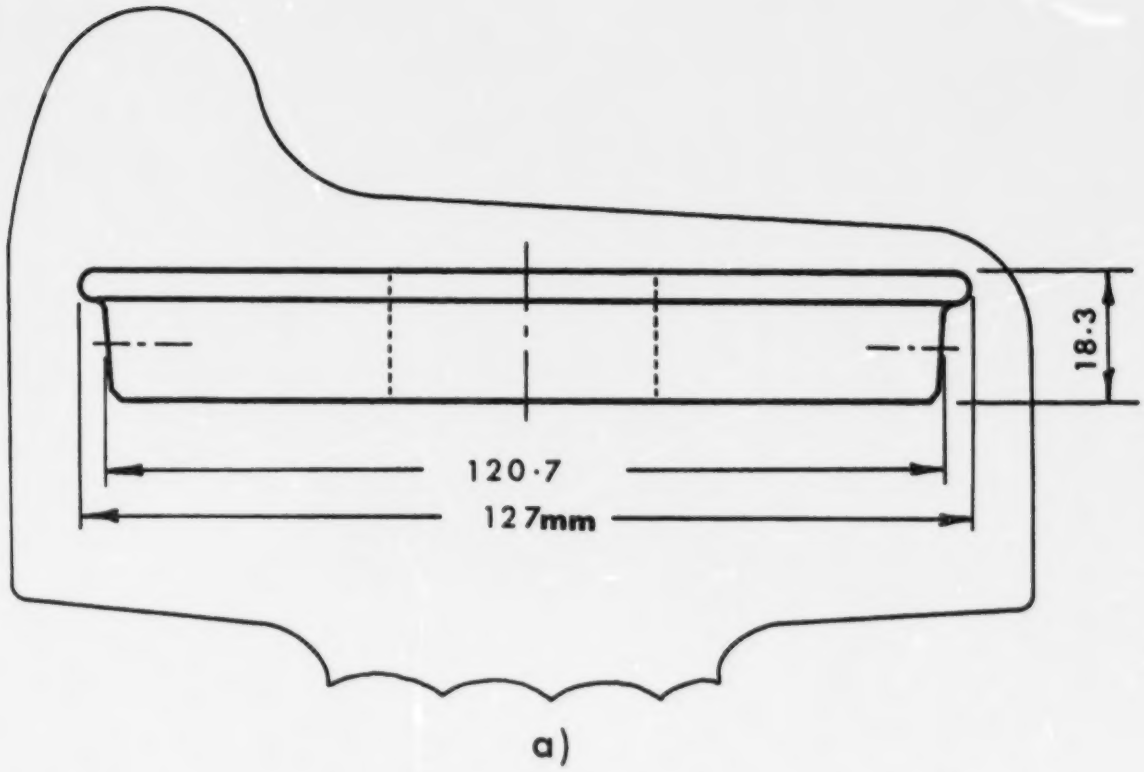

a)

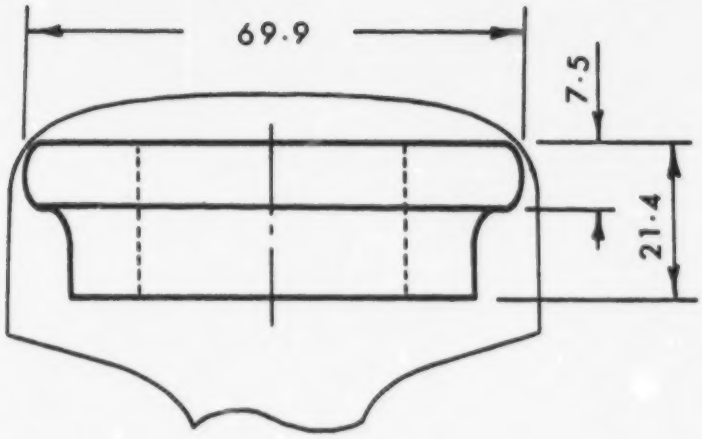

b)

Fig. 15: Dimensions of rail and wheel discs used in wear apparatus

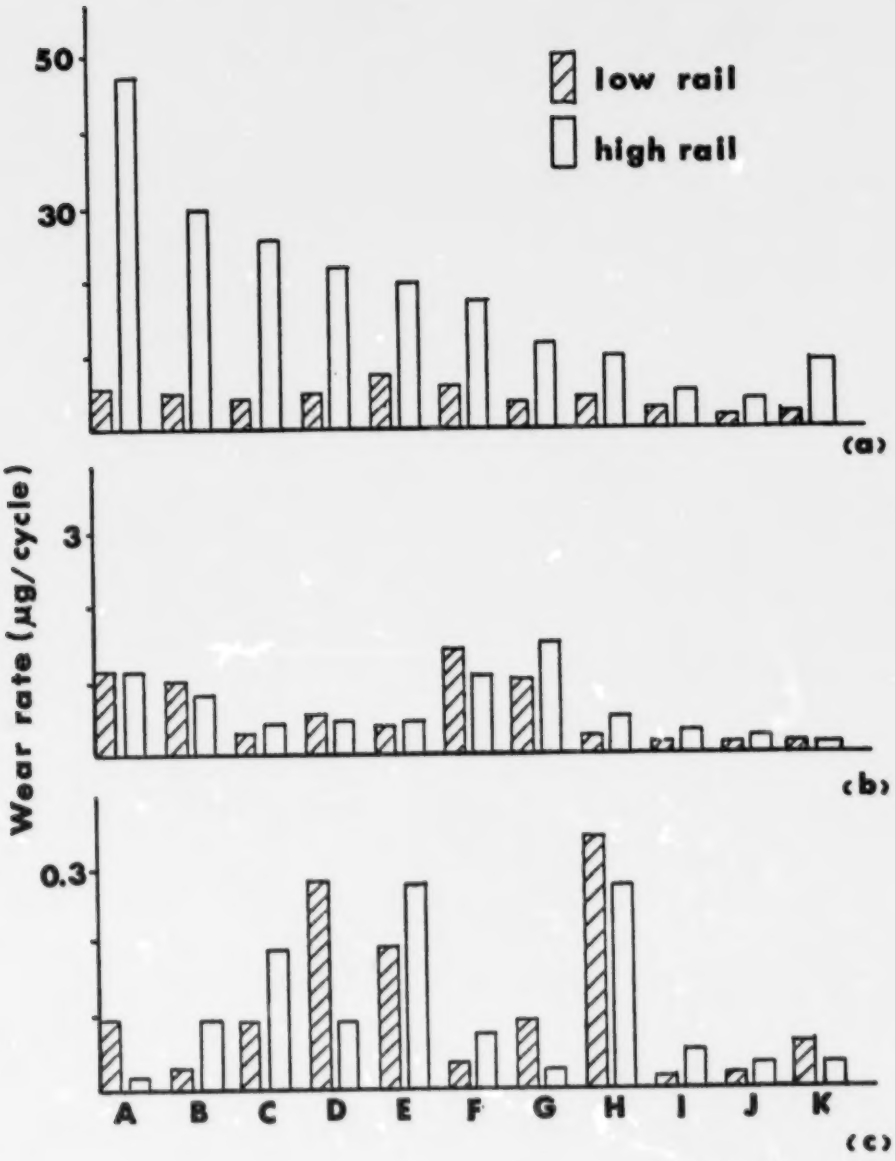

Fig. 16: Wear rates observed on commercial rail steels with: a) no lubrication, b) lubricated by grease - 20% sand mixture, c) lubricated by grease.
Steels: A - Standard carbon; B - Alloyed 1% Cr; C - Heat Cr-MoI; D - Russian FHT; E - Alloyed Cr-Cb; F - Fully heat treated; G - New head hardened; H - Australian head hardened; I - British Cr-enhanced; J - Japanese micro-alloyed head hardened; K - AWC 340. Note the scale changes in a), b) and c)

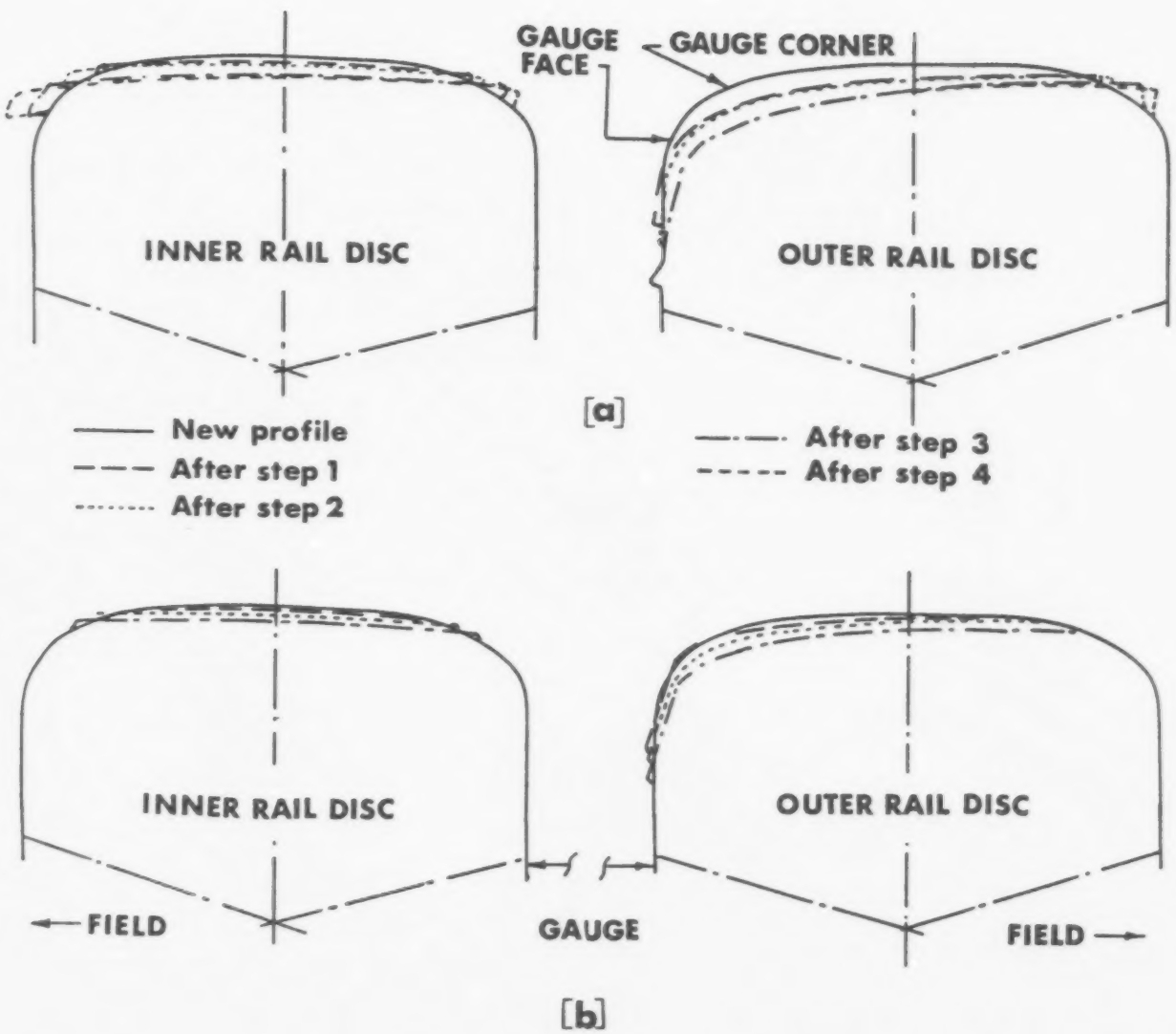

Fig. 17: New and worn profiles of low and high rail discs:
a) Steel A - standard carbon
b) Steel G - new head hardened

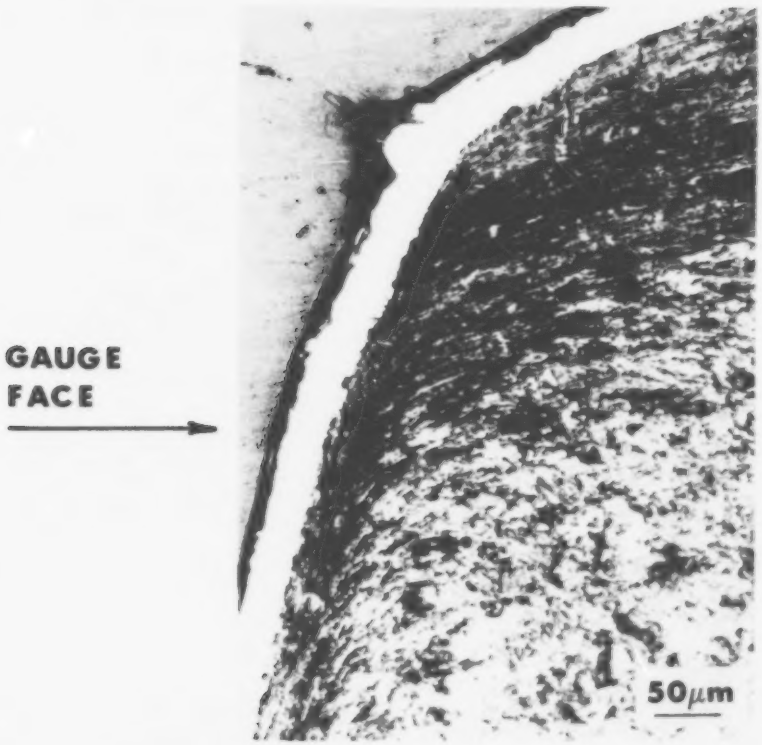

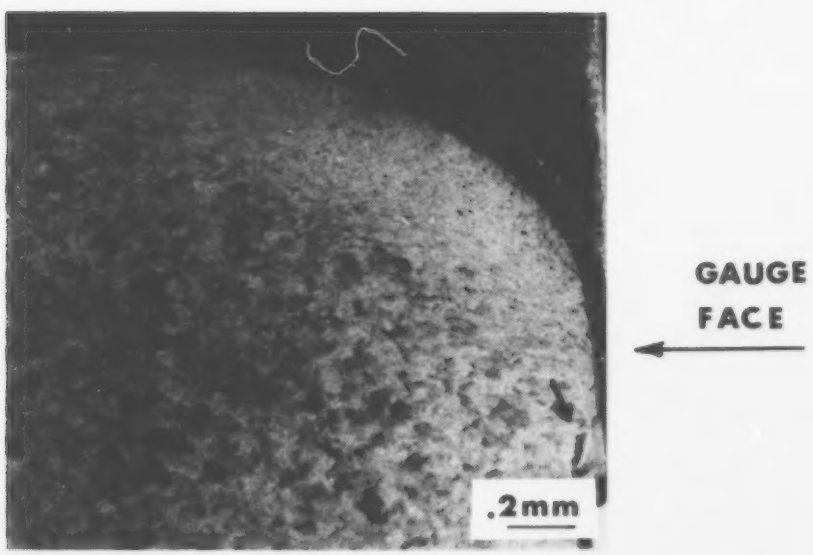

Fig. 18: a) plastic flow of metal into the gauge face area, where it is worn away
b) narrowing of gauge caused by plastic flow

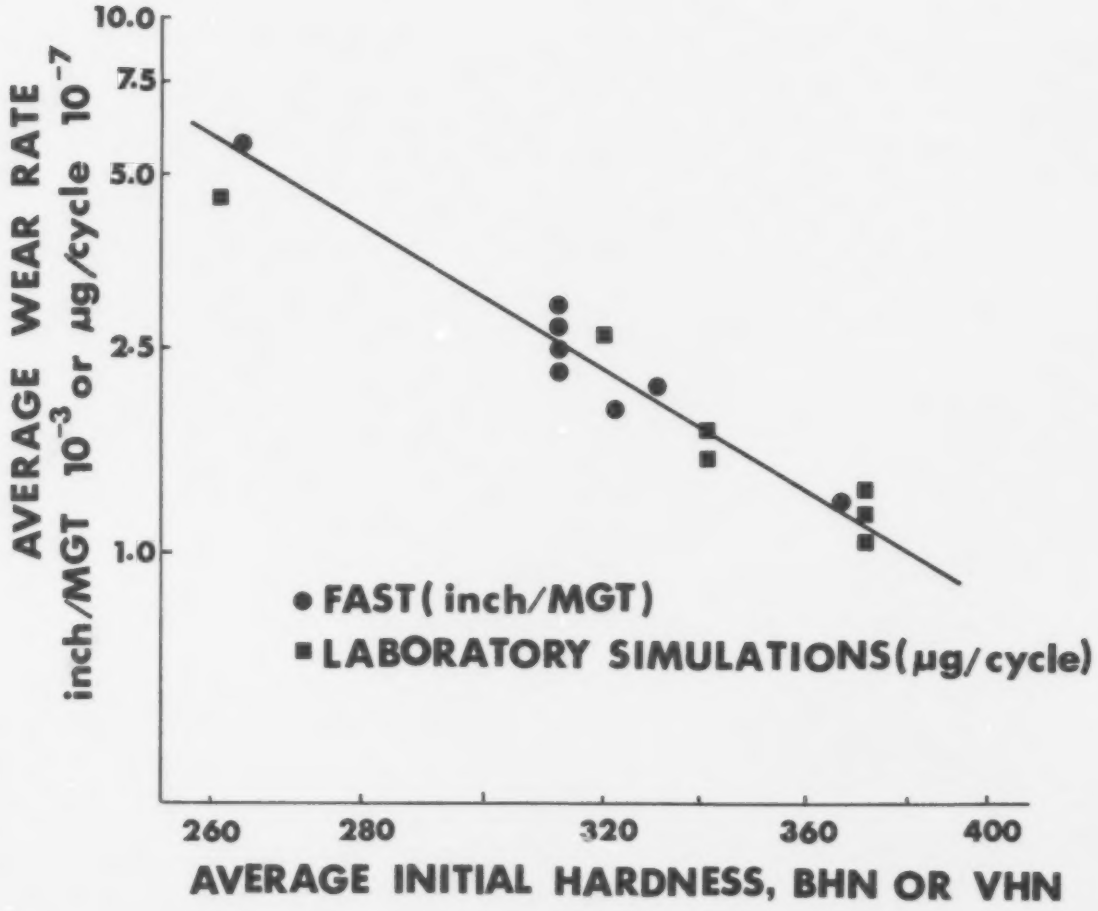

Fig. 19: Correlation of gauge face wear rates on the same rail steels tested at Facility for Accelerated Service Testing (FAST) and rail/wheel wear apparatus

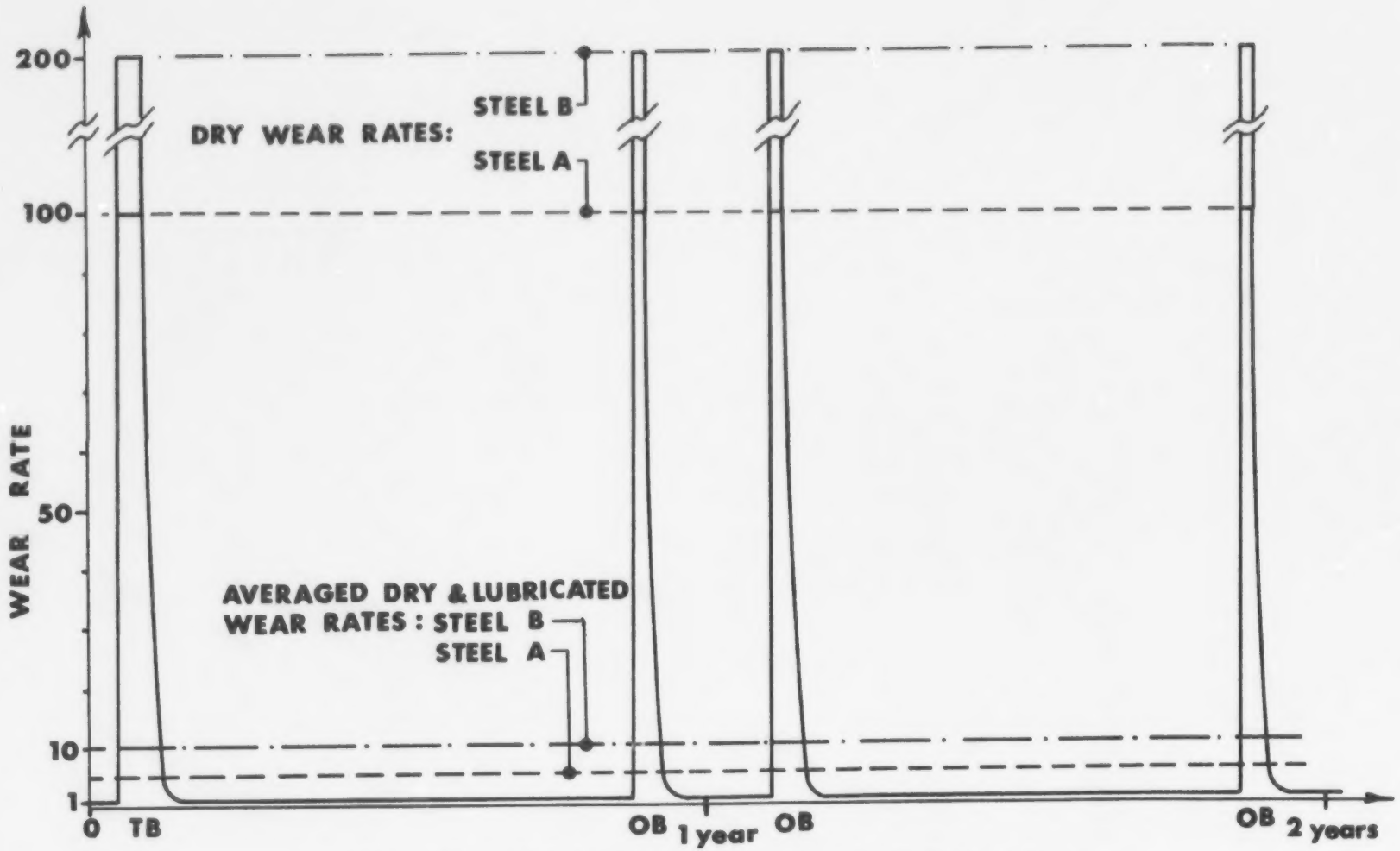

Fig. 20: Effect of lubrication breakdowns on the average gauge face wear rates. OB - one week and TB - two weeks lubrication breakdowns. Lubricated to dry wear rate ratios: Steel A - 1:100, Steel B - 1:200. Averaged lubricated to dry and lubricated wear rate ratios: Steel A - ≈ 1:5, Steel B - ≈ 1:10

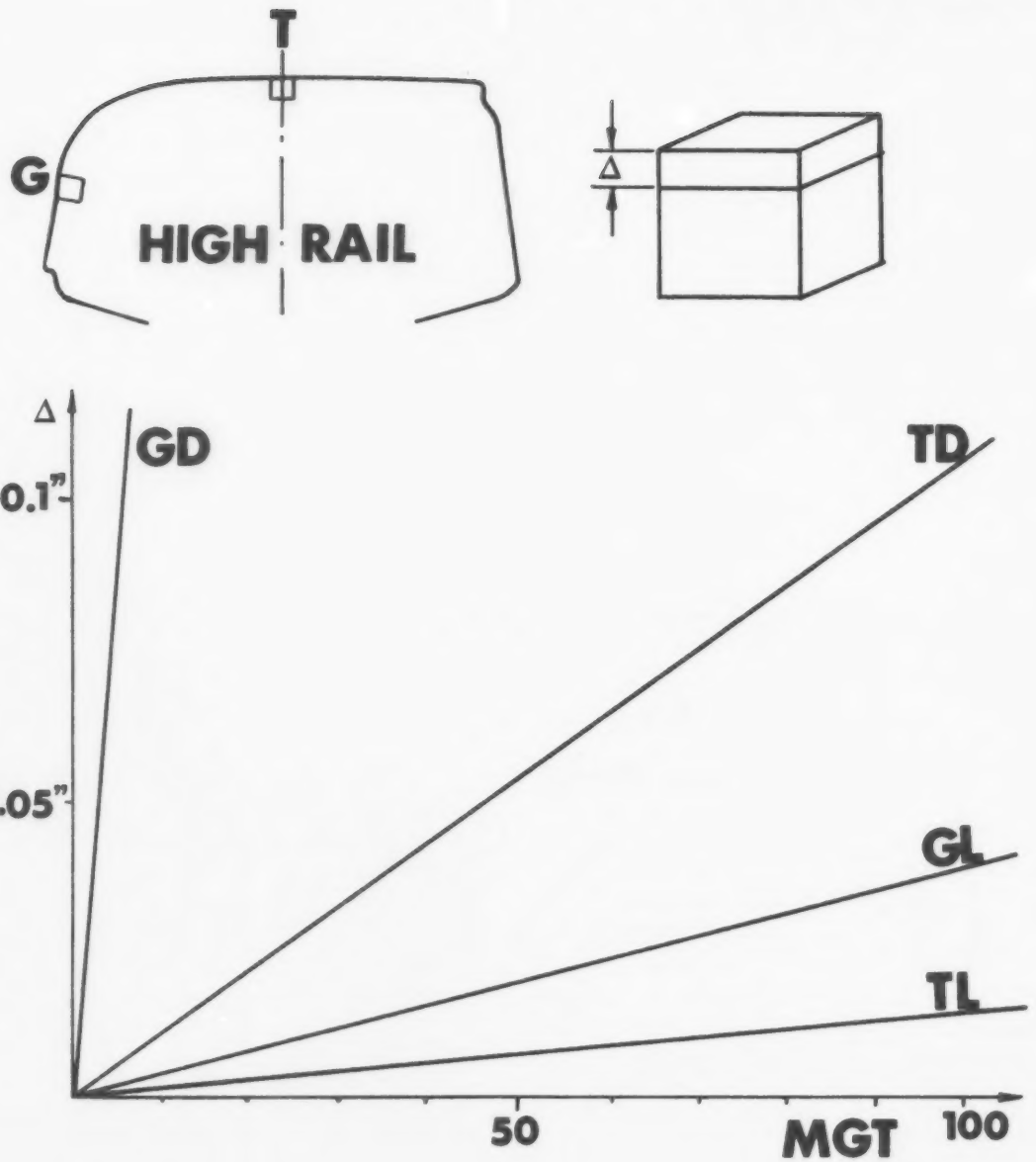

Fig. 21: Wear rates converted to surface recess of material. GD - gauge face dry i.e. rate of gauge face recess under dry conditions; TD - top, dry; GL - gauge face, lubricated; TL - top, lubricated

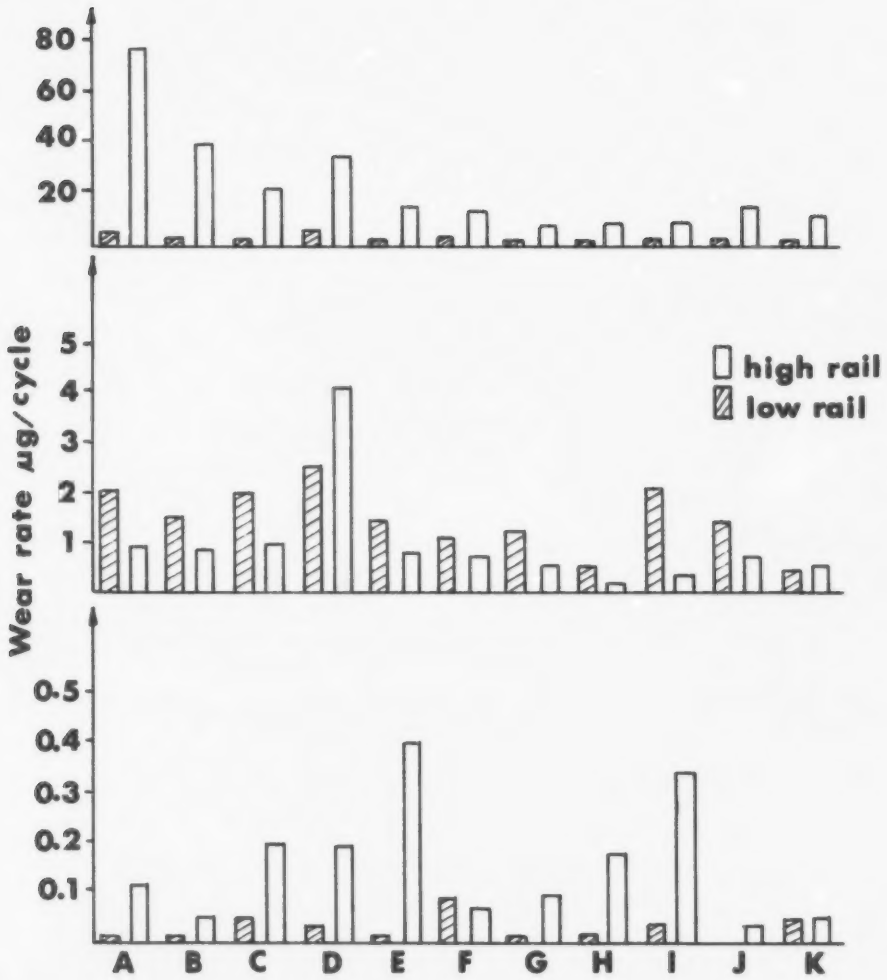

Fig. 22: Wear rates observed on experimental rail steels:
a) no lubrication, b) grease/20% sand lubrication,
c) grease lubrication.
Steels: A - C, D - F and G - I are tempered martensite,
bainite and pearlite respectively, J is nodular iron and
K is Cr-V pearlitic steel. Note scale changes in a), b) and c)

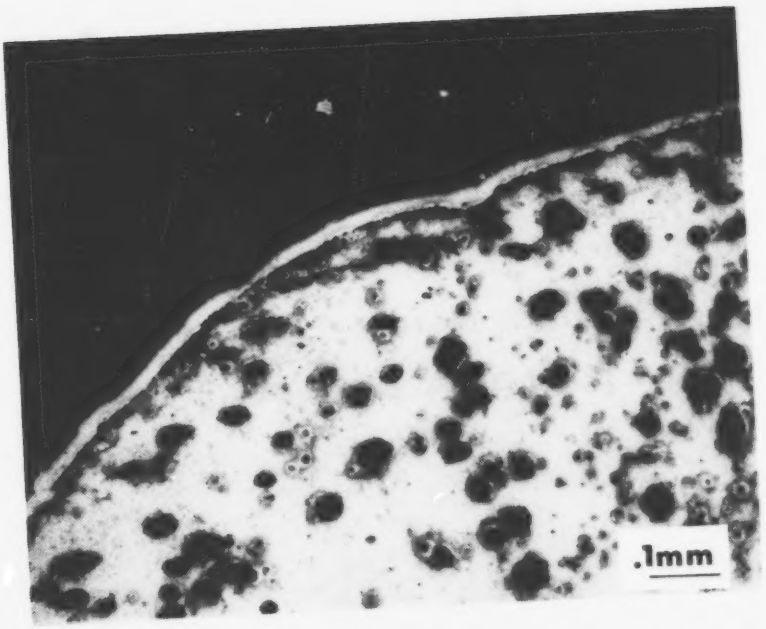

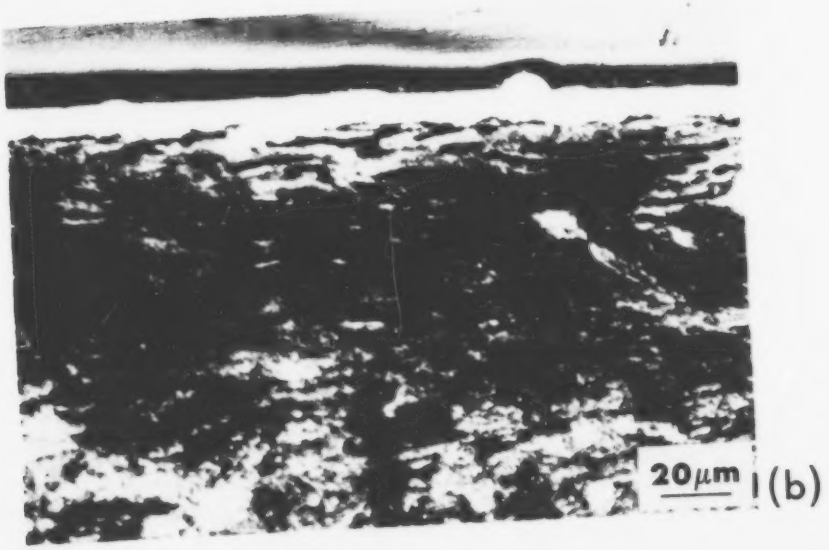

Fig. 23: a) gauge corner crossection of high rail disc with microstructure made from nodular iron
b) wear surface microstructure of adhesively worn rail steel

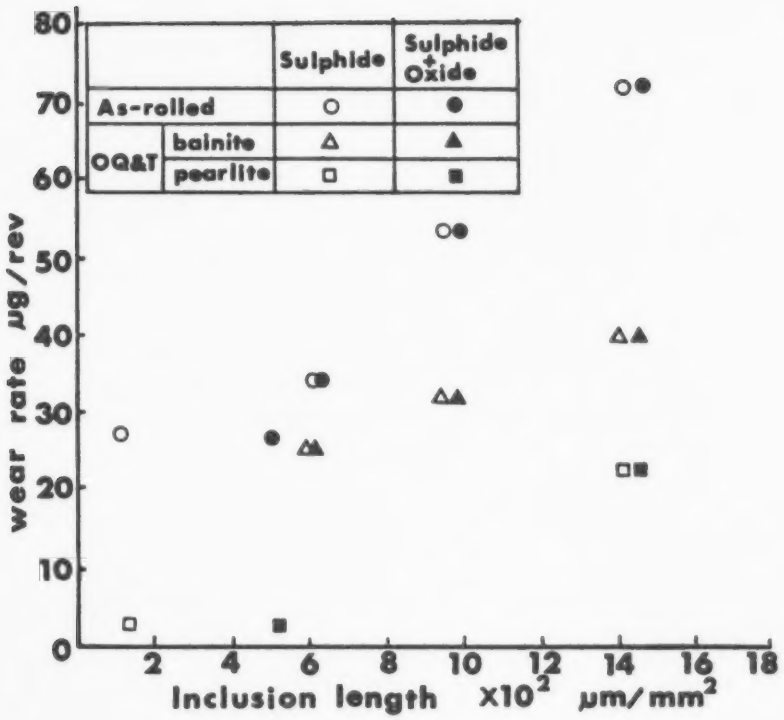

Fig. 24: Effect of sulphur inclusion density on adhesive wear

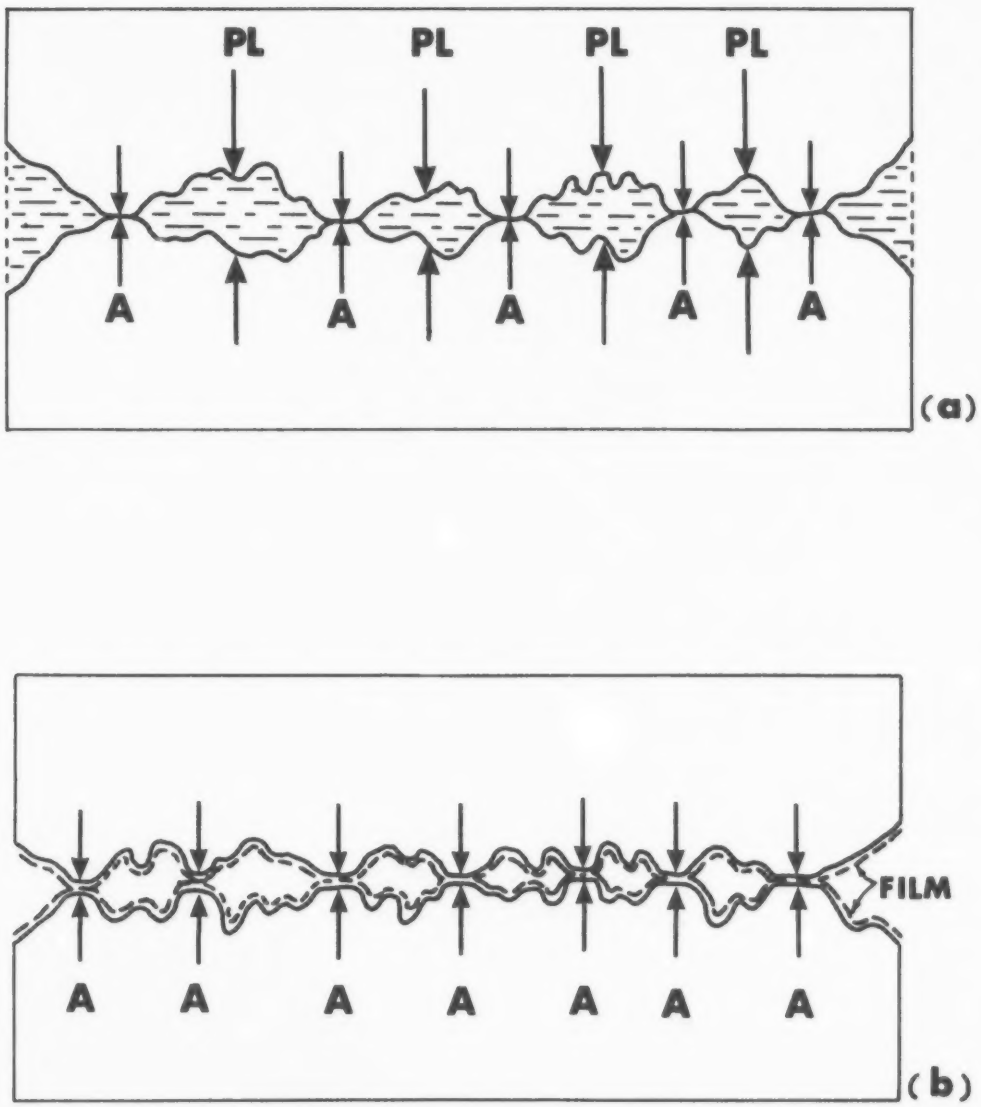

Fig. 25: Schematics of contact in:
a) partial-Elastohydrodynamic lubrication and
b) boundary lubrication.
A - load supported by asperities, PL - load supported by pressurized lubricant

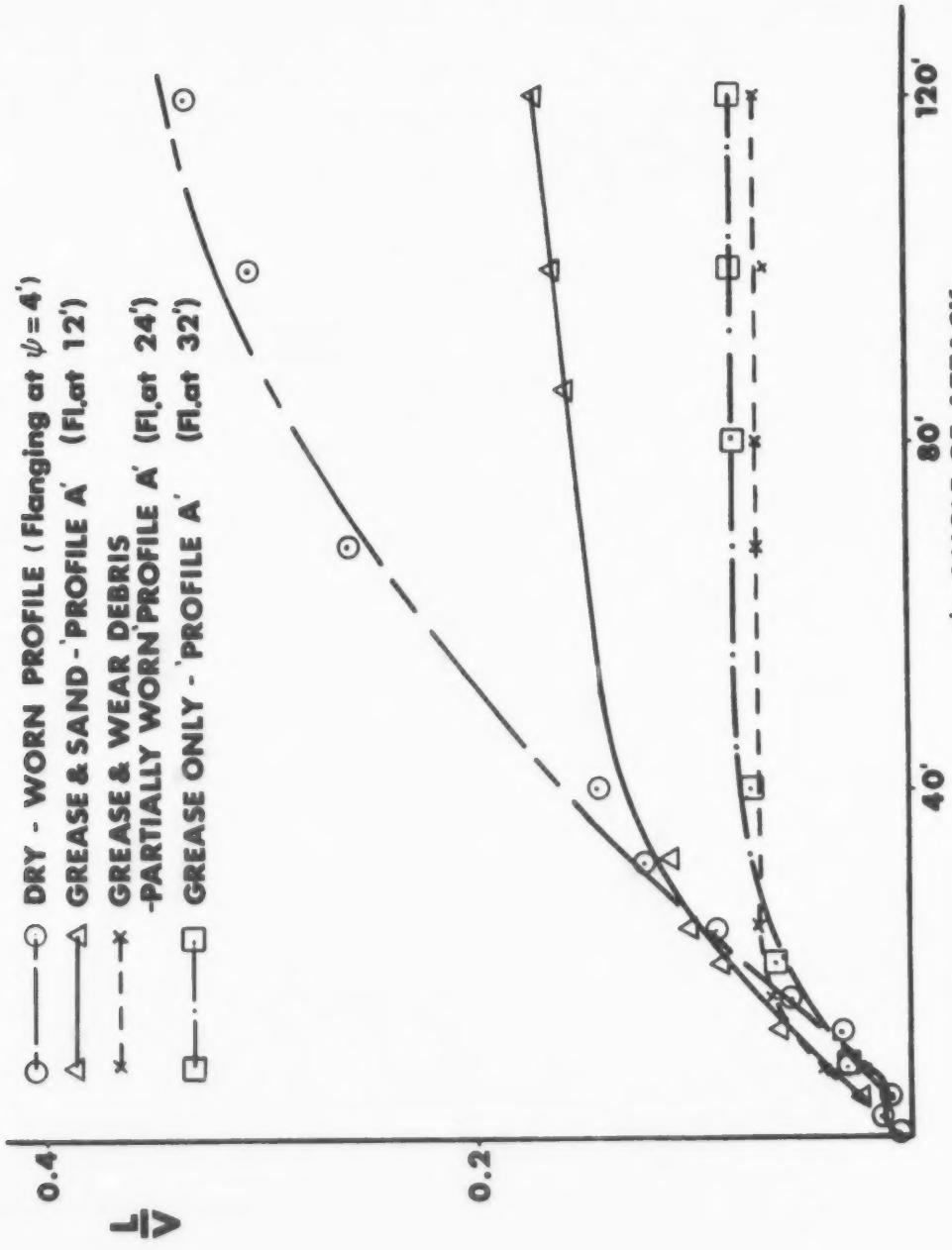

Fig. 26: Effect of lubrication on L/V ratio of low rail disc

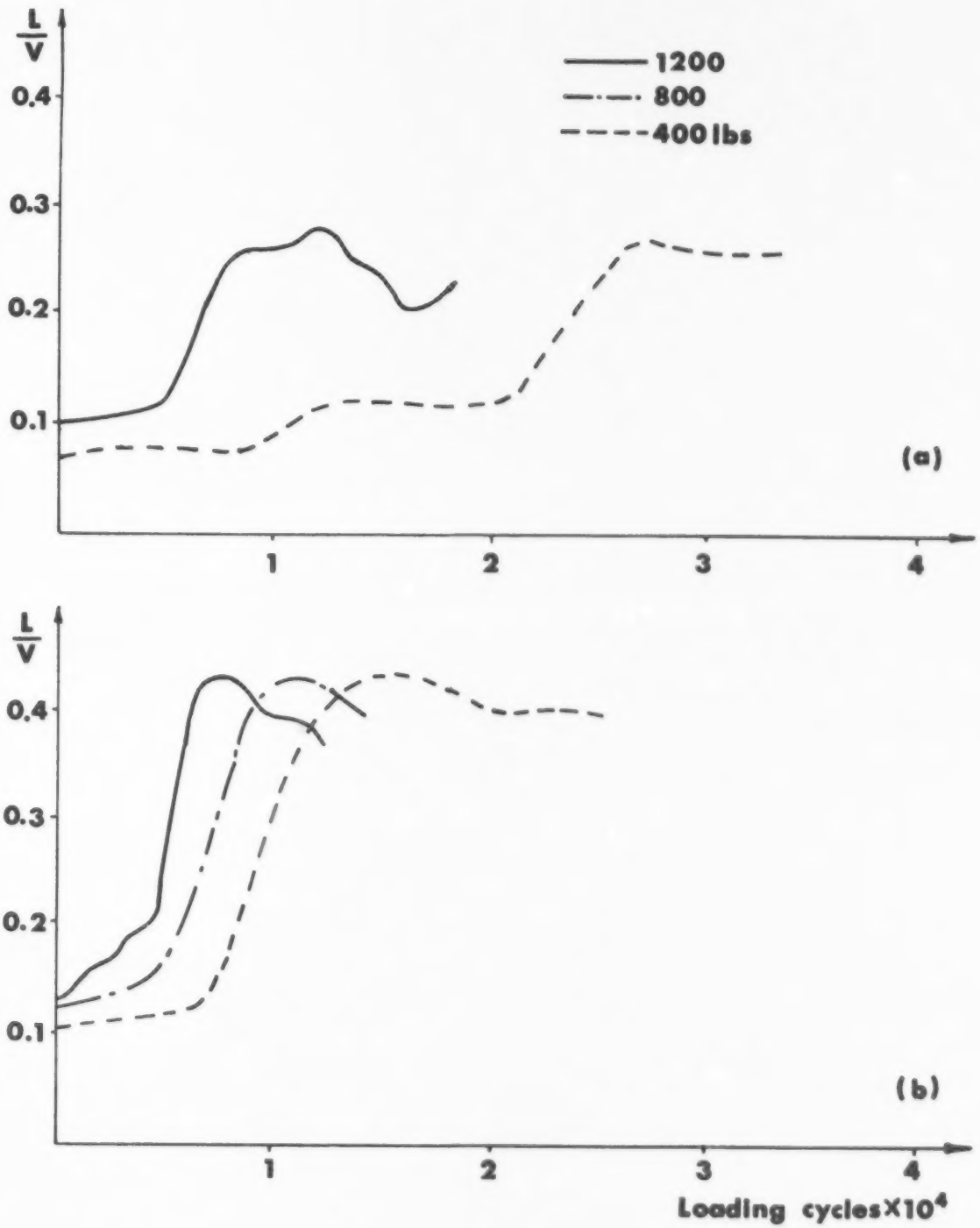

Fig. 27: Retentivity tests a) $\psi = 20'$
b) $\psi = 40'$
The consumption of lubricant is marked a by sudden increase in L/V ratio

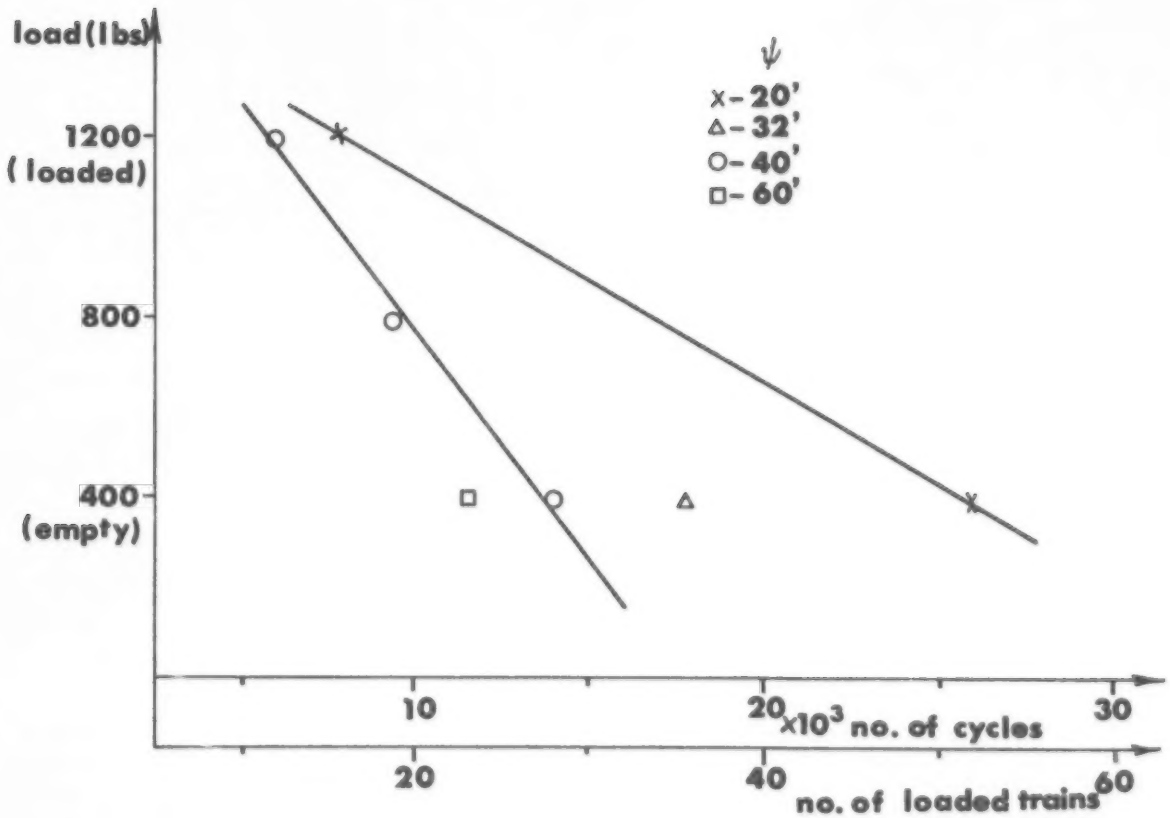

Fig. 28: Lubrication breakdown as function of load and angle of attack

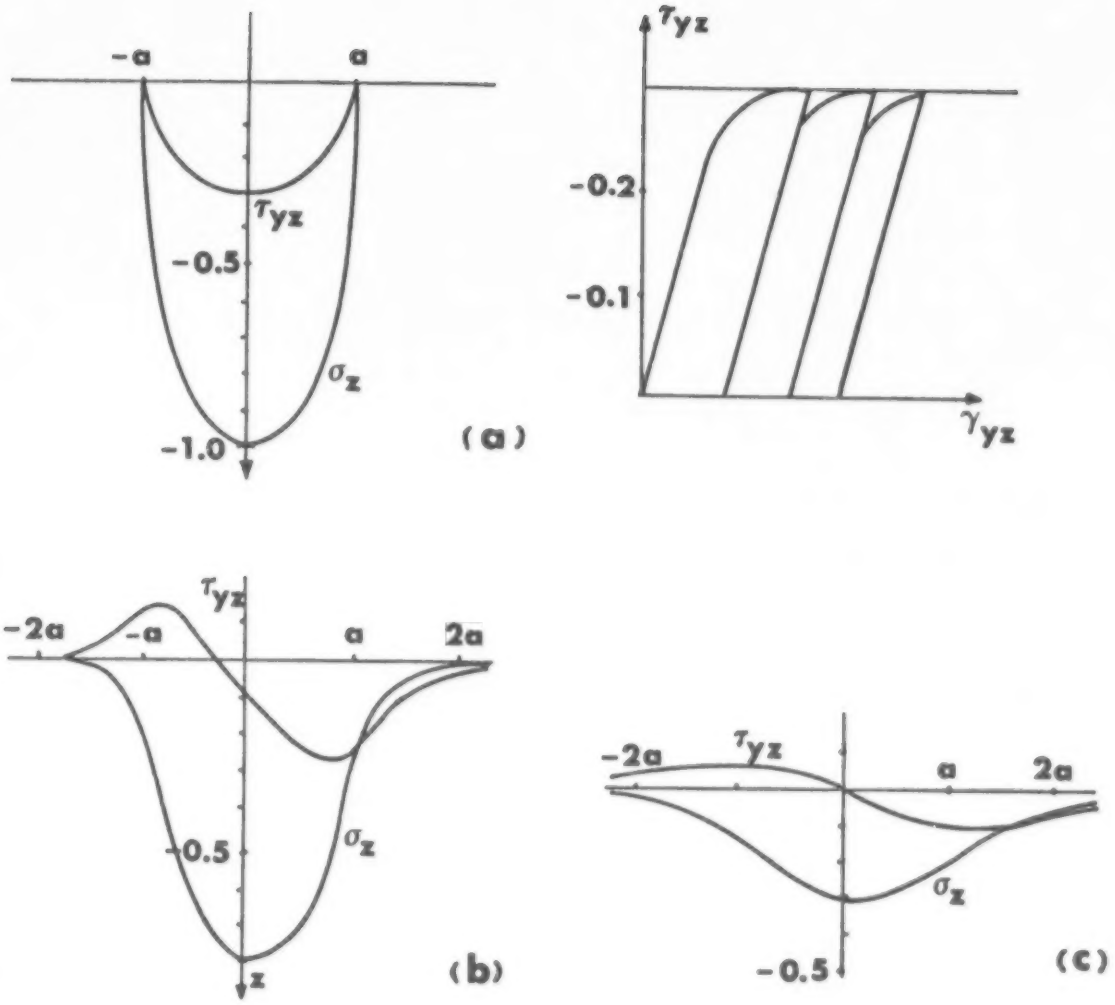

Fig. 29: Compressive σ_z and shear τ_{yz} stress distribution at the depth a) z = 0, b) z = 0.5a and c) z = 1.5a (Vertical load P = 1.0, lateral load Q = 0.3)

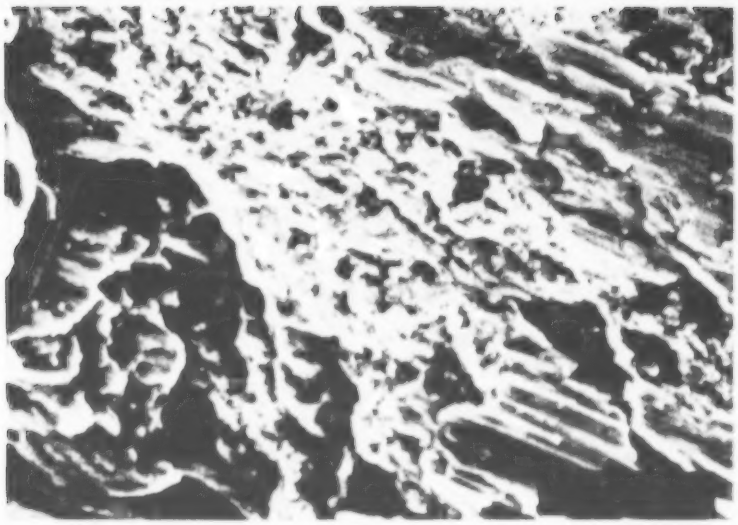

Fig. 30: Ductile shear fracture of rail material

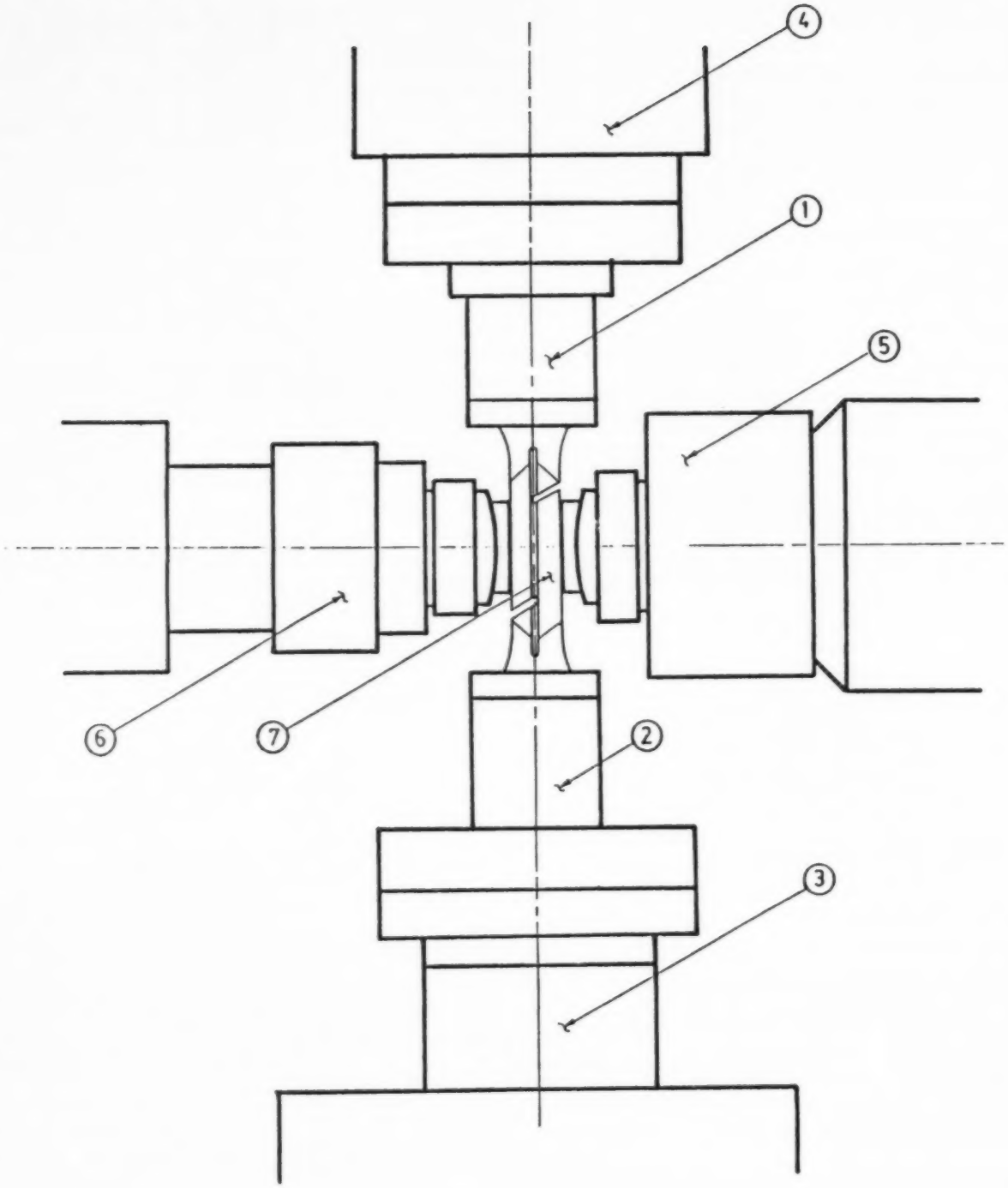

(1,2) -- Vertical Grips
(4) ---- Load Cell
(6) ---- Horiz. Load Cell
(3) -- Vertical Actuator
(5) -- Horiz. Actuator
(7) -- Biaxial Specimen

Fig. 31: Biaxial specimen with loads applied in the shear and compression directions

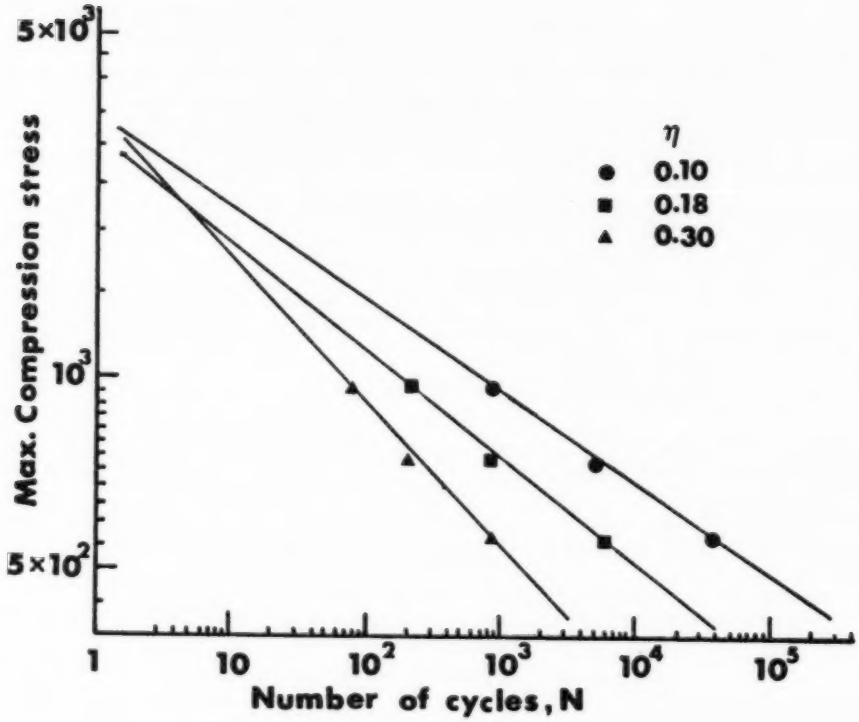

Fig. 32: Number of cycles to crack initiation by plastic instability with respect to maximum shear stress for different values of η

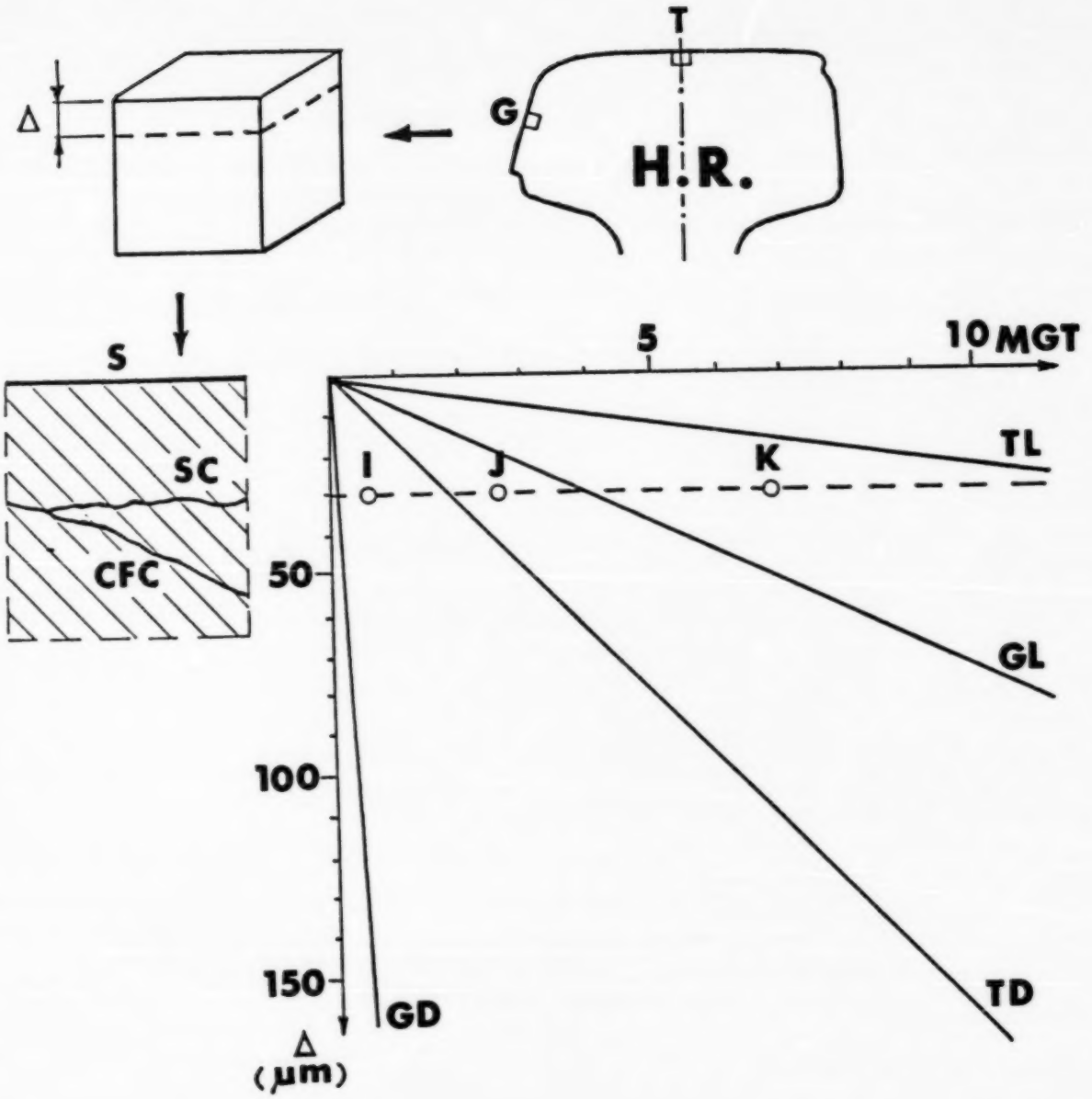

Fig. 33: Relationship between wear and surface fatigue crack initiation for 8° curve. Material: chromium alloyed steel (Figure 16, steel B). Cracks: SC - surface crack, CFC - contact fatigue crack, S - surface. Wear rates: GD - gauge face, dry. TD - top surface, dry, GL and TL - gauge face and top surface respectively lubricated. Surface crack initiation points: K - location B & C (Figure 3) lubricated, $\mu \approx .18$; J - location B & C, dry, $\mu \approx .3$, $p_0 \approx 1150$MPa (167ksi); I - location A, lubricated by grease and sand, $\mu \approx .18$, $p_0 \approx 2{,}500$MPa (363ksi).

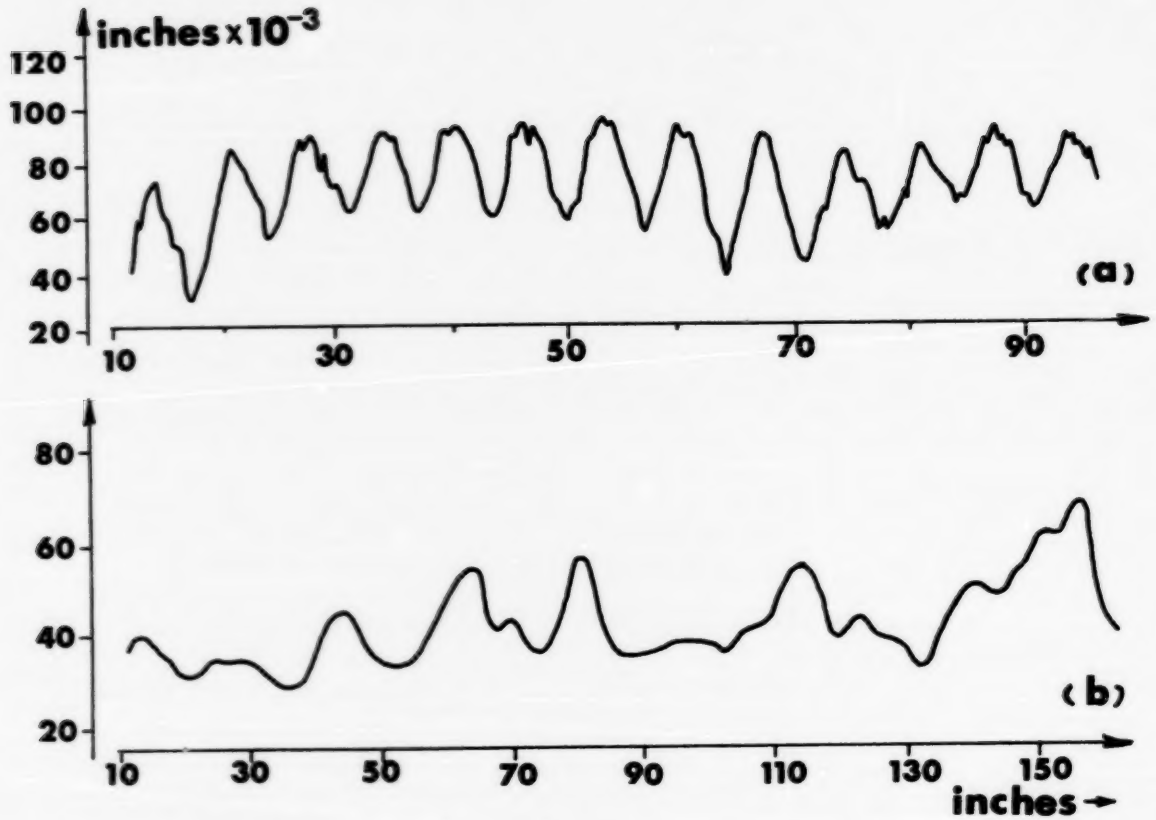

Fig. 34: Rail corrugation profiles
a) at FAST under dry conditions
b) in Canadian Rockies under lubricated conditions

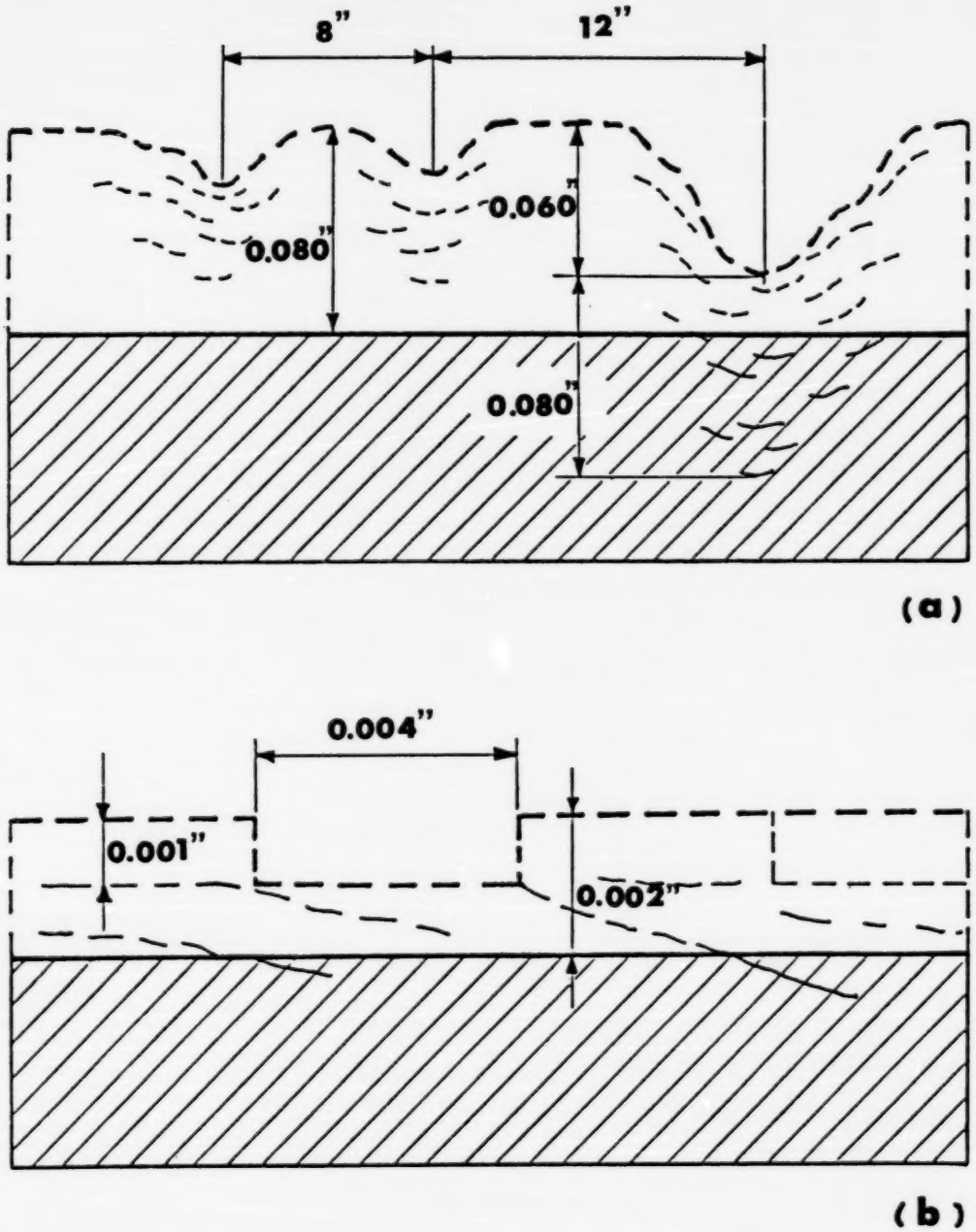

Fig. 35: Schematics of a) corrective and b) preventive grinding shown on a) longitudinal and b) transverse sections of the railhead

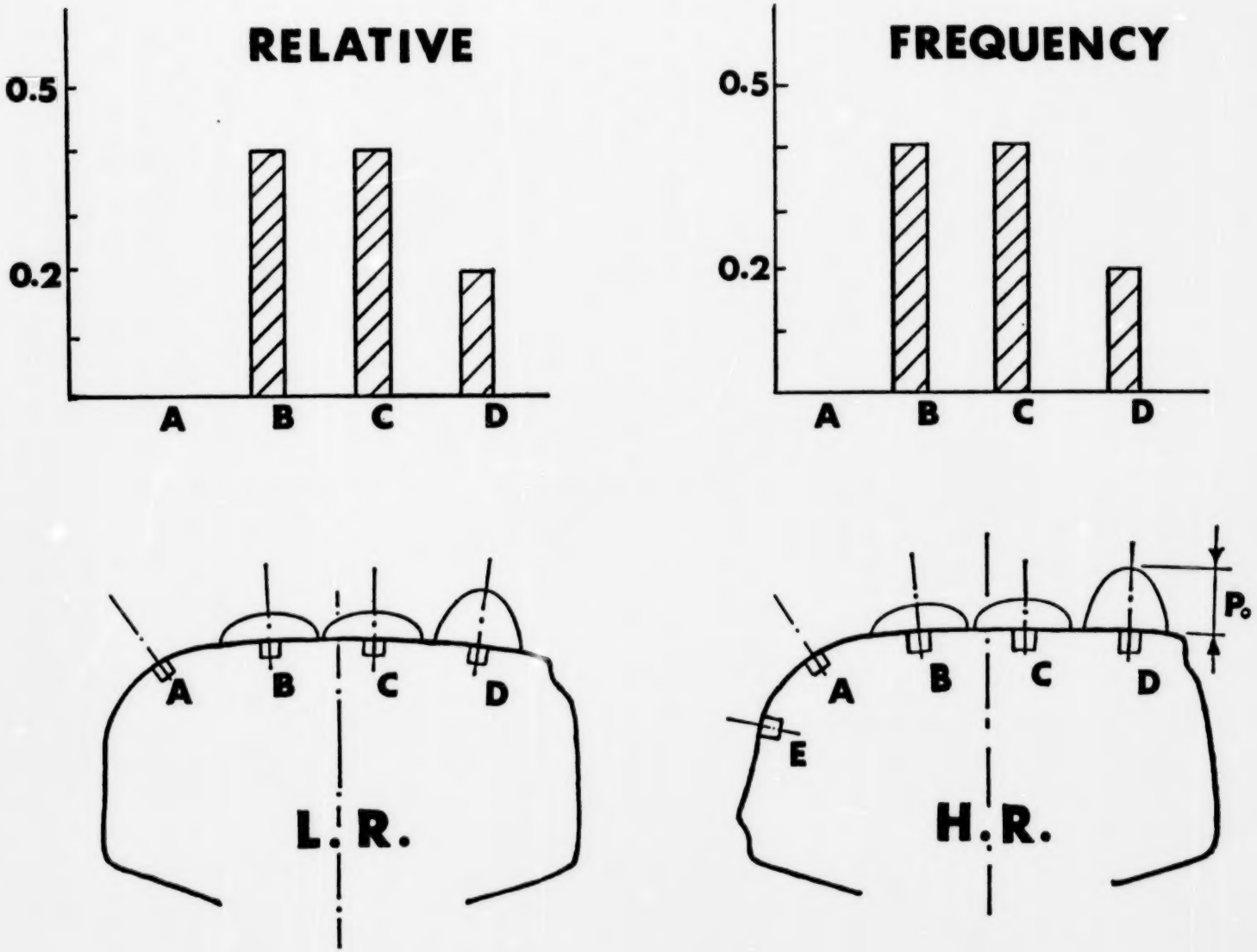

Fig. 36: Modified frequency histogram for preventively ground rails on 8° curve

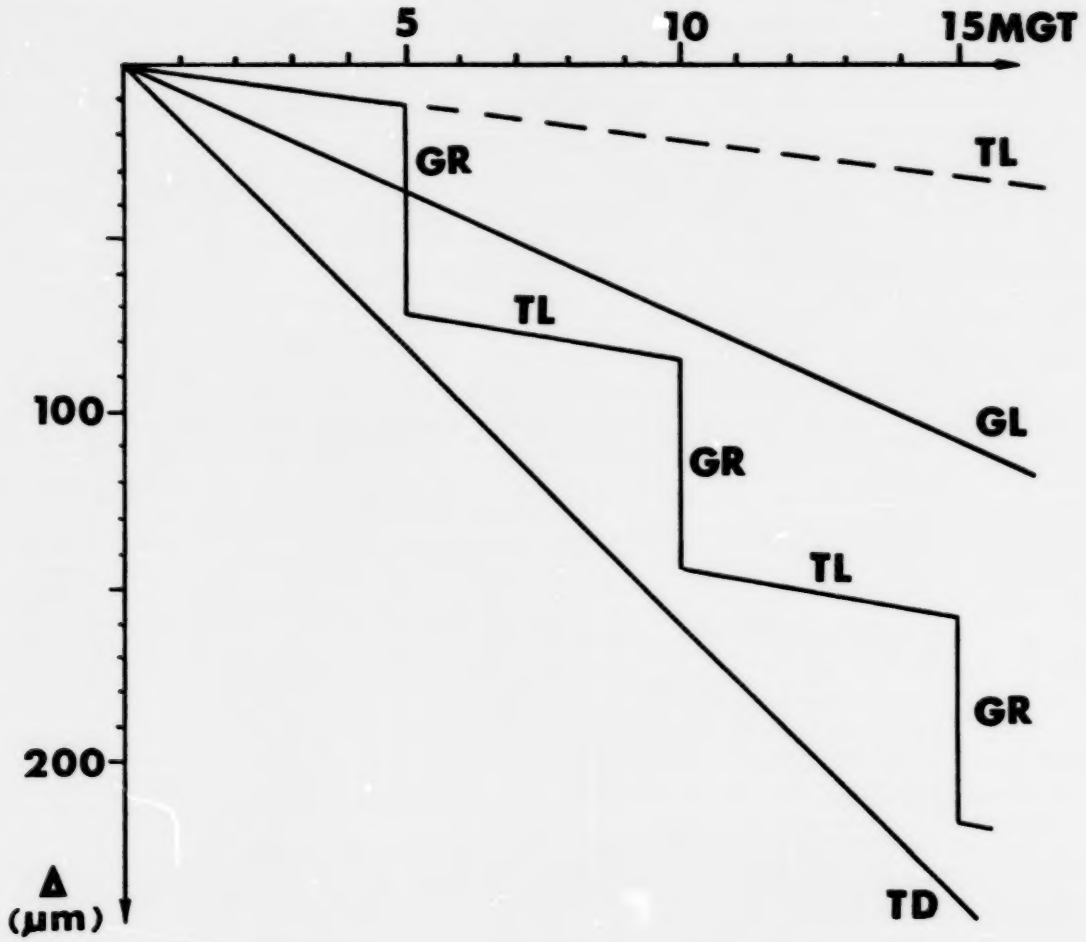

Fig. 37: Effect of preventive grinding on wear rates in lubricated 8° curve. Wear rates: TD - top, dry; TL - top, lubricated; GL - gauge face, lubricated; GR - removed by grinding

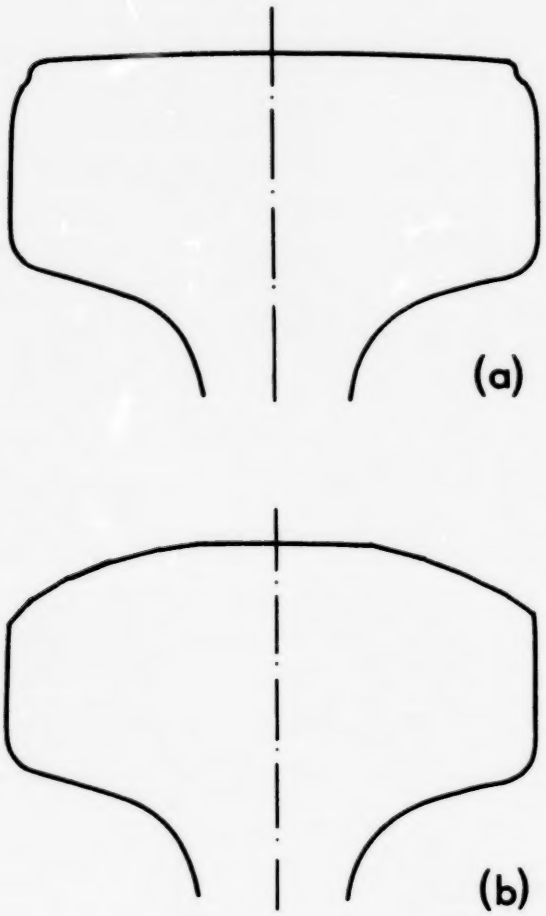

Fig. 38: a) "Flat" and b) "contour" grinding profiles

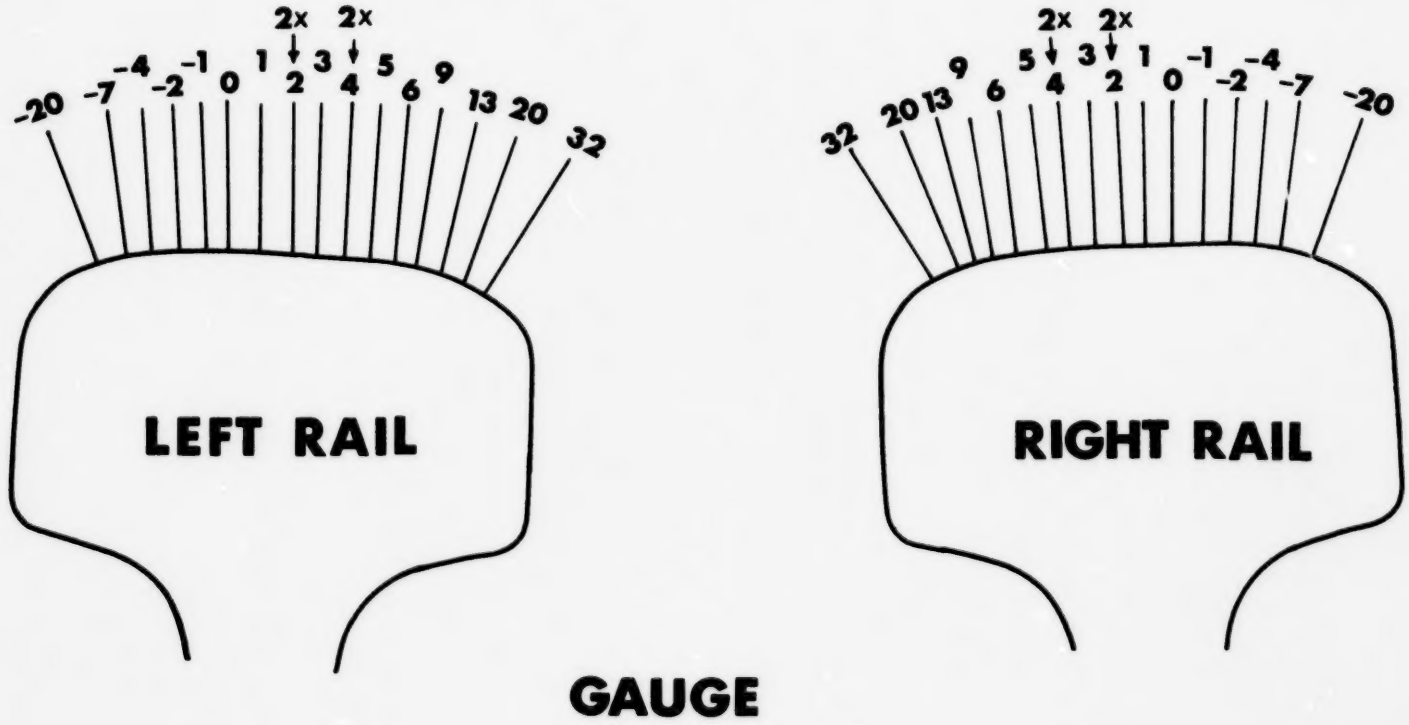

Fig. 39: Basic (tangent track) rail grinding pattern for 44 stone grinding train recommended for territories travelled by wheels with modified Heumann profile

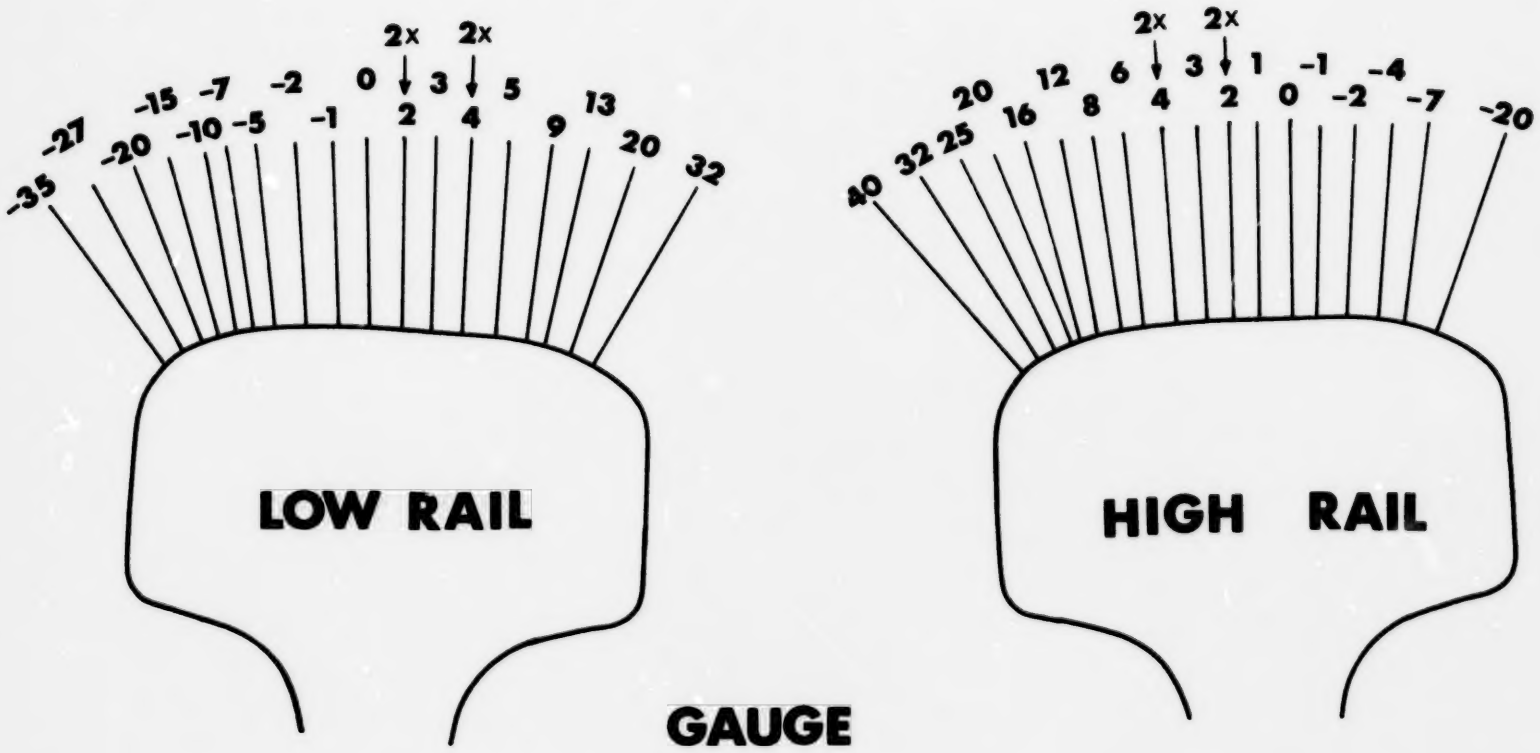

Fig. 40: Left hand curve rail grinding pattern for 44 stone grinding train recommended for territories travelled by wheels with modified Heumann profile

REPORT DOCUMENTATION PAGE/PAGE DE DOCUMENTATION DE RAPPORT

REPORT/RAPPORT	REPORT/RAPPORT
1a TR-WE-50	1b NRCC. 27491
SECURITY CLASSIFICATION/ CLASSIFICATION DE SÉCURITÉ Unclassified 2	DISTRIBUTION/DIFFUSION ☐ Controlled/Contrôlé ☒ Unlimited/Illimité 3

TITLE/SUBTITLE/TITRE/SOUS-TITRE

Wear and Contact Fatigue Model for Railway Rail

4

AUTHOR(S)/AUTEUR(S)

Kalousek, J.

5

SERIES/SÉRIE

DME Technical Report

6

CORPORATE AUTHOR/PERFORMING AGENCY/AUTEUR D'ENTREPRISE/AGENCE D'EXÉCUTION

National Research Council
Division of Mechanical Engineering
Tribology and Mechanics Laboratory

7

SPONSORING AGENCY/AGENCE DE SUBVENTION

8

DATE	FILE/DOSSIER	LAB. ORDER COMMANDE DU LAB.	PAGES	DIAGS	REFS
1986/10			61	40	47
9	10	11	12a	12b	12c

NOTES

13

DESCRIPTORS(KEY WORDS)/MOTS-CLÉS

Rail wear, lubrication, grinding, contact fatigue and rail life

14

SUMMARY/SOMMAIRE Based on a study of contact fatigue crack initiation and propagation, a new rail lubrication and grinding maintenance policy is proposed. It advocates avoidance of lubrication breakdowns in combination with light but frequent grinding. Absence of gauge face wear and corrugations and much improved rail life will result.

15

ADDRESS/ADRESSE

Dr. C. Dayson Head/Chef
Western Laboratories
Division of Mechanical Engineering
3650 Wesbrook Mall, Vancouver, B.C. V6S 2L2
604 666-2623

16

Revised 85.10
Révisée 85.10